Electrochemical Energy Reviews (2024) 7:18
https://doi.org/10.1007/s41918-024-00221-0

REVIEW ARTICLE

Li Alloys in All Solid-State Lithium Batteries: A Review of Fundamentals and Applications

Jingru Li[1] · Han Su[1] · Yu Liu[1] · Yu Zhong[1] · Xiuli Wang[1] · Jiangping Tu[1]

Received: 17 August 2023 / Revised: 17 January 2024 / Accepted: 22 March 2024

Abstract
All solid-state lithium batteries (ASSLBs) overcome the safety concerns associated with traditional lithium-ion batteries and ensure the safe utilization of high-energy-density electrodes, particularly Li metal anodes with ultrahigh specific capacities. However, the practical implementation of ASSLBs is limited by the instability of the interface between the anode and solid-state electrolyte (SSE). To mitigate this, considerable research has been dedicated to achieving enhanced stability at the anode/SSE interface. Among the current strategies for enhancing interface performance, the concept of Li-alloy materials is extensively used and well functionalized in various scenarios, including Li alloys as anodes, Li-alloy interlayers and Li alloys in the anode. Despite the notable achievements of Li-alloy materials in ASSLBs, the functionality, practicality and working mechanism of Li-alloys have not been fully elucidated. This review commences by providing an exhaustive and in-depth examination of the fundamental kinetics, thermodynamics, and mechanics, highlighting Li-alloy materials. Subsequently, through a systematic interconnection of material properties and their practical applications, we undertake a comprehensive analysis of the operative principles governing Li alloys. This analytical approach allows a thorough evaluation of the viability and utility of Li alloys within the context of ASSLBs. Finally, this review concludes by succinctly summarizing the future prospects and inherent potential of Li-alloy materials for further advancing the field of ASSLBs.

Keywords Li alloys · Anode · All-solid-state lithium batteries · Physicochemical properties · Applications

1 Introduction

Since their commercialization in the 1990s, lithium-ion batteries (LIBs) have revolutionized the use of power sources for electronic devices and vehicles by providing high energy densities and efficient rechargeability [1–3]. However, as the field of energy storage technology advances, the current energy density of LIBs is rapidly approaching its theoretical limit of approximately 300 Wh kg^{-1} [4–7]. This limitation renders LIBs inadequate for meeting the progressively escalating energy storage demands of contemporary society. Furthermore, the utilization of organic electrolytes and membranes in traditional LIBs causes flammability concerns, particularly when high-energy-density anodes (such as Li metal) and cathodes (such as layered oxides) are employed to extend the boundaries of energy density [8–11]. To address these challenges, there has been a significant surge in the development of all-solid-state lithium batteries (ASSLBs). ASSLBs have the potential to overcome the safety concerns associated with traditional LIBs by replacing the flammable components with solid-state electrolytes (SSEs) [12–14]. This fundamental shift from liquid electrolytes to SSEs inherently eliminates the risk of thermal runaway, ensuring the safe utilization of high-energy-density electrodes, particularly Li metal anodes, which have a remarkable theoretical specific capacity of 3 860 mAh g^{-1}. In addition, ASSLBs can be internally connected in series to deliver high energy density from the standpoint of practical production [15–18].

However, the practical implementation of ASSLBs presents a significant challenge with respect to the unstable

Jingru Li and Han Su have contributed equally to this work.

✉ Yu Zhong
yu_zhong@zju.edu.cn

✉ Jiangping Tu
tujp@zju.edu.cn

[1] State Key Laboratory of Silicon and Advanced Semiconductor Materials, Key Laboratory of Advanced Materials and Applications for Batteries of Zhejiang Province, School of Materials Science and Engineering, Zhejiang University, Hangzhou 310027, Zhejiang, China

Published online: 21 May 2024

interface between the anode and SSEs. This interface instability causes three primary concerns. First, notable side reactions ensue due to the substantial disparity in Fermi levels between the anode and SSE materials [19–21]. These reactions adversely affect the efficiency of the anode material, thereby impeding the overall battery performance. Second, the intrusion of Li metal into the electrolyte, caused by mechanical failures of the electrolytes or Li^+ and e^- flows reacting inside the electrolytes, creates a formidable issue [22–25]. This intrusion can result in the degradation of battery performance and, in severe cases, end in battery failure [26, 27]. Third, insufficient contact between the anode and SSEs can generate a large interfacial resistance, magnify the local current density and exacerbate Li metal intrusion [28–31].

To mitigate these concerns, considerable efforts have been dedicated to investigating the anode/SSE interfacial behaviors and to achieving enhanced performance and stability [32–35]. Therefore, a better understanding of the anode/SSE interface has been established in recent years. The thermodynamic and mechanical stability and the Li^+ transport kinetics at the interface are the main factors affecting the Li^+ stripping/plating regulations [36–38]. Among the present strategies for enhancing interface performance, the concept of Li-alloy materials is extensively employed and well functionalized in various scenarios. In summary, there are three major applications of Li-alloy materials in ASSLBs. (1) Li-alloy materials as the anode: by substituting active Li metal with more inert Li alloy materials, the side reactions between the anode and SSEs as well as Li metal intrusions can be theoretically suppressed (Fig. 1a). (2) Li-alloy interlayer: instead of directly serving as the component of the anode, Li-alloy materials are commonly constructed on the anode/electrolyte interface to ensure good contact and lower the interphase overpotential (Fig. 1b). (3) Li-alloy materials in the anode: in this situation, the bulk active material is still metallic Li, while Li-alloy materials in the bulk of the anode with high adsorption of Li atoms and fast Li^+ diffusion kinetics can lower the nucleation potential of crystalline Li, thereby regulating Li^+ plating (Fig. 1c).

Despite the notable achievements of Li-alloy materials in ASSLBs, the functionality, practicality and working mechanism of Li-alloys have not been fully elucidated. In addition, there are few systematic summaries of the physiochemical concepts of Li alloys. Our aim is to fill this gap in the literature and combine the fundamental concepts of Li alloys with their applications to provide useful insights for future studies. In this review, we first present a detailed discussion on the fundamental kinetics, thermodynamics and mechanics of Li-alloy materials. Then, by linking the properties and

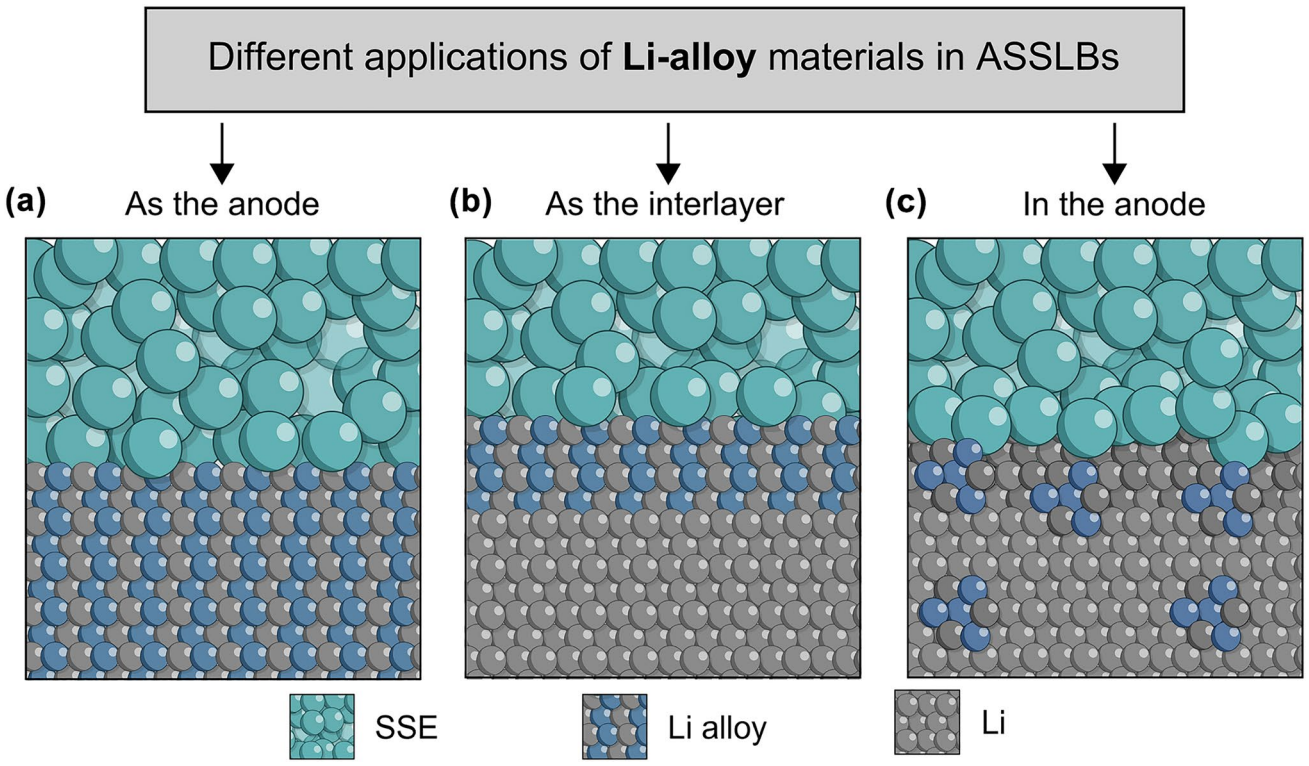

Fig. 1 Different applications of Li-alloy materials in ASSLBs. **a** Li alloy as the anode, **b** Li alloy as the interlayer, **c** Li-alloy materials in the anode

applications, we analyze the working principles and evaluate the applicability of the Li alloys. At the end of the review, the prospects and potentials of Li-alloy materials in ASSLBs are summarized.

2 Physicochemical Concepts of Li-Alloys

Due to its high chemical reactivity, lithium has the remarkable ability to form seamless alloys with a wide range of metals and metalloids, as illustrated in Fig. 2a. In addition, the low melting point of approximately 180 °C exhibited by lithium creates an advantageous environment for the preparation of Li alloy materials [39]. The history of Li alloys can be traced back to their initial application in the aerospace industry, where lithium-aluminum (Li-Al) alloys were employed because of their notable attributes of high mechanical strength and lightweight properties [40]. Subsequently, with the rapid growth of the LIB industry, a multitude of Li alloys have been developed to meet the escalating demand for advanced energy storage solutions [41, 42]. Within this section, a comprehensive discussion of the physicochemical

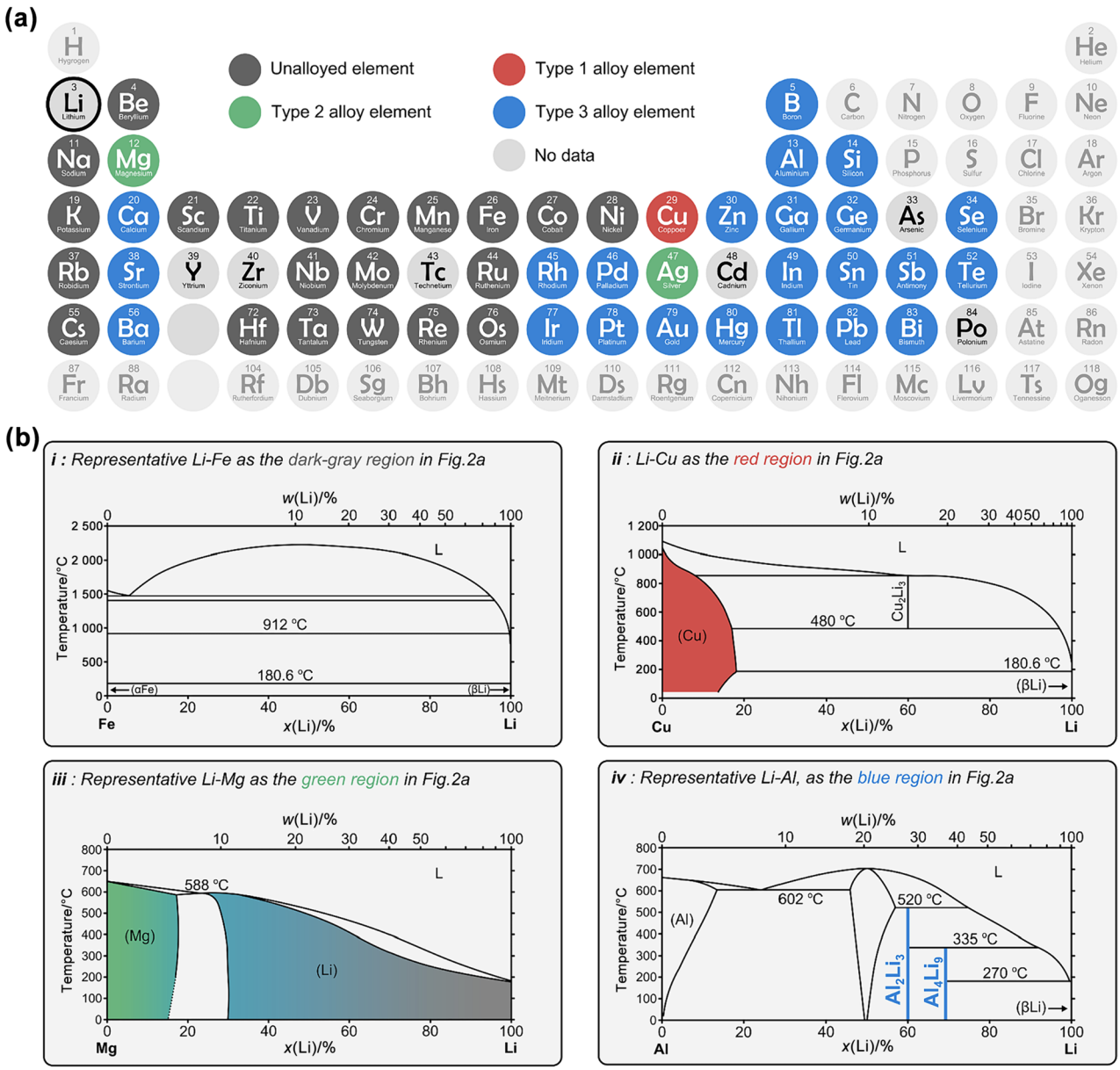

Fig. 2 Phase and phase diagram of Li alloys. **a** Metals/metalloids that can form alloys with Li in the periodic table. **b** (i) Representative phase diagram of the unalloyed Li-Fe system; (ii) phase diagram of the Type 1 Li-Cu system; (iii) representative phase diagram of the Type 2 Li-Mg system; (iv) representative phase diagram of the Type 3 Li-Al system

properties exhibited by Li alloys, with a particular emphasis on those associated with the electrochemical performance of alloys in ASSLBs, is provided.

2.1 Thermodynamics

2.1.1 Phase Diagram of Li Alloys

The alloying process between lithium and metals/metalloids is facilitated by the mutual diffusion of lithium and metal/metalloid atoms across their interface. When this chemical potential-driven diffusion reaches its thermodynamic steady state, the Li-metal/metalloid system will be in a specific alloy state on its corresponding phase diagram. By referring to the phase diagram of Li alloys, it becomes possible to analyze various aspects, including the solubility of metals in lithium or lithium in metals and the occurrence of phase-phase transitions. Figure 2b shows binary phase diagrams of three typical types of Li alloys based on the solubility of Li and alloying metals/metalloids [43–48]. Additionally, a representative phase diagram of the Li-Fe system that cannot form alloys is displayed in Fig. 2b(i).

Type 1: Li atoms exhibit discernible solubility within the metal matrix, while the metal cannot dissolve in the Li matrix.

Type 2: both Li and the metal exhibit mutual solubility, indicating that they can dissolve in each other to a certain degree.

Type 3: Li and metals/metalloids can only produce intermetallic compounds.

Among the reported Li alloys, only the Li-Cu system belongs to Type 1 (the red region in Fig. 2a) [49]. Notably, the dissolution of Li in Cu remains debatable, although the phase diagram predicts a room-temperature lithium solubility of ~ 13% (atomic percentage) [Fig. 2b(ii)]. In fact, Cu is commonly applied as a current collector in LIBs and as a counter electrode to test the Li stripping/plating Coulombic efficiency (CE) due to its inert property against Li metal and high electronic conductivity [50]. However, recent research has illustrated that an electrochemical solid solution of Li can occur when nano-copper is employed as the matrix to overcome unfavorable thermodynamics [51]. In the case of Type 2, both Ag and Mg (blue regions in Fig. 2a) possess mutual solubility toward Li because of their comparable crystalline structure and atomic size [52, 53]. Note that other metals exhibiting extremely low mutual solubility with Li are excluded from this type. As the representative Li-Mg phase diagram indicates [Fig. 2b(iii)], no new phase occurs during lithiation/delithiation in the solid-solution region, indicating that the alloying process does not require extra energy for the phase-phase transition; this facilitates lithiation and delithiation [54]. In addition, the absence of phase boundaries in the solid solution may promote Li diffusion kinetics across the interface. Owing to this, Li-Ag and Li-Mg alloying systems have garnered significant research attention for their potential utilization in ASSLBs [55–57]. Type 3 is the case for most Li alloys (green regions in Fig. 2a). Due to the absence of infinite solid solutions in reported Li alloys, intermetallic compounds, which are routine forms of Li alloys, have noteworthy implications in terms of their thermodynamics, mechanics, and kinetics. The extensive array of intermetallic compounds formed between Li and various metals/metalloids has significant importance in understanding the behavior and performance of these alloys. Exploring these aspects becomes imperative when assessing the potential utilization of these alloys in ASSLBs. In particular, the physiochemical changes that transpire during phase-phase transitions of intermetallic compounds assume a vital role in employing Li alloys as anode materials. An exemplary example is Al [Fig. 2b(iv)], which is renowned as one of the most promising anode materials for ASSLBs [58, 59].

2.1.2 Redox Potential and Specific Capacity of Li Alloys

Lithium metal has the lowest electrochemical potential of − 3.04 V [vs. standard hydrogen electrode (SHE)] due to its low ionization energy and small atomic size. When Li alloys are combined with other metals or metalloids through a conversion reaction, Li atoms infiltrate the host material. This process leads to a change in the redox potential of the resulting Li alloy, which follows a decreasing trend as the depth of Li alloying increases [60, 61]. As the Li alloy approaches its Li-rich state, the conversion reaction is halted. At this point, any further increase in the Li ratio within the system results in a redox potential equal to that of pure lithium. Figure 3a represents the average potential (vs. Li/Li^+) of metals/metalloids, which is a crucial factor when constructing anodes based on the conversion reaction between Li and metals/metalloids. From the perspective of high energy density, a low average potential is desirable. Among typical metals and metalloids, Li-Mg and Li-Ag alloys exhibit relatively low average potentials, indicating their potential application as anode materials [62, 63].

The conversion reaction includes the phase transition of Li alloys with characteristic redox potentials. Therefore, elucidating the changes in potential during the electrochemical process may contribute to a better understanding of Li alloy anodes.

Low-flow Coulometric titration rates are often employed to determine the redox potential of Li alloys to ensure complete phase transition [64]. In addition, from the standpoint of thermodynamics, the steady-state potential of Li alloys can be theoretically predicted. During the lithiation/delithiation process of Li alloys, the following reaction is assumed to describe the transformation from $Li_{x_1}M$ to $Li_{x_1}M$:

(a)

Alloy	Average potential/ (V vs. Li/Li⁺)
Sn	0.504
Si	0.400
Zn	0.310
Ag	0.175
Sb	0.948
In	0.300
Mg	0.032 5
Pb	0.423

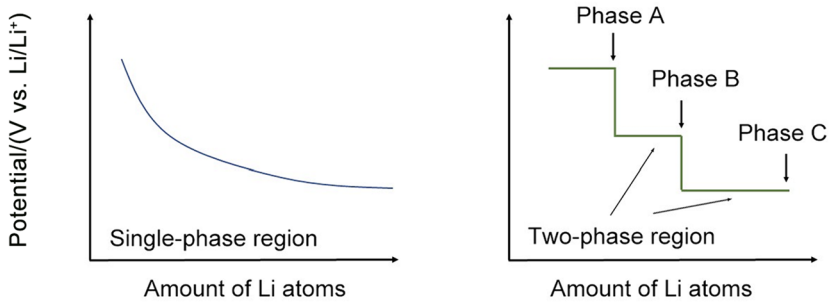

(c)

Alloy	Maximum capacity/ (mAh g⁻¹)
Sn	993
Si	3 579
Zn	410
Ag	670
Sb	660
In	1 012
Mg	2 150
Pb	582

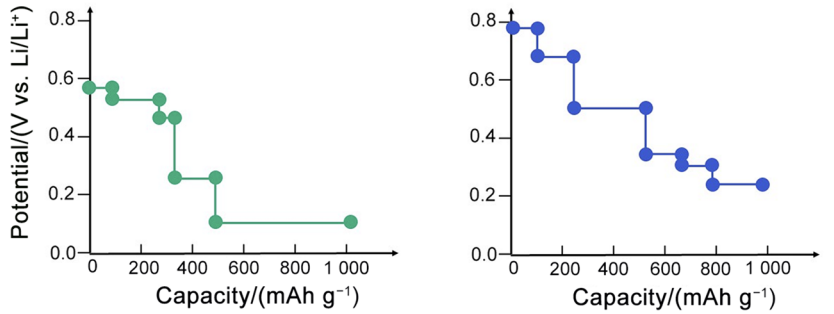

Fig. 3 Potential and capacity of Li alloys. **a** Average potential of typical Li alloys. **b** Schematic diagrams of the single-phase region and two-phase region. **c** Maximum capacity of typical Li alloys. **d** Theoretical potential-capacity diagram of Li-In (green) and Li-Sn (blue) alloys

$$\mathrm{Li}_{x_1}\mathrm{M} + \left(x_2 - x_1\right)\mathrm{Li} \leftrightarrow \mathrm{Li}_{x_2}\mathrm{M}\left(x_2 > x_1\right) \quad (1)$$

where M is the metal or metalloid and x is the number of Li atoms in the alloy.

Based on the phase diagram, two situations need to be considered (Fig. 3b) [62].

(1) Lithiation/delithiation occurs in the one-phase region (including the solid-solution region). The chemical potential of Li (μ_{Li}) changes with the Li activity (α). The relationship between the potentials (V) of $\mathrm{Li}_{x_1}\mathrm{M}$ and $\mathrm{Li}_{x_2}\mathrm{M}$ can be calculated from the difference in μ_{Li} between A and B.

$$V_{\mathrm{Li}_{x_2}\mathrm{M}} - V_{\mathrm{Li}_{x_1}\mathrm{M}} = -\frac{\Delta\mu_{\mathrm{Li}}}{\left(x_2 - x_1\right)F} = -\frac{RT\left(\ln\alpha_{\mathrm{Li}_{x_2}\mathrm{M}} - \ln\alpha_{\mathrm{Li}_{x_2}\mathrm{M}}\right)}{F\left(x_2 - x_1\right)} \quad (2)$$

where R, T, and F are the gas constant, thermodynamic temperature, and Faraday constant, respectively.

(2) Lithiation/delithiation occurs in the two-phase region. Due to the phase equilibrium condition, μ_{Li} is constant for any phase composition within this region. Hence, a constant potential is observed in this region. The potential (V) corresponding to the two-phase region has the following relationship with the reaction Gibbs free energy (G).

$$V_{\mathrm{Li}_{x_2}\mathrm{M}-\mathrm{Li}_{x_1}\mathrm{M}} = -\frac{\Delta G}{F\left(x_2 - x_1\right)} = \frac{G_{\mathrm{Li}_{x_2}\mathrm{M}} - G_{\mathrm{Li}_{x_1}\mathrm{M}}}{F\left(x_2 - x_1\right)} + \frac{G_{\mathrm{Li}}}{F} \quad (3)$$

First-principles studies have been commonly employed to determine the theoretical redox potential of Li alloys by considering the stable structure presented in calculated or reported phase diagrams [65]. Due to the negligible contributions of pV (where p and V stand for the pressure and volume, respectively) and thermal energy during the equilibrium phase transitions of Li alloys, the Gibbs free energy is typically approximated by the internal energy in most investigations. Consequently, the potential in two-phase regions can be straightforwardly obtained by calculating the internal energy values of $\mathrm{Li}_{x_1}\mathrm{M}$, $\mathrm{Li}_{x_2}\mathrm{M}$, and Li and substituting them into Eq. 3. Importantly, most theoretical studies focus solely on the potential of two-phase regions in Li alloys and disregard the potential changes in the one-phase region. This methodology is generally reasonable and aligns well with the actual scenario since the phase diagram of most Li alloys is dominated by two-phase regions. However, caution needs to be exercised when dealing with Li alloys that exhibit a wide range of one-phase regions, particularly Li-Ag and Li-Mg alloys capable of forming solid solutions. Neglecting the one-phase regions may result in significant deviations between the predicted and realistic potentials for Li alloys with specific compositions. A feasible strategy to determine the potential diagram for those kinds of alloys is to apply the Li concentration to simulate the Li activity, which is rather difficult to measure. In addition, for a more precise prediction of an Li alloy potential, the evolution of the phase structures during the electrochemical

process should be effectively characterized to provide solid inputs. For instance, the phase structure of the Li-rich alloys ($Li_{17}Sn_4$ and $Li_{22}Sn_5$) in the Li-Sn system has been a debatable subject, and this ambiguity can lead to misleading results in potential calculations [66].

Owing to the reversible conversion reaction between Li and metals/metalloids, the specific capacity (C) of Li alloy materials during the transformation from $Li_{x_1}M$ to $Li_{x_2}M$ can be calculated via the following equation:

$$C = \frac{F\left(x_2 - x_1\right)}{M_{\mathrm{w}}\left(\mathrm{Li}_{x_1}\mathrm{M}\right)} \tag{4}$$

where M_w represents the molecular weight.

Based on this, the maximum specific capacity of each metal and metalloid is summarized in Fig. 3c; this capacity corresponds to the transition from the metal to its Li-richest alloy state. Li-Si alloys possess the highest specific capacity compared with that of their counterparts, indicating the promising potential of using Li-Si alloys as anode materials [67]. Additionally, since the potential and specific capacity of Li-alloy materials can both be derived when assuming an $Li_{x_1}M$ and $Li_{x_2}M$ transition, the potential-capacity diagram during the lithiation/delithiation process can be created. Figure 3d shows the correlation between the potential and the specific capacity of the Li-In and Li-Sn alloy systems according to theoretical calculations [65]. By comparing the theoretical potential-capacity diagram with the practical potential-capacity diagram of different alloy systems, information on the phase transition and reaction polarization during the electrochemical alloying/dealloying process can be obtained. The construction of a theoretical potential-capacity diagram can aid in the identification of promising alloy-based anode materials with high energy density.

2.1.3 Crystal Structure of Li Alloys

During the lithiation or delithiation process of the metal parent phase, new Li alloy phases gradually form at the interface of the parent phase, leading to the creation of a distinct metal/alloy interface. The newly formed Li alloy phase often has a dissimilar lattice volume and crystalline type compared to that of the parent phase, resulting in significant interfacial effects. The lattice mismatch between the newly generated subphase and the parent phase categorizes the phase boundaries into three types: coherent phase boundaries, semicoherent phase boundaries, and incoherent phase boundaries. When the lattice mismatch is minimal, coherent phase boundaries tend to form; this refers to atoms at the interface being simultaneously located at the junction of the two-phase lattice. The atoms on the coherent phase boundary cooperate seamlessly, causing minimal distortion and leading to the lowest energy state for this phase boundary. However, if the interplanar spacing of two adjacent crystals at the phase interface differs greatly, achieving complete correspondence becomes impossible. As a result, dislocations occur at the interface to reduce the elastic strain energy. If the atomic arrangement of the two phases at the interface remains partially matched, these interfaces are referred to as semicoherent phase boundaries. Furthermore, when the atomic arrangement of the two phases at the phase interface is highly dissimilar, only an incoherent phase boundary can be formed [68] (Fig. 4a).

Due to the varying phase interface energy associated with different phase interfaces, these disparities can significantly influence the mass transfer and mechanical characteristics of the interfaces. Concurrently, distinct types of phase interfaces may manifest distinctive interface behaviors arising from their inherent interface properties. Consequently, in this review, we advocate that the crystal structure of alloy phases and their consequential structural changes during alloying needs to be more thoroughly researched because this is a pivotal aspect frequently disregarded in Li alloy applications.

An examination of the crystal structures of representative Li-Sn alloys with different lithium contents, as shown in Fig. 4b, reveals that phase transitions in Li alloys within the two-phase region are frequently accompanied by the emergence of new phases exhibiting markedly different crystal structures [66]. Consequently, alloys undergoing these phase transformations commonly exhibit semicoherent and incoherent phase boundaries. Remarkably, the majority of the binary Li alloy systems feature an Li-richest phase that has a face-centered cubic structure similar to metallic Li (Fig. 4c). However, exceptions do exist, such as Li_9Al_4, which possesses a monoclinic crystal structure deviating from the typical face-centered cubic arrangement observed in other Li-richest phases (Fig. 4d) [69]. This highly asymmetric crystal structure can produce substantial phase boundary energy. Therefore, understanding and addressing the implications of these crystallographic disparities in Li alloy systems warrant close examination in the pursuit of comprehensive material design and development.

2.2 Kinetics

Li-ion diffusion within alloys assumes a paramount role in delineating the electrochemical performance. As illustrated in Fig. 5a, the alloys exhibit two discernible modes of lithium diffusion: interstitial and vacancy diffusion. These modes are further elucidated by two underlying mechanisms: direct hopping and coordination. Computational investigations rooted in first-principles simulations have enabled the quantification of lithium migration barriers within conventional Li-In and Li-Sn alloy systems [70]. The outcomes reveal a discernible shift in the prevailing diffusion

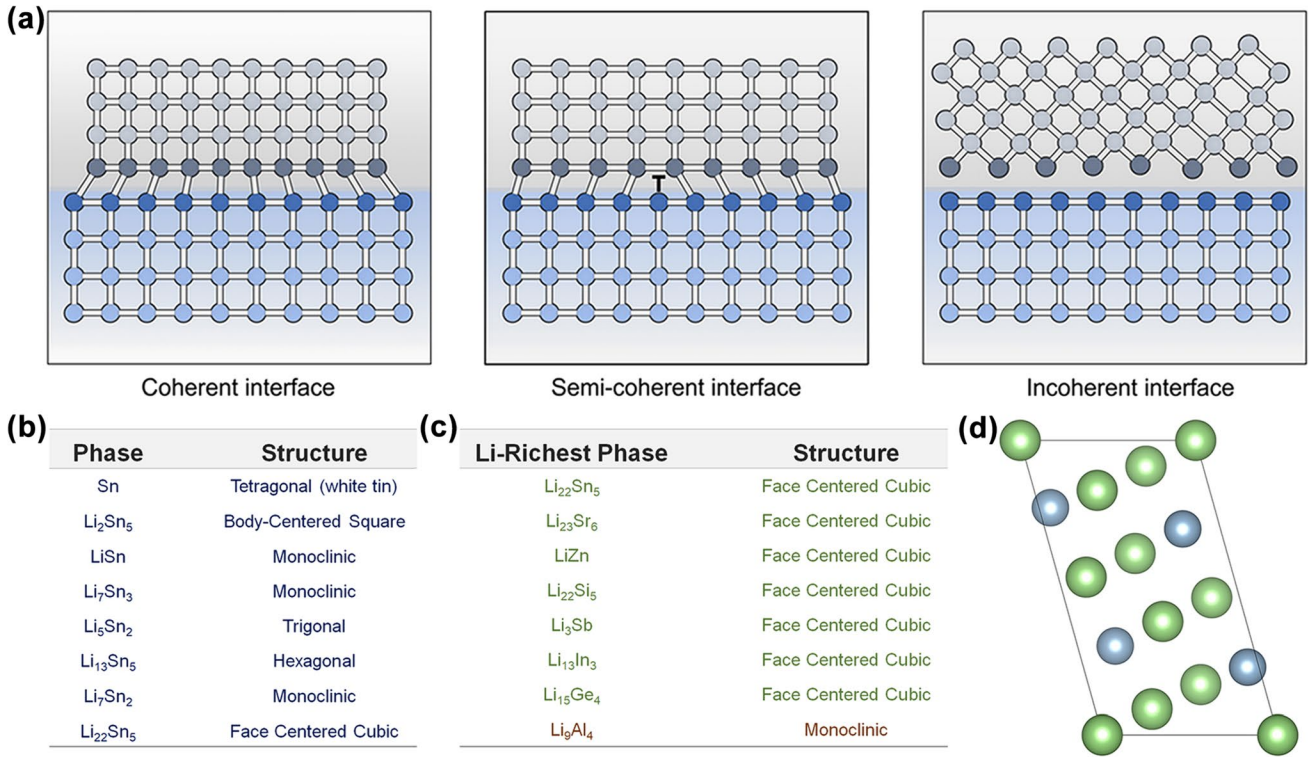

Phase	Structure
Sn	Tetragonal (white tin)
Li_2Sn_5	Body-Centered Square
LiSn	Monoclinic
Li_7Sn_3	Monoclinic
Li_5Sn_2	Trigonal
$Li_{13}Sn_5$	Hexagonal
Li_7Sn_2	Monoclinic
$Li_{22}Sn_5$	Face Centered Cubic

Li-Richest Phase	Structure
$Li_{22}Sn_5$	Face Centered Cubic
$Li_{23}Sr_6$	Face Centered Cubic
LiZn	Face Centered Cubic
$Li_{22}Si_5$	Face Centered Cubic
Li_3Sb	Face Centered Cubic
$Li_{13}In_3$	Face Centered Cubic
$Li_{15}Ge_4$	Face Centered Cubic
Li_9Al_4	Monoclinic

Fig. 4 Phase boundary structure and crystal structure of Li-alloys. **a** Schematic illustration of coherent, semicoherent and incoherent phase interfaces. **b** Crystal structure of Li-Sn alloys with different ratios of Li atoms. **c** Crystal structure of the Li-rich phase in typical Li alloys. **d** Monoclinic structure of Li_9Al_4

mechanism, transitioning from interstitial direct hopping to vacancy diffusion, coupled with interstitial coordination, as the lithium content increases in both Li-Sn and Li-In alloys. Notably, the diffusion barriers observed in Li-In alloys generally exhibit a lower magnitude than their Li-Sn counterparts (Fig. 5b, c), as corroborated by an independent study [65]. Moreover, the electrochemical performance of Li-alloy anode-based cells, specifically those with the Li-In configuration, consistently surpasses that of their Li-Sn anode-based counterparts. This difference in performance can be attributed to the greater binding strength inherent in the Li–Sn bond than in the Li–In bond. However, these discussions are confined to the intrinsic diffusion behavior transpiring within the bulk alloy matrix in the absence of external driving forces such as chemical potential gradients.

A critical metric for evaluating lithium-ion diffusion behavior is the diffusion coefficient, which can be ascertained through various experimental methodologies. During the course of electrochemical cycling, alloy anodes typically undergo multiple phase transitions in conjunction with alterations in the lithium transport kinetics and the morphological configuration of the alloy. A recent report extensively probed the alloying dynamics of Li-In alloys through a series of electrochemical tests, as depicted in Fig. 5d [71]. As shown in Fig. 5e, the diffusion coefficient, obtained from galvanostatic intermittent titration technique (GITT) profiles, exhibits an initial stable value exceeding 10^{-10} cm^2 s^{-1} ($0 < x < 1$ in Li_xIn), signifying a steady alloying process predominantly impelled by chemical potential gradients. With the progression of lithiation, chemical diffusion assumes a subordinate role, with the rate-limiting step transitioning to charge transfer at the electrode-electrolyte interface. Upon attaining the critical lithium content ($x > 1.25$ in Li_xIn), the diffusion coefficient inferred from GITT profiles decreases to less than 10^{-12} cm^2 s^{-1}, even lower than the diffusion coefficient of elemental lithium (10^{-11} cm^2 s^{-1}). This decrease signifies a transformation in kinetics from an alloying-centered process to one predominantly involving lithium deposition. A similar evolutionary pattern in the diffusion coefficient has been documented in the context of the Li-Al alloy system [72, 73]. However, the specific value of the diffusion coefficient is substantially influenced by the morphological attributes of the samples. In the case of Li-Mg alloys prepared utilizing the kinetically controlled vapor formation and deposition (KCVD) technique, the resultant porous structures with columnar pores effectively provide enhanced electrolyte infiltration [42]. Consequently, the diffusion coefficients associated with KCVD-produced Li-Mg alloys exhibit a magnitude range spanning from

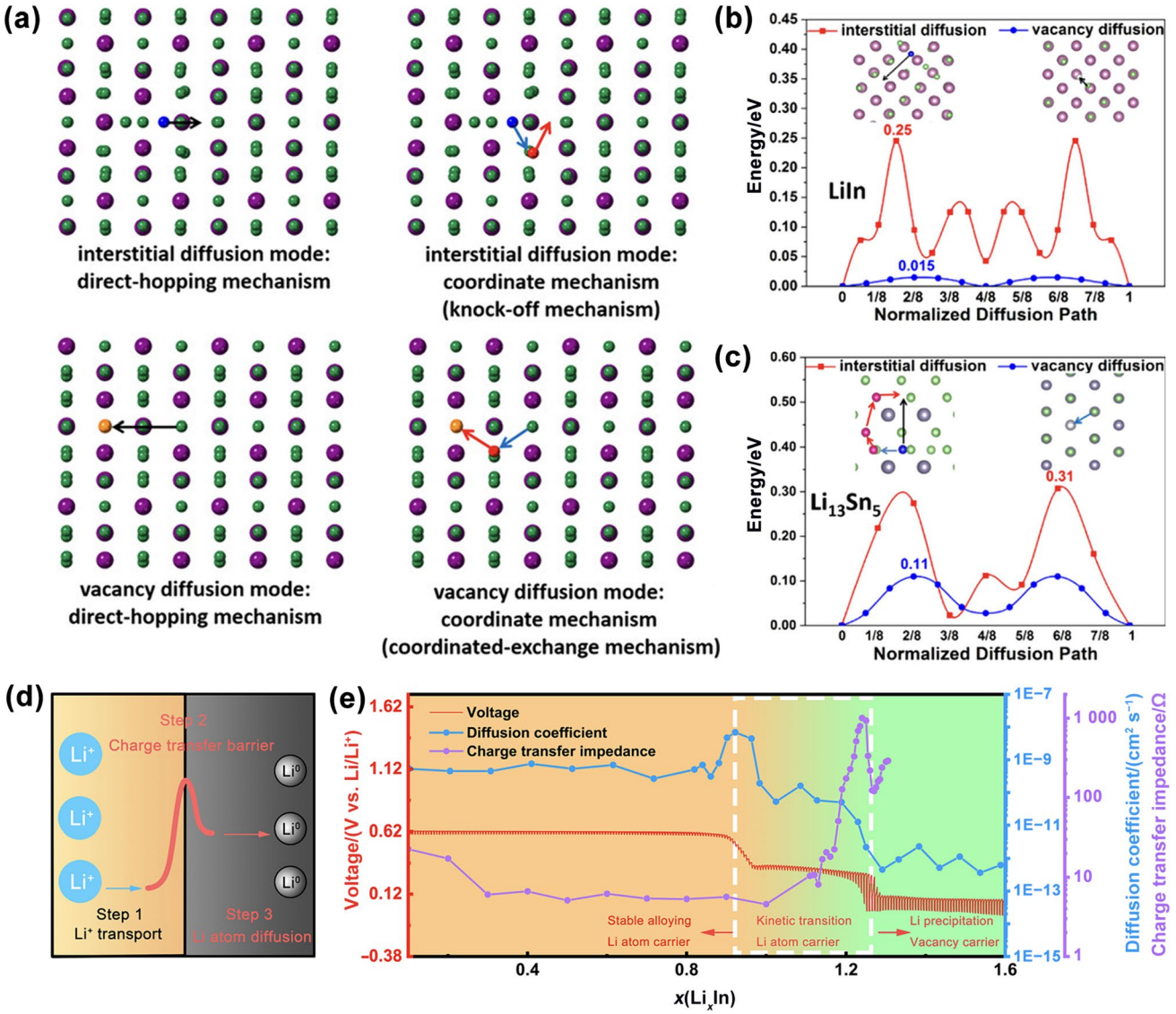

Fig. 5 Diffusion kinetics in Li alloys. **a** Schematic illustration of the diffusion modes and the two mechanisms in each mode. The lowest energy barriers of the Li transport in **b** Li-In alloy and **c** Li-Sn alloy. Reprinted with permission from Ref. [70]. Copyright © 2022, American Chemical Society. **d** Schematic illustration of the interfacial Li transport process. **e** Evolutions of the diffusion coefficient and charge transfer impedance as a function of the Li content in Li_xIn and the GITT profile. Reprinted with permission from Ref. [71]. Copyright © 2021, AAAS

1.2×10^{-7} to 5.2×10^{-7} cm^2 s^{-1}, representing an order of magnitude disparity when compared with values reported in the extant literature [74, 75].

Based on the discussion above, lithium dendrites also exist in alloy anodes when the rate of Li deposition exceeds its diffusion into the alloys. Evident Li accumulation at the anode/electrolyte interface occurs if the critical Li content is reached during lithiation because alloys with high Li content always exhibit an extremely low Li diffusion coefficient, as shown in Fig. 6a, b [71]. Another scenario leading to Li dendrite formation is cycling at high rates, where Li ions fail to diffuse into the alloy in time to support the subsequent alloying process at high current densities. Instead, these ions combine with incoming electrons, leading to the deposition of metallic Li at the interface [76]. This phenomenon was verified by a recent investigation on the critical current density (CCD) of several alloy anodes in Li_6PS_5Cl-based symmetric cells [41]. Based on the fluctuating voltage profiles of the $LiZn_2$ symmetric cell in Fig. 6c, the Li-Zn alloy ($LiZn_2$) anode suffers from a short circuit at a current density of 2 mA cm^{-2}. Soft short circuits also occur at current densities of 10 and 12 mA cm^{-2} for symmetric cells with Li_2Si and Li_7Sn_3 electrodes, respectively. For the Li-Zn|LPSCl|Li-Zn cell displayed in Fig. 6c, direct Li deposition at the

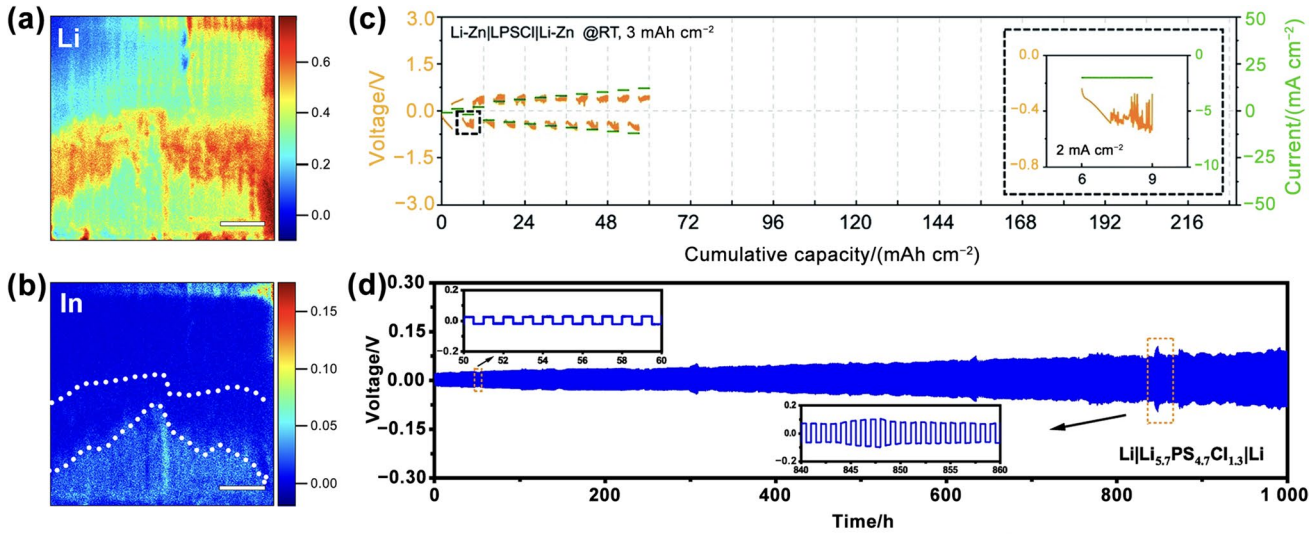

Fig. 6 Li accumulation at the interface and the voltage profiles of different anodes. Cross-sectional elemental mapping images of **a** Li and **b** In at the failure stage ($x = 1.5$ in Li_xIn) characterized by time-of-flight secondary ion mass spectroscopy (ToF-SIMS). Scale bar: 10 μm. Reprinted with permission from Ref. [71]. Copyright © 2021, AAAS. **c** Voltage and current profiles of the Li-Zn|LPSCl|Li-Zn cell at step-increased current densities. Reprinted with permission from Ref. [41]. Copyright © 2022, The Royal Society of Chemistry. **d** Typical voltage profile of a symmetric Li|LPSCl|Li cell. Reprinted with permission from Ref. [79]. Copyright © 2022, Nature Publishing Group

anode/electrolyte interface is likely the specific cause of the short circuit at a high current density. A recent report indicated that the change in crystal structure during lithiation of Li-Zn alloys was accompanied by a significant energy barrier for further alloying [77]. Additionally, the Li diffusion kinetics within the Li-Zn alloy are limited, which impedes the timely transport of Li from the surface to the bulk, particularly under high current density conditions. Considering these factors, direct Li deposition rather than Li alloying is kinetically favored, thereby leading to localized Li accumulation at the electrode/solid electrolyte interface. Driven by an electric field, these Li deposits tend to propagate into SSEs along the grain boundaries, pores and other defects, causing short circuits in the cell. The growth of alloy dendrites can also be activated when the cell is subjected to a high current density and high cycling capacity, as discussed in Sect. 3.1.1.2. Symmetric cells fail due to dendrite formation; moreover, full cells may also encounter short circuits induced by dendrites. These instances can be recognized by a lower rate of voltage increase or voltage fluctuation while charging the cell [78].

In addition, symmetric cells with alloy anodes typically exhibit zigzag voltage profiles during each plating/stripping process, in contrast to the flat voltage profile of a square wave observed with bare Li, as shown in Fig. 6d. These changes are closely related to the Li transport kinetics in the electrode. Additionally, the phase transitions accompanied by changes in the electrode potential can also account for the sloped voltage profile of alloy anodes [65, 80–82].

2.3 Mechanics

The mechanical aspects, encompassing the mechanical properties of SSEs, SSE/electrode interfaces, and electrodes, have recently received considerable attention due to their great influence on the performance of energy storage cells [81, 83–85]. However, despite their crucial significance, the understanding of the mechanical issues associated with ASSLBs is insufficient, primarily due to the lack of advanced characterization techniques and well-defined theoretical models in this domain. Specifically, investigations pertaining to the mechanical behavior of Li alloy materials within ASSLBs are notably scarce. To address this gap, the objective of this section is to elucidate the inherent mechanical properties of Li alloy materials based on existing literature. Additionally, a comprehensive analysis of the mechanical aspects concerning the application of alloy materials in ASSLBs is presented.

The insertion and extraction of lithium atoms in Li alloys induce significant changes in their molar volume. Prior research on LIBs shows that these volumetric variations can lead to electrode cracking, delamination, and pulverization, resulting in compromised structural integrity [86–90]. Currently, the prevailing theory supports the notion that the stress change inside alloy materials is the primary cause of their mechanical degradation. Here, we use the lithiation process of silicon (Si) particles as an illustrative example. Upon lithiation, Si particles exhibit a typical core-shell structure, wherein the outer shell transforms into amorphous

Li_xSi (with x approximately equal to 3.75), while the core layer remains as an unlithiated Si crystal. At the interface between the lithiated shell and the unlithiated core, the lithium concentration undergoes an abrupt change from 0 to nearly 3.75. Due to the lack of a transitional region for gradual volume alteration, volume expansion primarily occurs at this interface. In the initial lithiation stage, the hoop stress at the interface is mainly compressive, and no cracks appear at this point. However, as lithiation progresses, the initially lithiated outer layer is pushed outward due to the subsequent lithiation of the underlying material. This phenomenon converts the compressive stress in the original outer layer into tensile stress, which acts as the driving force for the formation of surface cracks [86, 91, 92]. During the subsequent delithiation process, the stress accumulated during the previous lithiation process can be released to a certain extent through the volume shrinkage of the alloy materials. However, this process often introduces new tensile stresses that exacerbate crack propagation. Over time, pulverization of the alloy materials can occur [85, 93]. Additionally, the volume shrinkage of alloy materials during delithiation can result in delamination at the interface, representing another form of mechanical failure in alloy anodes.

The violent volume change also facilitates additional side reactions between the electrode and the electrolyte, leading to a reduced CE and electrode utilization within the battery. In the LIBs using liquid electrolytes, during lithiation, the Li alloy structures expand toward the electrolyte, followed by contraction during delithiation. This cyclic process causes the solid-electrolyte interphase (SEI) formed during lithiation to fracture as the nanostructure shrinks during delithiation, which exposes fresh silicon surfaces to the electrolyte. Subsequently, a new SEI forms, leading to its gradual thickening with each charge/discharge cycle (Fig. 7a) [94]. This situation can also occur at the electrolyte/electrode interface in the ASSLBs. The SEI generated by the reaction of the lithiated alloy and the SSE breaks during the lithiation process of the alloy such that the active ingredients in the alloy anode are continuously consumed during the cycle. In addition, the anisotropy of alloy expansion also leads to uneven stress inside the alloy particles, resulting in internal cracking. An instructive example is Si, which undergoes a pronounced anisotropic expansion of approximately 280% during the lithium intercalation process. This volumetric expansion induces numerous internal fractures, significantly diminishing the CE of the battery. Intriguingly, germanium (Ge), which belongs to the same main group as

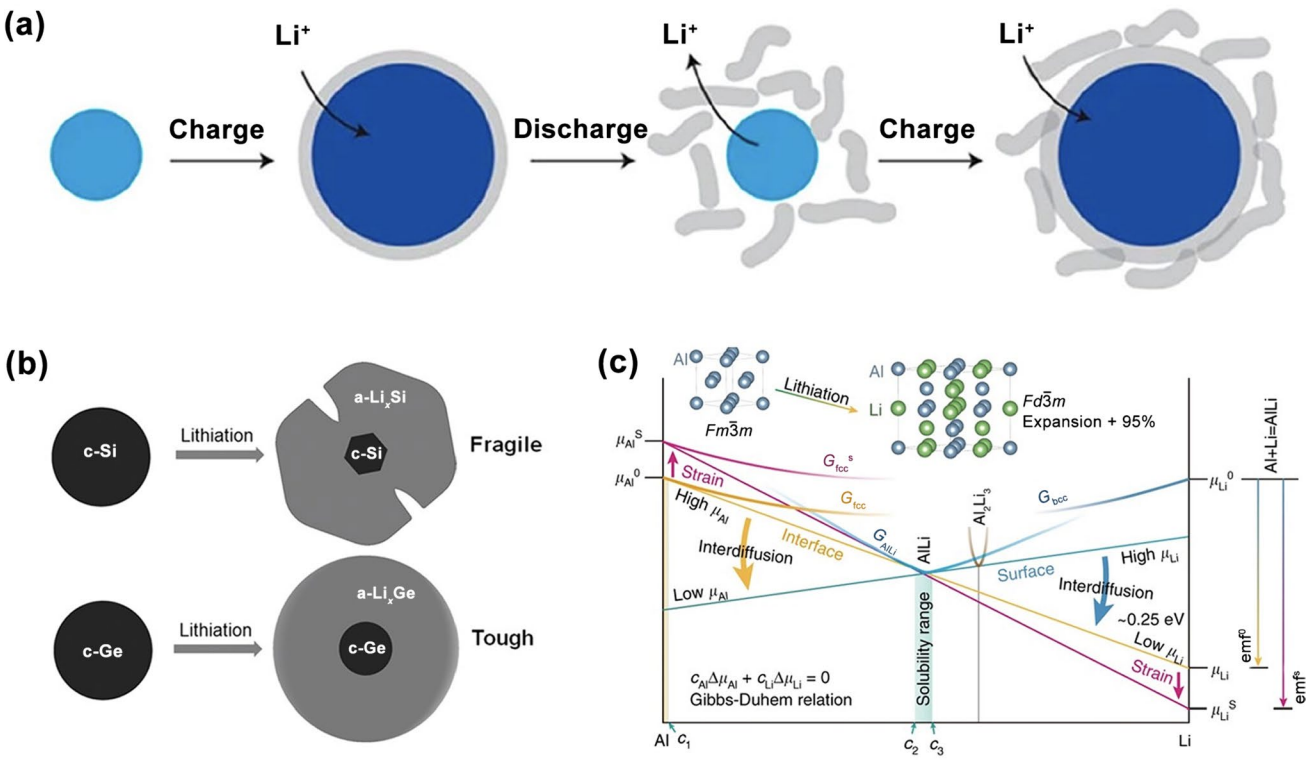

Fig. 7 Mechanical degradation of Li alloys. **a** Schematic illustration of the degradation mechanism of Li alloys in typical LIBs. Reprinted with permission from Ref. [94]. Copyright © 2012, Nature Publishing Group. **b** Comparison of Si and Ge during lithiation. Reprinted with permission from Ref. [95]. Copyright © 2013, American Chemical Society. **c** Gibbs free energy diagram of Li-Al alloys. Reprinted with permission from Ref. [89]. Copyright © 2020, Nature Publishing Group

Si, exhibits remarkable robustness against volume expansion (Fig. 7b) [95]. This resilience can be attributed to the absence of anisotropic lithiation, which effectively mitigates the occurrence of excessive local stress within the material. Moreover, recent research has indicated that the hardness of a metal matrix can induce varying strain effects during Li compound formation [89]. When plastic deformation occurs in the Al matrix, a significant number of dislocations are introduced, leading to an increase in the Gibbs free energy of the deformed Al matrix. This alters the two-phase equilibrium state, causing a shift in μ_{Li} (Fig. 7c). This phenomenon appears to be a primary factor contributing to the inhomogeneous lithiation observed in the softer Al electrode. The soft Al matrix cannot withstand the internal stress generated by the electrochemically growing AlLi phase, leading to volume expansion and plastic deformation of the matrix. As a result, Li tends to preferentially insert into these unstable regions to gain a chemical potential advantage. Conversely, an appropriately hard matrix can prevent plastic deformation, impeding the growth of AlLi due to the elastic stress in the Al matrix. In these cases, no preferential region for Li insertion exists within the appropriately hard matrix, promoting homogeneous lithiation throughout the remaining Al matrix on the surface and resulting in a uniform in-plane reaction.

Specifically, in the context of ASSLBs, wherein conduction heavily depends on rigid solid-solid contacts, the fracture and pulverization of intact alloy particles during cycling, coupled with the formation of voids owing to the shrinkage of delithiated alloys, will drastically increase the tortuosity of the charge carrier transport pathways, thereby increasing the overall battery resistance. In addition, due to their specific pressure conditions during operation, ASSLBs are significantly influenced by volume variations, which directly impact the pressure within the battery system and subsequently affect its electrochemical performance [96–99]. In the case of an ASSLB constrained by a constant volume, the total volumetric strain of the active materials in both electrodes during lithium insertion and extraction leads to pressure changes within the cell. The resulting stress from the net volumetric strain is determined by the elastic and plastic deformation of various materials within the cell. Han et al. [100] summarized this relationship in Eq. 5, where Δp represents the pressure change within the elastic limit, ε_{vol} denotes the volumetric strain, and K signifies the bulk modulus of the cell composite.

$$\Delta p = \varepsilon_{vol} K \tag{5}$$

In their later investigation, the pressure dynamics of ASSLBs were studied by using Si, Ge, and Sn as active materials for the composite anode, NCM111 for the composite cathode, and argyrodite as the ion transport medium during operation (Fig. 8a). The research findings identified the considerable volume fluctuations in the Li alloy electrode as the primary source of pressure variation within the battery; these fluctuations were attributed to the larger partial molar volume of Li (~9 cm^3 mol^{-1}) than that of NCM111 (~ 1–2 cm^3 mol^{-1}) (Fig. 8b). Additionally, the study emphasized the pivotal role of the particle size in determining the extent of pressure evolution. Notably, when employing alloy materials with smaller particles, the pressure variation during battery cycling was comparatively mitigated.

Moreover, in addition to its impact on carrier transport between the alloy and the SSE, as well as changes in the internal pressure of ASSLBs, the mechanical properties of the alloy play a significant role in the failure mechanism of the battery. The difference in ductility between alloys and lithium necessitates an exploration of the pressure required to maintain close contact between the alloy and electrolyte interface [101]. Furthermore, similar to the issue of contact loss observed with the use of lithium metal, contact loss can potentially occur at the interface between Li alloys and SSEs. This loss can lead to an excessive local current density during subsequent deposition, resulting in uneven lithium growth. Therefore, the deformation rate of various Li alloys during cycling needs to be investigated [39]. Additionally, based on the prevailing fracture mechanism, different hardness levels of alloy materials should theoretically cause varying degrees of electrolyte fracture when they interact with defects on the electrolyte surface [23]. However, comprehensive failure mechanisms for ASSLBs incorporating Li alloys are currently lacking. For that reason, the connection between the mechanical properties of the alloy and the failure mechanism of the ASSLB needs to be established through a combination of advanced characterization techniques and theoretical analysis.

3 Application of Li-Alloys in ASSLBs

As an example of prospective electrode materials for ASSLBs, Li-metal anodes have attracted significant amounts of attention in research and development. Although notable progress has been achieved in their advancement, the effective control of the lithium plating and stripping processes has proven considerably more challenging than initially envisioned [102–104]. Notably, issues such as side reactions between lithium and most SSEs, the growth of lithium filaments leading to short circuits, and the loss of interfacial contact present formidable obstacles to overcome [105–107]. In this context, Li alloys provide an enticing alternative approach to establishing a stable electrolyte-electrode interface, facilitating extended cycling capabilities in ASSLBs.

Research on Li alloys in ASSLBs dates back to the 1980s. As shown in Fig. 9, recent years have witnessed a growing

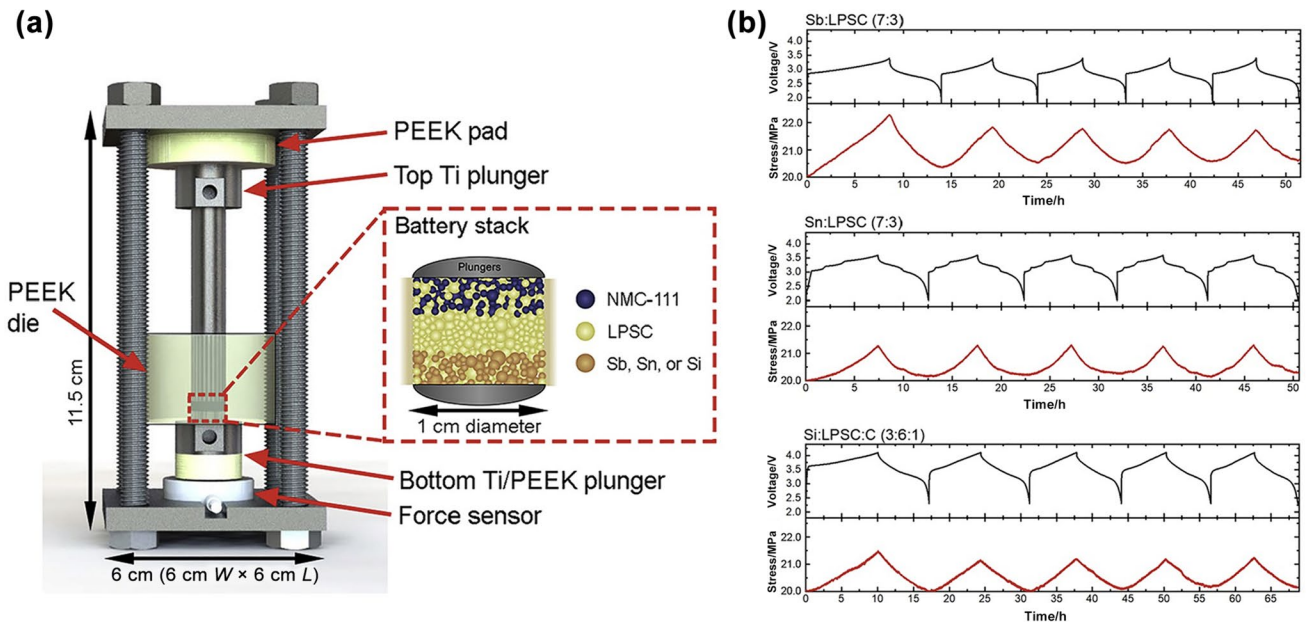

Fig. 8 Stress-volume evolution of ASSLBs using Li alloys as the anode. **a** Schematic illustration of the testing cell. **b** Evolution of the cell voltage and stress during the discharging/charging tests. Reprinted with permission from Ref. [100]. Copyright © 2021, Elsevier

number of breakthroughs in this field. Broadly, the applications of Li alloys in ASSLBs can be categorized into three groups: (1) serving as the anode, (2) functioning as the interlayer, and (3) serving as functional components within the anode. Typically, an alloy layer or bulk material demonstrates a higher lithium diffusivity than pure metallic Li, favoring efficient lithium transport toward the interface and enabling uniform lithium plating. Furthermore, the incorporation of lithium into other metals can effectively reduce the lithium chemical potential, thus suppressing the electrochemical decomposition of SSEs. Additionally, the alloy host provides stable sites for lithium insertion/removal while maintaining physical/electrical contact. Moreover, since lithium atoms within the matrix are not directly deposited onto the substrate, the issue of lithium dendrite formation can theoretically be circumvented [41, 117–119]. Subsequently, we will conduct a comprehensive review of the research results based on this classification. The reports mentioned in Fig. 9 are also discussed in detail in the subsequent sections.

3.1 Li Alloy Anodes

In this section, we explore the comprehensive elucidation of the mechanisms underlying the enhanced performance of Li alloy anodes. Furthermore, we discuss pertinent issues related to Li-metal alloy anodes. Finally, a dialectical perspective on Li-metal alloy anodes is provided, with a balanced assessment of their potential and limitations in the context of solid-state battery technology.

3.1.1 Benefits of Li Alloy Anodes

3.1.1.1 Enhanced Interfacial Stability The majority of SSEs exhibit instability as they come in direct contact with metallic lithium. The first-principles calculation results of the reduction potential of SSEs to metal lithium indicate that despite achieving ionic conductivity levels that approach or even surpass those of liquid electrolytes [e.g., $Li_{10}GeP_2S_{12}$ (LGPS)] [120–122], severe side reactions still occur between the SSE and metallic Li [123–125]. These side reactions cause the formation of a mixed conductor interface (MCI) or SEI [126–129], wherein the MCI, characterized by both electronic and ionic conductivity, triggers further side reactions, ultimately leading to battery failure.

In addressing this challenge, the utilization of alloy-based anodes provides a potential solution. Specifically, employing an alloy anode effectively lowers the chemical potential of lithium in the anode while elevating the electrode's potential versus lithium. As a thermodynamic consequence, this approach reduces the occurrence of the side reactions between the anode and the SSE (Fig. 10a). By modulating the electrode potential of the anode through alloying, the likelihood of detrimental side reactions at the interface between the anode and SSE can be minimized, thus enhancing the stability and longevity of the battery system. For instance, Li-In alloy anodes have been successfully applied in ASSLBs. Within the two-phase region of In and Li-In, the Li-In anode exhibits a potential of ~ 0.62 V versus Li/Li^+ [109, 130, 131]. Due to its relatively high potential, this anode material is conducive to pairing with halides or LGPS

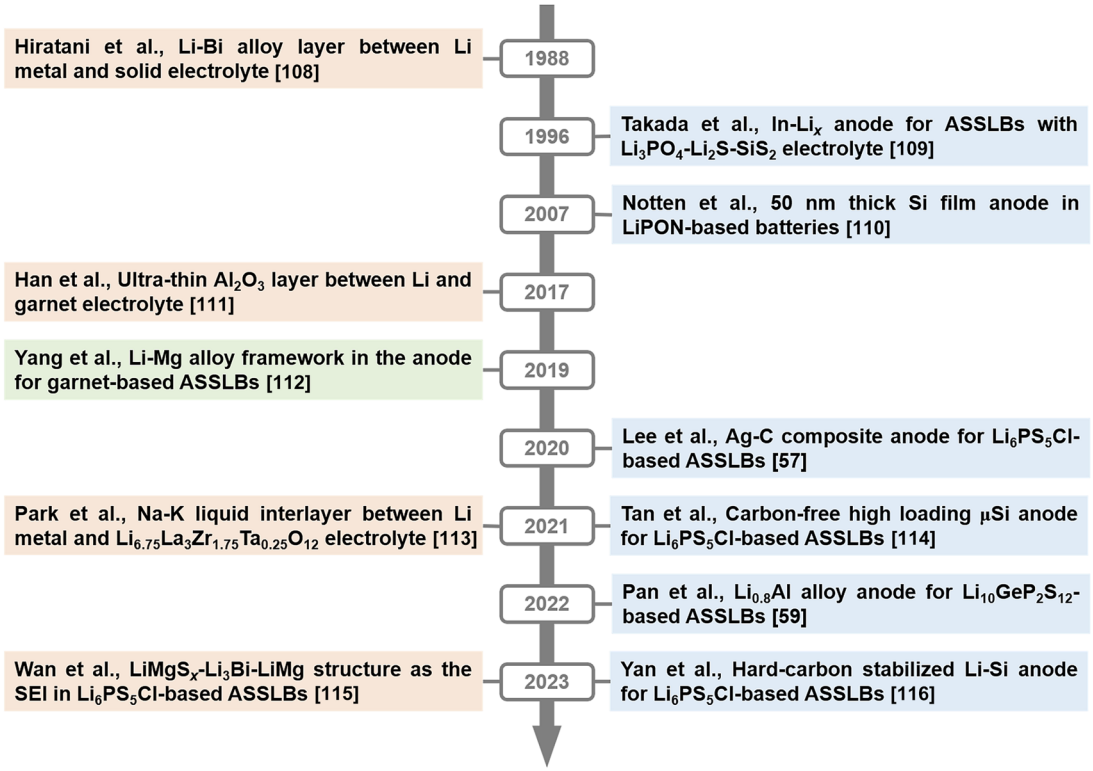

Fig. 9 Timeline diagram illustrating the representative works in the field of Li alloys in ASSLBs [57, 59, 108–116]

electrolytes, wherein their compatibility can lead to the formation of continuous MCI upon interaction with metallic lithium [120, 121, 132–134]. However, prudent consideration is necessary when examining the side reactions occurring between the Li-In anode and the SSE. Contrary to the assumption of an absence of side reactions between Li-In alloys and SSEs, thermodynamically, the electrode potential of Li-In alloy anodes remains lower than the reduction

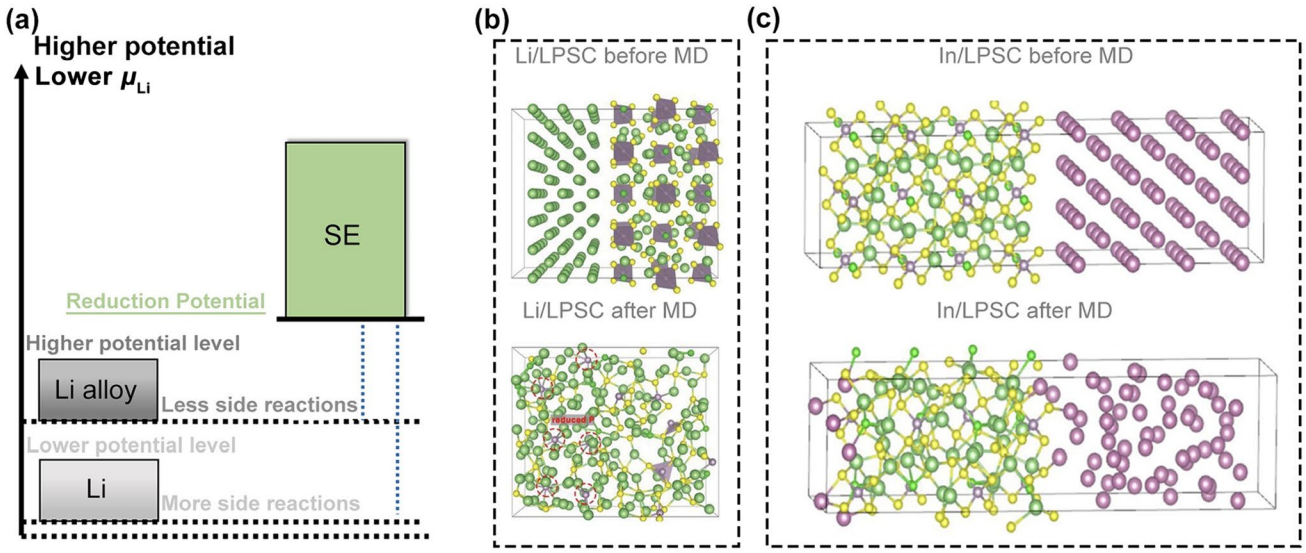

Fig. 10 Enhanced interfacial stability of Li alloys. **a** Thermodynamic explanation of the enhanced interfacial stability. **b** AIMD simulation of the Li/Li$_6$PS$_5$Cl interface. Reprinted with permission from Ref. [135]. Copyright © 2022, Wiley-VCH. **c** AIMD simulation on the In/Li$_6$PS$_5$Cl interface. Reprinted with permission from Ref. [78]. Copyright © 2021, Nature Publishing Group

potential of the majority of SSEs, particularly sulfides. As a consequence, side reactions between Li-In and the SSE still occur, warranting careful attention to this aspect in the context of battery performance and stability assessments. From a theoretical standpoint, a comparison of the interfacial behaviors of metallic Li and Li-In with those of the typical argyrodite-type sulfide solid electrolyte Li_6PS_5Cl reveals intriguing insights. In the interfacial ab initio molecular dynamics (AIMD) simulation of lithium and Li_6PS_5Cl, a substantial reduction in P in the sulfide solid electrolyte occurs, leading to the concomitant generation of Li_2S and LiCl (Fig. 10b) [135]. In contrast, when In is used as the anode material, the AIMD results indicate the presence of a partially similar Li-In-S structure, with no pronounced reduction in P observed (Fig. 10c) [78]. These theoretical findings indicate that while reactions still occur between In and the SSE, they manifest in a less aggressive manner than metallic Li. This highlights the feasibility of using In as an alternative anode material to mitigate the interfacial side reactions. However, further investigations are warranted to comprehensively explore the compositional evolution of the interface between In and the electrolyte, refining the understanding of the interfacial dynamics and the potential for employing In as an effective means to suppress the detrimental side reactions.

3.1.1.2 Mitigation of Dendrite Growth The occurrence of lithium dendrites is also observed in ASSLBs, although the precise mechanisms responsible for their formation and the ensuing battery failure remain debatable. Insights acquired from liquid lithium metal batteries indicate that lithium metal deposition does not occur in a planar manner but rather causes dendritic growth in an unconfined environment [136–140]. This conversion-dominated electrode chemistry inherently leads to uncontrollable microscale intrinsic changes in electrochemically active materials during electrochemical cycling. In contrast, the introduction of alloys as anode materials shifts the electrode chemistry toward alloy reactions, wherein the dominant mechanism centers around reversible alloying and dealloying of the alloy anode without direct Li deposition/dissolution on the surface. This theoretical form of alloy-based electrochemistry has the potential to inhibit the growth of lithium dendrites and the occurrence of contact loss, thereby addressing a critical concern in the context of performance and safety.

However, as outlined in the mechanical considerations, the volumetric effect poses a significant challenge to the stability of alloy anodes, limiting the selection of materials that can maintain their intrinsic structure over the entire state of charge (SOC) range ($0\% - 100\%$). Currently, only graphite anode materials demonstrate the ability to preserve structural integrity while avoiding dendritic crystalline growth within a specified current range [141, 142]. In the case of Li-In alloys, which are commonly employed in ASSLBs, the phase transition range during battery operation is carefully managed and tightly confined to the two-phase region of In-LiIn, with the explicit purpose of circumventing mechanical failures resulting from excessive phase transitions [130]. A similar technique was also used for the application of Li-Al systems in ASSLBs [59]. Nevertheless, the issue of dendrite growth persists when alloy anodes are subjected to high current and loading conditions. Recent investigations focusing on Li-In anodes have revealed that when limiting the phase transition of Li-In alloy anodes to the two-phase region of Li-LiIn, the ASSLB assembled with the Li-In anode and a high cathode loading demonstrated favorable performance at 3.8 mA cm^{-2} [78]. However, this ASSLB using Li-In anode still experienced short circuiting after nearly 900 cycles. Upon using a high-resolution scanning electron microscope (SEM) to examine the failed anode/electrolyte interface, evident intrusion of In into the electrolyte was observed, indicating the growth of Li-In dendrites. In contrast, under the same conditions, the use of lithium metal as the anode led to pronounced electrolyte fractures and substantial contact loss between the lithium and electrolyte interface, thereby limiting the full cycle life of the battery to only 17 cycles (Fig. 11a). Based on these results, the incorporation of lithium alloys can decelerate the progression of dendrite invasion into SSEs and partially maintain contact between the anode and the electrolyte interface; however, lithium alloy incorporation does not provide a complete solution to dendrite issues (Fig. 11b). Hence, when practical scenarios involving high current densities and large capacities for ASSLBs employing alloys as anodes are contemplated, the anode-electrolyte interface, especially in terms of failure mechanisms, needs to be carefully considered for subsequent research endeavors.

3.1.2 Applications of Li Alloy Anodes

Notably, the replacement of metallic Li with Li alloys as the anode inevitably leads to a reduction in anode energy density due to considerations encompassing both specific capacity and average potential. However, this decrease in energy density is outweighed by the significant increase in the interfacial stability observed between Li alloys and SSEs, surpassing that of the lithium/SSE interface. Consequently, this trade-off in energy density is considered to be acceptable in light of the promising prospects for improved interface characteristics. Furthermore, a comprehensive assessment of the average potential from the metal phase to the Li-rich phase, alongside the theoretical maximum specific capacity of Li alloy anodes, is presented in Sect. 2.1.2. Notably, despite the

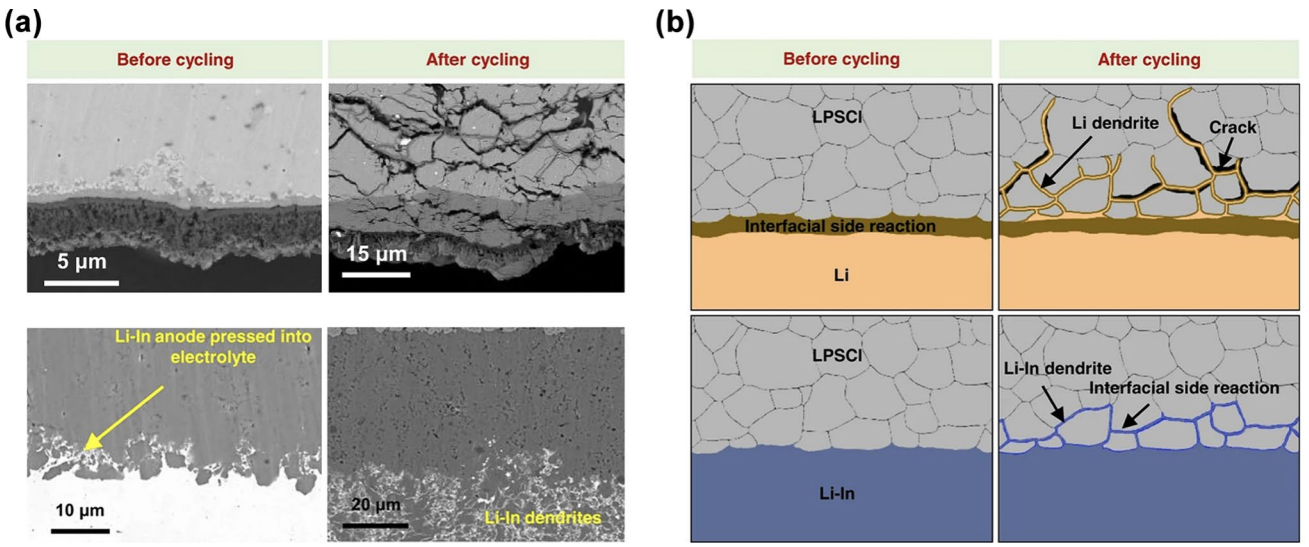

Fig. 11 Comparison of Li and Li-In dendrite growth. **a** SEM images of the anode/electrolyte interface before and after cycling. **b** Schematic diagram of the anode/electrolyte interface before and after cycling. Reprinted with permission from Ref. [78]. Copyright © 2021, Nature Publishing Group

aforementioned decrease in energy density, Li alloys still demonstrate a substantial enhancement when compared to traditional graphite anodes employed in conventional Li-ion batteries. A detailed exploration and analysis of this topic are available in a recent scholarly discussion addressing the promise of Li alloys in ASSLBs [143].

When contemplating the design of high-energy-density ASSLBs, strict control over the capacity ratio (N/P ratio) between the anode and cathode becomes essential. Additionally, meeting the strategic demand for energy densities exceeding 500 Wh kg^{-1} necessitates an anode capacity far surpassing that of the conventional graphite anode, with a theoretical specific capacity of 372 mAh g^{-1} [144, 145]. These requirements indicate that relying on the two-phase domain phase transition as the overall reaction of the electrode process for alloy anodes is impractical. As previously discussed in the mechanics section, when Li alloys gradually intercalate Li from their initial metal phase to the most Li-rich phase, this process induces a substantial volume expansion, rendering the electrode susceptible to conducting network collapse and eventual battery failure. Furthermore, the phase transition of an alloy typically involves the generation of various intermediate phases with different crystalline structures, resulting in significant differences in lattice parameters and, consequently, substantial grain boundary energy. These disparities can lead to internal structural damage within the alloy particles. In the context of commonly employed Li-In anodes in ASSLBs, numerous published reports reveal that the actual specific capacity of Li-In alloy anodes often falls below 200 mAh g^{-1} during cycling, while the areal capacity of the utilized Li-In alloy significantly exceeds that of the cathode [78, 146–149]. Under these conditions, the phase transformation of the Li-In alloy to the two-phase region of In-LiIn is confined; this confinement effectively suppresses the volume expansion and mechanical failure while maintaining a relatively constant potential of 0.62 V against metallic Li, thereby inhibiting the occurrence of side reactions. However, this interfacial stability is achieved at the expense of energy density. What's worse, under high current and large capacity cycling conditions, Li-In dendrites still exhibit growth in the battery, ultimately leading to battery failure after a certain number of cycles.

Hence, the development of a viable alloy anode material mandates strategic modification of the mechanical-chemical failure behavior within the phase transition range aligned with high specific capacity and low average voltage conditions. These alterations in the alloys' property are imperative for concurrently enabling elevated energy density while effectively fulfilling the essential roles of restraining dendrite growth, mitigating contact degradation, and suppressing detrimental interface side reactions. Depending on the type of alloying element, alloy anodes can be further categorized as Li-metal alloy anodes or Li-metalloid alloy anodes.

3.1.2.1 Li-Metal Alloy Anodes In a recent development, Samsung reported the attainment of an Ag-nano particle/C composite anode with remarkable capacity and stability enhancements (Fig. 12a, b) [57]. Employing comprehensive transmission electron microscopy (TEM) analyses, a noteworthy observation emerged wherein the Ag nanoparticles (NPs) underwent fragmentation into smaller entities sub-

sequent to the initial charging cycle (depicted in Fig. 12c). These results indicated the formation of Li_9Ag_4 alloys within the charging process. Intriguingly, a distinct phenomenon occurred, wherein a substantial proportion of both Ag and Li ions migrated toward the current collector side upon the completion of charging (Fig. 12d). This dynamic repositioning culminated in the persistence of fragmented particles solely within the confines of the Ag-C nanocomposite layer, thereby suppressing the dendrite growth. Furthermore, the increased mechanical robustness exhibited by the composite Li alloy anode was examined and was attributed to the active participation of the carbon component in the underlying electrochemical processes. The investigators postulated that the C particles served a dual role: first, they enabled efficient Li-ion conduction within the composite structure; second, their notable modulus of ~ 200 GPa provided the capacity for mechanical reinforcement to the Ag-C nanocomposite layer. This multifaceted involvement of carbon was instrumental in enhancing the overall mechanical integrity of the composite anode. In addition, as Ag is soluble in Li, no significant changes in the crystalline structure occurred during lithiation, thus facilitating lithiation. The collective insights gained from Ag-C composite alloy anodes provide valuable contributions to the understanding and advancement of high-performance Li alloy anode materials for practical energy storage applications.

Li-Al alloys are also an applicable choice for anodes of ASSLBs. Given the lighter nature of aluminum (Al) atoms compared to indium (In) atoms, Al has a higher theoretical specific capacity of 990 mAh g^{-1}. In addition, the average lithiation/delithiation potential of Al is 0.3 V versus Li/Li^+, a value significantly lower than that of In. Due to its high specific capacity and low average potential, the Al-based anode has been recognized as one of the most promising alloy-anode materials for high-energy-density ASSLBs. As reported by Kanno et al. [150], the application of an Li-Al alloy anode was able to mitigate the reduction of the thio-LISICON electrolyte ($Li_{3.25}Ge_{0.25}P_{0.75}S_4$), as shown by the low and stable resistance of the battery during cycling. Pan et al. [59] also achieved an ultralong lifespan of LGPS-based symmetric cells for more than 2 500 h at 0.5 mA cm^{-2} by using $Li_{0.8}Al$ electrodes to enhance the interfacial stability. Moreover, the $Li_{0.8}Al$|LGPS|S full cell with a low N/P ratio of 1.125 was assembled in their work and demonstrated an impressive cell-level specific energy of 541 Wh kg^{-1}, which affirmed the promising prospects of Li-Al anodes. The performance of Al-based alloys was further improved in recent research by Liu et al., in which the microstructure of Al foil was engineered by adding 5% (atomic content) In [151]. The In laminae uniformly distributed in the Al matrix were lithiated prior to the Al, generating the Li-In alloy phase with high lithium diffusivity. This Li-In alloy phase remained unchanged after discharging, which played a crucial role in improving the reversibility of the phase transition between Al and LiAl and promoting the facile (de) lithiation of Al. Consequently, the ASSLB with the non-prelithiated $Al_{94.5}In_{5.5}$ foil (30 μm in thickness) as the anode demonstrated stable cycling for 200 cycles at a high current density of 6.5 mA cm^{-2}.

New anode compositions involving two or more alloys may also improve the performance of alloy anodes. Therefore, an efficient screening method needed to be established. Zhong et al. [152] successfully achieved high-throughput fabrication of Sn-Co-Sb alloys with various composition in

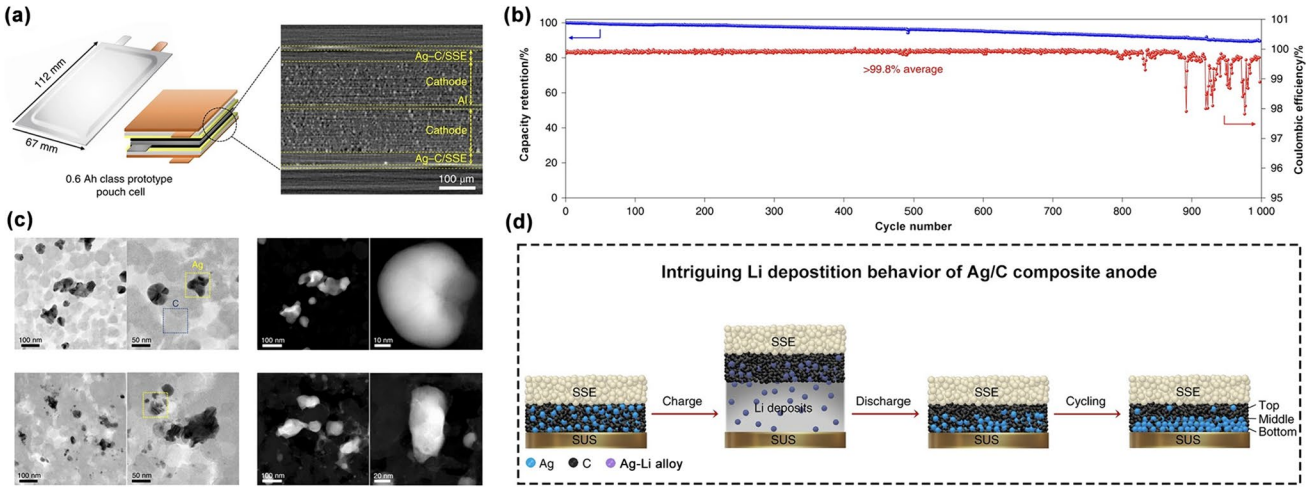

Fig. 12 Ag-C composite anode for ASSLBs. **a** Construction of an all-solid-state pouch cell using an Ag-C composite anode. **b** Cycling performance of the all-solid-state pouch cell using the Ag-C composite anode. **c** TEM images of the Ag particles inside the anode before and after charging. **d** Intriguing Li deposition behavior of the Ag-C composite anode. Reprinted with permission from Ref. [57]. Copyright © 2020, Nature Publishing Group

a large sample via the well-designed gradient electrodeposition method. This novel method provides a feasible way for rapid screening of alloy materials with multiple components and also provides some inspiration for future research.

3.1.2.2 Li-Metalloid Alloy Anodes Metalloids usually refer to elements with intermediate properties between those of metals and nonmetals, which include boron, silicon, germanium, arsenic, antimony, and tellurium. Among these materials, boron, silicon, germanium, and antimony have been reported as anodes in LIBs. A summary of their basic properties is provided in Table 1.

The widely reported Li-B alloys have the unique structure of free lithium contained in a solid skeleton composed of Li_7B_6 [156]. These materials are not strict alloy anodes because both the free Li and the Li_7B_6 skeleton in Li-B alloys can contribute to the electrochemical capacity. Initially, discovered in the 1970s, Li-B alloys with 70% (atomic content) Li have been widely applied as anodes in thermal batteries because most Li-B alloys can remain solid at elevated temperatures up to 650 °C [157]. However, the electrochemical performance of Li-B anodes in nonaqueous electrolytes at ambient temperature remains unsatisfactory and is notably affected by the cutoff voltage [153, 158–160]. In detail, a high cutoff voltage leads to a large amount of Li being stripped from the alloy anode, resulting in the collapse of the porous skeleton and poor reversibility. In addition, operating a cell with an Li-B anode at a low cutoff voltage can ensure stable performance but will result in limited discharge capacity [153].

As listed in Table 1, Ge has a maximum capacity of 1 624 mAh g^{-1} when lithiated to $Li_{22}Ge_5$ [154]. It is generally presumed that cracking and material pulverization caused by a 260% volume change are the main causes of the rapid capacity decay of the Ge anodes in cells with liquid electrolytes [161, 162]. However, as we mentioned in Sect. 2.3, Ge nanoparticles can maintain structural stability without cracks during lithiation/delithiation, ascribed to the more isotropous distribution of strain inside the nanoparticles during lithiation [95]: this behavior is in sharp contrast to the behavior of Si nanoparticles. Hence, it is proposed that the accumulation of insulating SEI components such as Li_4Ge_2H at the interface may be the cause of the rapid capacity decay in traditional LIBs [163]. In addition, the high cost of Ge poses a significant barrier to the commercialization of Ge-based anodes.

Antimony (Sb) metals with unique two-dimensional layered structures exhibit a high electronic conductivity of 2.5×10^6 S m^{-1}, which ensures excellent kinetics [155, 164, 165]. Additionally, the volume change in Sb (135%) after Li-ion insertion is much lower than that in Si or Ge, which is beneficial for maintaining the structural stability of the electrode. However, the electrochemical performance of Sb significantly lags behind that of graphite anodes, commercialized anode materials with layered structures [166–169]. Moreover, the severer issue lies in the toxicity of Sb to the environment, causing the commercialization of Sb-based alloy anodes to be challenging.

Si is abundant and environmentally friendly and has potential to be a promising anode material with theoretical capacities comparable to those of Li metal. The lithiation potential of Si (0.4 V vs. Li/Li^+) can prevent direct Li plating and Li dendrite formation. Its low cost enhances its appeal for commercialization [170–172]. Based on comprehensive considerations of energy density, safety, stability and cost, Si-based anodes remain the most promising choices for ASSLBs. Extensive research efforts over the years have led to substantial progress in mechanistic studies, battery design, and large-scale material production for ASSLBs incorporating Si-based anodes, thereby continually advancing the prospects for commercialization. An in-depth discussion of the application of Si-based anodes in ASSLBs is presented as follows.

In most cases, poststudies about Si anodes are based on LIBs. The violent volume change of Si, the ongoing growth of the SEI, and the low Columbic efficiency are all challenging problems [86, 87, 173]. Specifically, the volume of Si expands by ~ 280% after total lithiation, which indicates that Si anodes suffer from cracking and pulverization after repeated expansions/contractions, as displayed in Fig. 13a. The generated cracks can block or destroy the pathways for the electrons and Li^+ ions. A portion of the active material may even lose electrical contact with the current collector. In addition, fresh surfaces of Li-Si alloys are exposed to electrolytes due to the violent volume change. Lithiated Li-Si alloys are highly reactive toward traditional LIB electrolytes; therefore, the SEI will immediately be generated on their surface. However, the SEI is not stable enough to withstand

Table 1 Summary of the basic properties of common metalloid anodes

Metalloid anode	Lithiated phase	Theoretical specific capacity/(mAh g^{-1})	Volume change/%	Potential/(V vs. Li/Li^+)	References
B	Li_7B_6	2 892	\	0.82	[153]
Ge	$Li_{22}Ge_5$	1 624	260	0.5	[154]
Sb	Li_3Sb	660	135	0.8	[155]
Si	$Li_{22}Si_5$	4 200	280	0.4	[87]

intense volume changes; thus, the continuous consumption of electrolytes occurs to reconstruct the SEI [174]. Consequently, batteries with Si anodes always exhibit low CEs and deteriorating electrochemical performance. Additionally, the trapped Li in the Si anode due to limited diffusion kinetics (Fig. 13b) is another cause of the low CE, which causes increased research interest in the prelithiation of the Si-based anodes [175–177].

In the context of ASSLBs, Si-based ASSLBs exhibit promising commercial prospects [67, 179–181]. First, the mechanical strength of SSEs can aid in the compensation of the volume change of Si anodes in theory. In addition, ASSLBs are usually assembled and tested under external pressure to ensure intimate interfacial contact. Soft Li can easily deform and penetrate the SSE under pressure, leading to a short circuit. However, using Si with a higher modulus as the anode can prevent these occurrences. The hardness of Li-Si alloys has been reported to always be lower than that of pristine Si. Hence, lithiated Li-Si can deform plastically under external pressure, maintaining close contact with SSEs for excellent reversibility during cycling [114]. Moreover, both Si and Li-Si alloys exhibit better thermodynamic stability toward SSEs. Furthermore, the immovability of SSEs will reduce the contact area between the anode and SSE, thereby further reducing the occurrence of side reactions in the battery [182].

However, the issue of a low initial CE still needs to be addressed in Si-based ASSLBs. Some SSEs, especially sulfides, have narrow electrochemical stability windows and tend to decompose below 1.7 V [183, 184]. Since the lithiation of Si occurs only when the potential is less than 0.4 V versus Li^+/Li, side reactions will proceed via interactions between the Si anode and P cations in the sulfide electrolyte when the potential is less than 1.5 V (vs. Li^+/Li); these results are confirmed by both theoretical predictions (Fig. 13c, d) and experiments [178]. These side reactions contribute to extra capacity during the first charge of the battery. However, the byproducts (SiP_2, SiP, and Li_5SiP_3) with higher electrode potentials than Si show restricted reversibility within the cutoff voltage of the Si anode. Consequently, selecting an appropriate SSE that matches the Si anode is also crucial for ASSLBs [185, 186].

Composite Si Anodes. The structural design of Si-based anodes is a topic of intense debate. One view advocates for the incorporation of Si (and carbon materials) with SSEs to form a composite anode, mimicking the situation in LIBs where the liquid electrolyte can fully wet the anode. Sulfide electrolytes with high ionic conductivity and excellent mechanical properties are the most promising candidates

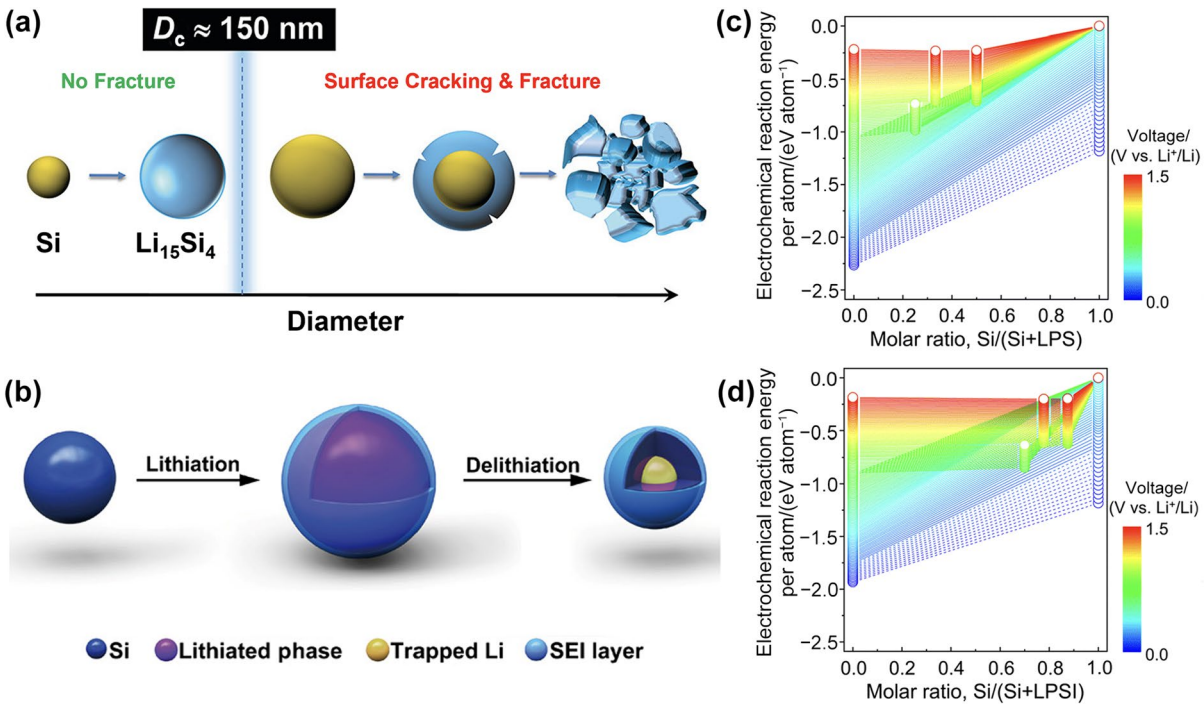

Fig. 13 Failure mechanisms of the Si anodes. **a** Volume effects of the Si anode. Reprinted with permission from Ref. [86]. Copyright © 2012, American Chemical Society. **b** Li trapped in the Si anode during delithiation. Reprinted with permission from Ref. [176]. Copyright © 2019, AAAS. Calculated electrochemical reaction energy between Si and **c** $75Li_2S$-$25P_2S_5$ and **d** $70(0.75Li_2S$-$0.25P_2S_5)$-60LiI electrolytes, confirming the side reactions between the Li-Si anode and the sulfide electrolytes. Reprinted with permission from Ref. [178]. Copyright © 2023, The Royal Society of Chemistry

among SSEs for serving as the ionic conducting framework in composite Si anodes. The pioneering work of Trevey et al. involved mixing nano Si, acetylene black and $77.5Li_2S{\cdot}22.5P_2S_5$ at a mass ratio of 1:1:5 via ball milling to form the composite Si anode [187]. The results showed that the ASSLB with a composite Si anode achieved a much greater capacity retention than the LIB, benefitting from the composite structure and the internal generated pressure during the powder compaction process.

The performance of the composite Si anodes can be affected by various factors, including the mass ratio, size distribution, mixing method, applied carbon materials, and the type of SSE [188–190]. Smaller electrolyte particles are more conducive to constructing an efficient ionic conductive path and fully releasing the capacity [190]. To improve the specific energy density of the battery, the amount of electrochemically inert components, especially SSEs, should be minimized as much as possible. Recently, an inspiring result was reported for the Si-based ASSLB. Figure 14a shows the preparation process of the composite Si anode, in which a mixture of Si nanoparticles, Li_6PS_5Cl electrolyte, and carbon black with a mass ratio of 6:3:1 was ball milled at 400 r min^{-1} for 2 h. This composite Si anode enabled a cell-level energy density of 285 Wh kg^{-1} (without current collectors) in the assembled Swagelok-type ASSLB [84]. Furthermore, by preparing a bipolar stacked ASSLB, as displayed in Fig. 14b, the cell-level energy density could be increased to 204 Wh kg^{-1} (with current collectors), with the output voltage reaching 8.2 V (Fig. 14c) [191]. The uniform mixing of Si with SSEs and the carbon inside the composite anode created a more sufficient contacting area and reduced the local current density, which was crucial for improving the rate performance of the cell. However, sulfide electrolytes tend to be thermodynamically unstable toward Li-Si, indicating that an enlarged contact area between Si and the electrolyte may intensify interfacial side reactions. Additionally, carbon has been reported to promote the decomposition of sulfide electrolytes, further degrading the long-term stability of composite anodes [114, 192]. Hence, further research is required to explore the most suitable composition to fully leverage the merits of the composite Si anodes.

Diffusion-Dependent Si Anodes. Another view is that Si or Si-C composites are sufficient for use as anodes in ASSLBs, a concept referred to as diffusion-dependent electrodes. In this way, the cell-level energy density can be greatly improved. Notten et al. first applied a 50 nm thick Si film in LiPON-based batteries [110]. A cross-sectional SEM image of the cell is displayed in Fig. 15a. According to their reports, the discharge capacity of the assembled Si|LiPON|$LiCoO_2$ cell remained stable for 60 cycles, and postmortem characterization indicated an intact interface without any cracks between the thin Si film and LiPON electrolyte after cycling. Subsequent studies of LLZTO-based ASSLBs confirmed that the cycling stability was significantly affected by the thickness of the Si film [193]. A drastic Si volume change resulted in rapid capacity decay when the thickness of the Si film approached or exceeded 900 nm. Only Si films with thicknesses less than 180 nm could maintain close contact with the LLZTO electrolyte.

However, the high loading of Si anodes is imperative for improving the cell-level energy density. Therefore, as shown in Fig. 15b, the columnar Si anode (col-Si) with a high areal loading exceeding 3.0 mAh cm^{-2} was developed via physical vapor deposition (PVD) [182]. The col-Si anode exhibited unique 1D breathing phenomena during lithiation, and the intrinsic pores inside could compensate for the volume expansion to maintain structural stability, ensuring the stable cycling of the col-Si|LPSC|NCM full cell for more than 100 cycles. Nevertheless, due to the high cost of PVD, col-Si was unsuitable for mass production. In 2021, Tan Darren et al. [114] reported the application of a 99.9% (by weight) micro-silicon anode prepared via slurry casting in sulfide-based ASSLBs (Fig. 15c), which demonstrated a record high capacity retention of 80% after 500 cycles at 1 C (5 mA cm^{-2}) in the assembled full cell. In a recent study by Yan et al. [116], an Li-Si alloy anode was fabricated via direct pressing of an Si-containing film and Li foil together and exhibited improved kinetics and structural stability compared with those of the bare Si anode due to the low hardness of the Li-Si alloy and prerelease stress during lithiation. However, soft short circuits still existed, especially under high-rate and high-capacity conditions. To address this, hard carbon was mixed with Li-Si alloy as a stabilizer to construct an inner connected ionic/electronic conductive network, which helped to suppress the dendrite growth (Fig. 15d). As a consequence, the hard-carbon-stabilized Li-Si anode demonstrated a remarkable capacity retention at 1 C (5.86 mA cm^{-2}).

3.1.3 Failure Mechanisms

Numerous research articles have investigated the failure mechanisms of ASSLBs [194, 195]. A recent review by Liu et al. [196] comprehensively addresses the failure modes at Li metal anode/solid-state electrolyte (SSE) interfaces, covering electric, chemical, electrochemical, and mechanical aspects. Inspired by this review, we conducted a parallel discussion on the failure mechanisms of ASSLBs with Li alloy anodes. As mentioned earlier in Sect. 3.1, owing to the higher potential and lower reducibility of the alloy compared to those of pristine Li, the application of alloy anodes effectively improves the (electro) chemical stability of the anode-electrolyte interface. Therefore, chemical and electrochemical failures stemming from excessive (electro) chemical decomposition of thermodynamically unstable

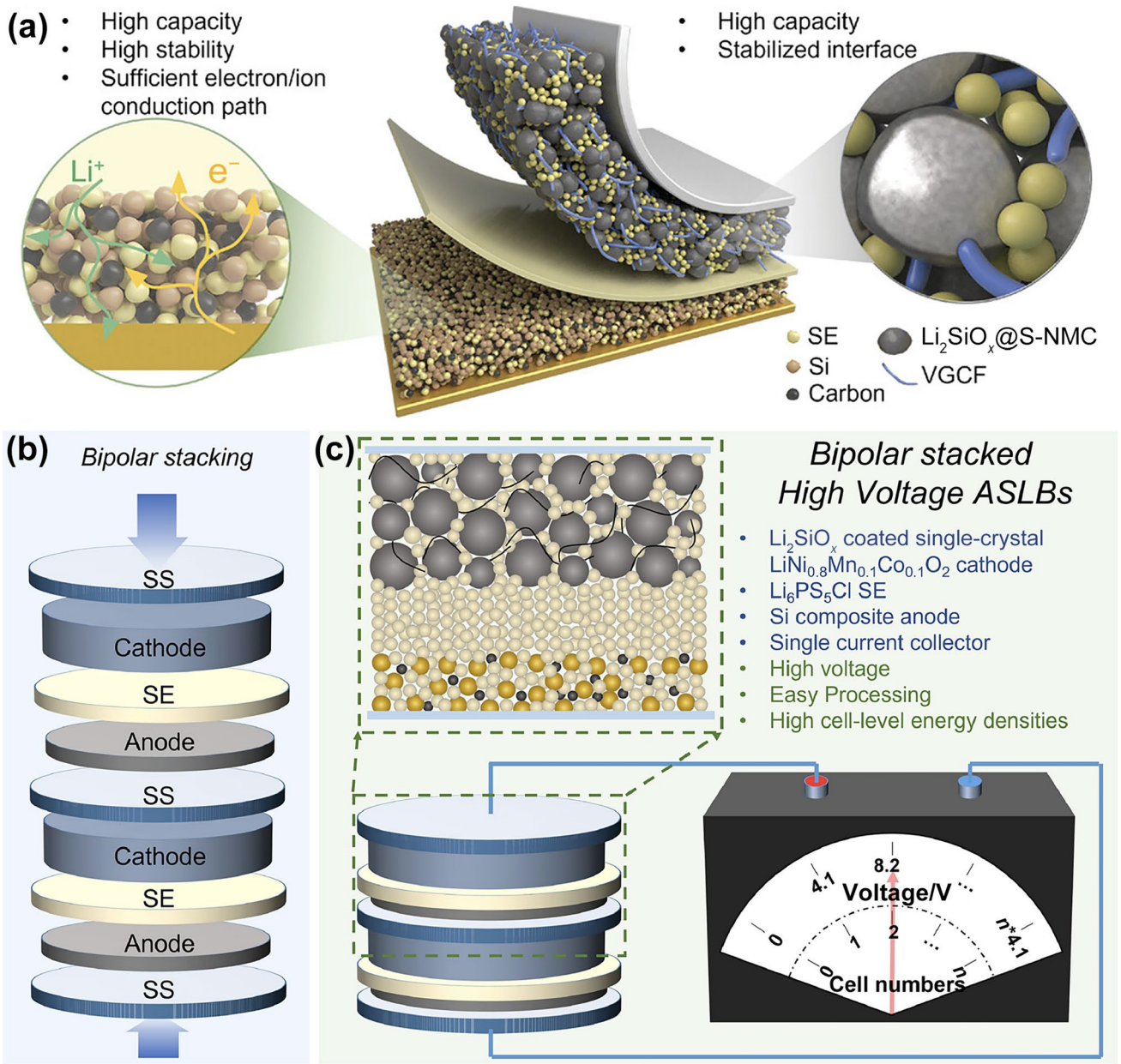

Fig. 14 Design of the composite Si anodes. **a** Schematic illustration of the composite Si anode in high-energy all-solid-state batteries. Reprinted with permission from Ref. [84]. Copyright © 2022, Wiley-VCH. **b** Structure and **c** advantages of bipolar-stacked all-solid-state batteries. Reprinted with permission from Ref. [191]. Copyright © 2022, Wiley-VCH

solid-state electrolytes at interfaces are uncommon in ASSLBs with alloy anodes. The following discussion will primarily concentrate on the electric failure and mechanical failure of ASSLBs with Li alloy anodes.

(1) Electric failure. Electric failure refers to the dendrites being propelled by an electric field. The use of alloys as anodes theoretically suppresses the formation of Li dendrites since alloying reactions typically occur at higher potentials where the necessary conditions for lithium deposition are not met. However, the kinetics of alloy anodes have a significant impact on their performance. If the diffusion of Li within the alloy is sluggish or hindered, direct Li deposition rather than Li alloying will be kinetically favored, thereby leading to the accumulation of Li at the anode/electrolyte interface. Due to the inherent defects on the surface of SSEs, the distribution of the electric field at the anode/electrolyte interface tends to be inhomogeneous, which promotes the development of these Li accumulations into Li dendrites. Additionally, harsh working conditions, such as high cathode loading and high rates, can stimulate the growth of alloy dendrites

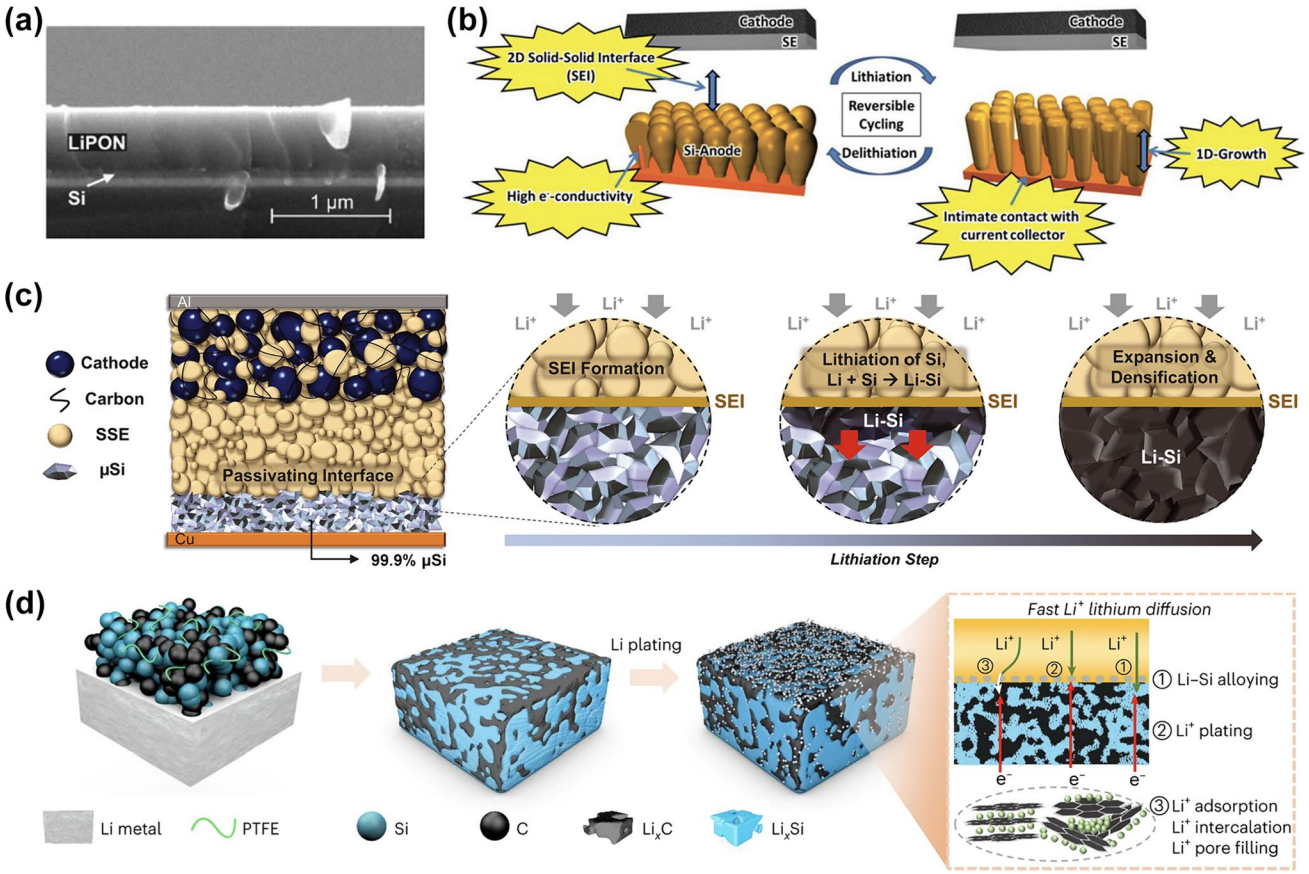

Fig. 15 Design of the diffusion-dependent Si anodes. **a** Cross-sectional SEM image of the Si/LiPON interface after cycling. Reprinted with permission from Ref. [110]. Copyright © 2007, Wiley-VCH. **b** Schematic illustration of the contact between col-Si and SSEs and the 1D breathing behavior of the col-Si anode during lithiation. Reprinted with permission from Ref. [182]. Copyright © 2020, Wiley-VCH. **c** The 99.9% μSi anode and its lithiation process in an all-solid-state full battery. Reprinted with permission from Ref. [114]. Copyright © 2021, AAAS. **d** Mechanism of the hard carbon-stabilized LiSi anode. Reprinted with permission from Ref. [116]. Copyright © 2023, Nature Publishing Group

(such as Li-In dendrites), leading to short circuiting of the cell. Moreover, both the inherent electronic conductivity of the electrolyte itself and defects within the electrolyte may trigger the direct Li deposition within the solid electrolyte [27]. Therefore, additional methods are needed to improve the electronic insulation of the interface and optimize the structure and composition of SSEs.

(2) Mechanical failure. The significant volume change in alloy anodes always poses a threat to the structural stability of ASSLBs. Anode expansion during lithiation increases the internal stress of the battery, as these volume changes cannot be accommodated by the rigid and immovable SSEs. Consequently, persistent stress concentration leads to mechanical damage in the SSEs, including the development of microcracks. Interfacial contact loss induced by void formation is also an important form of mechanical failure [197]. Lu et al. [198] conducted an in-depth investigation into the evolution of interfacial voids and highlighted the significant influence of current density and capacity on void formation kinetics. Specifically, the applied current density affects the void nucleation process, while the capacity controls the void evolution process. A higher current density results in smaller but more numerous void nuclei. As the capacity gradually increases, these void nuclei develop in 2D or 3D directions, ultimately forming void defects with varying structures. These voids block the mass transport, leading to the rapid failure of the cell. Additional findings from Lee et al. [199] indicate that a reduced anode thickness also accelerates the occurrence of interface contact loss; this is related to the intensified friction between the anode and the SSE. Regarding the mechanism behind void formation, diffusion and coalescence of vacancies are probably the primary causes of void generation. However, a recent report by Li et al. [200] contested this speculation, leaving the internal mechanism of void formation an open question. While the aforementioned studies primarily focus on the behavior of bare Li anodes, the conclusions drawn from these investigations are equally applicable to lithiated alloy anodes and composite lithium

anodes with alloys. These newly emerged defects trigger electrical failure of the cell due to exacerbated heterogeneity in the distribution of Li^+ flux within the battery. Once dendrites are formed, the stress concentration at the dendrite tips will also aggravate the cracking of electrolytes. This type of failure is often referred to as "chemomechanical failure" or "electro-chemo-mechanical failure" in the literature [195, 201]. A more drastic volume change of the anode correlates to severer degradation in battery performance [202]. Therefore, a rational structure design is crucial for ASSLBs.

In general, batteries rarely experience failure due to a singular cause. Therefore, a thorough and comprehensive analysis is required to conduct failure analysis.

3.2 Li-Alloy Interlayers

3.2.1 Better Interfacial Contacts

The inherent affinity of certain alloys for Li metal enables alloys to serve as effective interlayers between the Li anode and SSEs via interactions between Li and lithiophilic alloys or alloy compounds. A previous report on the construction of an Li-alloy interlayer for better interfacial contact involved sputtering a thin layer of Au on the clean surface of the SSE pellet, primarily via magnetron sputtering or vacuum evaporation [203, 204]. The spontaneous alloying process between Au and Li facilitates seamless contact between the anode and SSE. In addition, the Li-Au interlayer can also suppress void formation during Li dissolution, which is essential for improving the reversibility of the Li anode [203]. Recently, metal compounds, such as fluorides and nitrides, have been commonly employed at the Li/garnet interface through magnetron sputtering, drop casting, or spin coating to modify the surface of garnet electrolytes [205–210]. Generally, the original surface of garnet-type electrolytes is always contaminated with a lithiophobic Li_2CO_3 layer, which results in large interfacial resistance [211, 212]. After modifying the surface of garnet-type electrolytes with these metal compounds, the interfacial contact could be significantly improved by the conversion reactions between Li metal and metal compounds. For instance, Shi et al. prepared an SnN_x-coated $Li_{6.4}La_3Zr_{1.4}Ta_{0.6}O_{12}$ (LLZTO) pellet via magnetron sputtering, which was then exposed to molten Li to accelerate the conversion reactions between SnN_x and Li [207]. Consequently, the resulting Li_ySn/Li_3N layer covered all grain boundaries and voids, ensuring a uniform distribution of Li^+ flux and a dendrite-free morphology (Fig. 16a). As a result, the symmetric cell consisting of optimized interfaces showed a remarkable lifespan of 985 h at 0.1 mA cm^{-2} with a low and stable overpotential. Notably, the reactions between these coating compounds and Li metal at room temperature could increase the roughness of the anode, possibly compromising interfacial contact and impeding mass transport through the interface [98]. Additionally, reactions at room temperature can be sluggish and inadequate, further compromising the overall electrochemical performance of the cell. Therefore, an additional step involving an elevated temperature beyond the melting point of Li metal is widely used to accelerate the complete reactions between Li and the introduced compounds, as elucidated in the report by Shi et al. [207]. However, a high temperature raises safety concerns during the preparation process. The viability of these methodologies for prospective commercialization has yet to be determined. Recently, a functional Li anode with a composition gradient of LiF-LiAl-Li was reported for garnet-based ASSLBs through reactions between molten Li and AlF_3. The significant difference in interfacial energy between the Li/LiF and Li/LiAl alloy interfaces led to a spontaneous composition gradient. The inner LiAl alloy layer close to the Li metal enabled a low interfacial resistance, while the LiF layer close to the LLZTO electrolyte worked as a rigid shell to prevent the formation of Li dendrites. As a consequence, this tactic substantially increased the critical current density (CCD) of the Li symmetric cell to more than 3.0 mA cm^{-2} (Fig. 16b) [213].

Additionally, liquid alloys with low melting points provide promise for enhancing the interfacial contact between the anode and SSEs. The unique fluidity of liquid alloys at room temperature ensures good interfacial contact, as well as the ability to heal interfacial defects, such as voids that arise during cycling. In this context, mercury, the sole metal that remains liquid at room temperature and atmospheric pressure, was investigated [214–216]. An Li-Hg alloy with 1.3% (molar content) Li could completely wet the LLTO pellet and the Li_2S-P_2S_5 sulfide electrolyte, significantly reducing the interfacial resistance. As displayed in Fig. 16c, the Li-Hg alloy interface spontaneously underwent a phase transition between liquid and solid with the plating and stripping of Li, exhibiting an excellent self-healing ability to ensure dynamic interface stability [215]. Moreover, a liquid Na-K alloy at room temperature could also promote interfacial contact. Additionally, the Na-K alloy interlayer remained stable at the interface because neither Na nor K could alloy with Li metal [113]. However, the fluidity of liquid alloys in the interlayer could also cause specific problems. The SSE pellet is not dense but has several pores and cracks inside it. Therefore, the liquid alloy at the interface may infiltrate into the SSEs along these defects, resulting in short circuiting of the cell.

3.2.2 Increased Interfacial Stability

As discussed in Sect. 3.1.1, although the electrode potential of the alloy is lower than the reduction potential of SSEs, the long-term stability of ASSLBs with alloy anodes is still achievable [65, 85, 150, 217–219]. In addition to the theoretical predictions in Fig. 10c, a flexible SEI shell composed

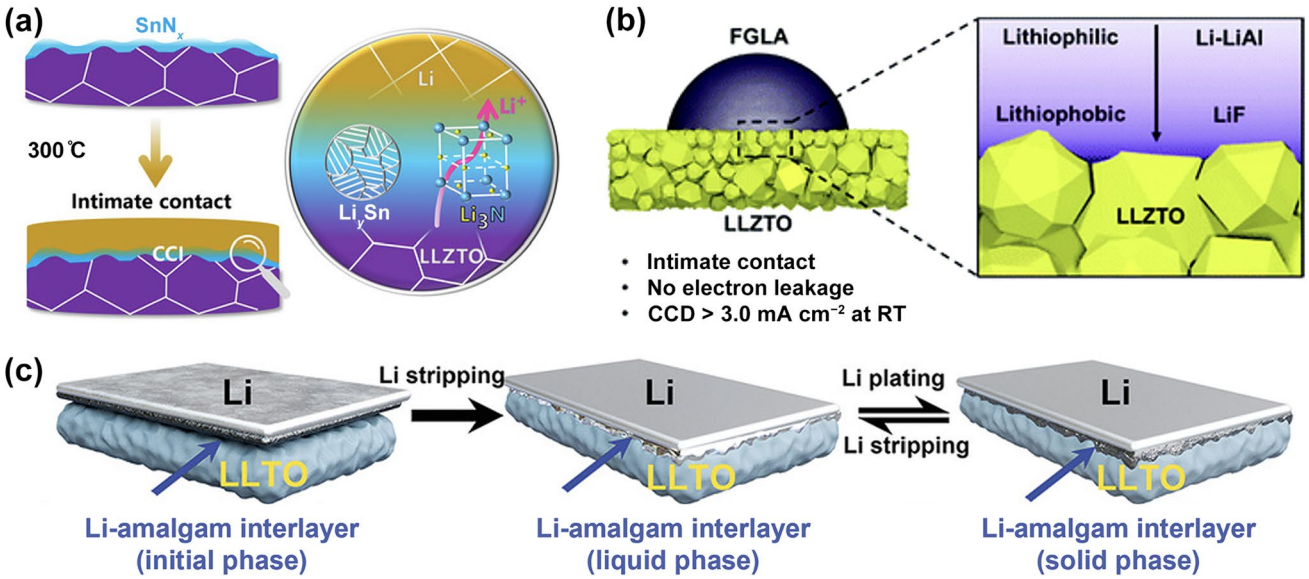

Fig. 16 Li-alloy interlayers for better interfacial contact. **a** Schematic illustration of the interfacial contact between molten Li and SnN_x-coated LLZTO electrolyte. Reprinted with permission from Ref. [207]. Copyright © 2020, Wiley-VCH. **b** Gradient LiF-LiAl-Li anode and its merits. Reprinted with permission from Ref. [213]. Copyright © 2022, The Royal Society of Chemistry. **c** Evolution of the Li-Hg alloy interlayer during cycling. Reprinted with permission from Ref. [215]. Copyright © 2020, Wiley-VCH

of In_2S_3 was characterized on the surface of the cycled Li-In anode, as shown by the in-depth XPS profile in Fig. 17a; this shell can contribute to the kinetically stable interface [117]. Therefore, using alloys as the interlayer may also contribute to providing better interfacial stability from this perspective. Nevertheless, in a recent review, the interfacial stability of Li alloy interlayers/SSEs was questioned [220]. All alloys are electronic conductors, which indicates that the alloy interlayer, or the interlayer rich in alloy components, might aggravate the decomposition of electrolytes or cause direct Li deposition on the top of the interlayer. However, some studies have shown rather controversial results in which Li alloy interlayers could still enhance the interfacial stability. For instance, the Ag-Li intermetallic layer prepared by rolling Ag and Li foils together greatly improved the interfacial stability between the Li anode and Li_6PS_5Cl electrolyte [56]. In detail, the cross-sectional SEM images in Fig. 17b showed the reversible change in thickness of the Li layer under the Ag-Li interlayer during charging/discharging, while the thickness of the Ag-Li layer remained constant throughout the entire process. Additionally, X-ray microscopy (XRM) images and XPS spectra confirmed that the interface was still flat and stable after 30 cycles of discharging/charging; these results indicated that no severe side reactions occurred between the LPSC electrolyte and the Ag-Li interlayer. The low electronic conductivity of Li-Ag alloys and the excellent ionic transport property of the Ag-Li interlayer were considered to be the main factors preventing direct Li deposition above the Ag-Li interlayer. However, the Li^+ transport kinetics through the interlayer significantly influenced the performance. The abovementioned results are often obtained at low rates. The transport of Li^+ through the alloy interlayer can be blocked or not timely enough at high current densities, leading to the direct deposition of Li metal above the alloy interlayer. Additionally, some alloy elements in the interlayer may gradually diffuse into and eventually dissolve in Li metal via inherent thermodynamic compatibility, producing new concerns regarding the stability of the Li-alloy interlayer [220]. Hence, additional studies need to be devoted to exploring the inner mechanisms of alloys, improving the interfacial stability and understanding the evolution of interfacial structures.

Recently, it was proposed that mixing alloy components with insulating inorganics can help to decrease the electronic conductivity of the interphase while retaining the benefits of Li alloy-rich interphase [139, 221–223]. Through in situ reactions between metal chloride and Li metal, an Li alloy-rich SEI with the incorporation of the insulating LiCl was prepared to increase the interlayer resistivity to an order of magnitude of 10^4 Ω cm, which was significantly greater than that of the native SEI layer on Li metal or the reported amorphous carbon layer. This high resistivity was sufficient to ensure the deposition of Li below the composite layer [224]. In addition, Zhao et al. [225] noted that there could be a positive impact of the alloy components at the interface of Li anode/sulfide electrolytes, which could enhance the electrochemical performance of the cell once a delicate balance between alloy-induced interfacial deterioration and alloy-regulated uniform

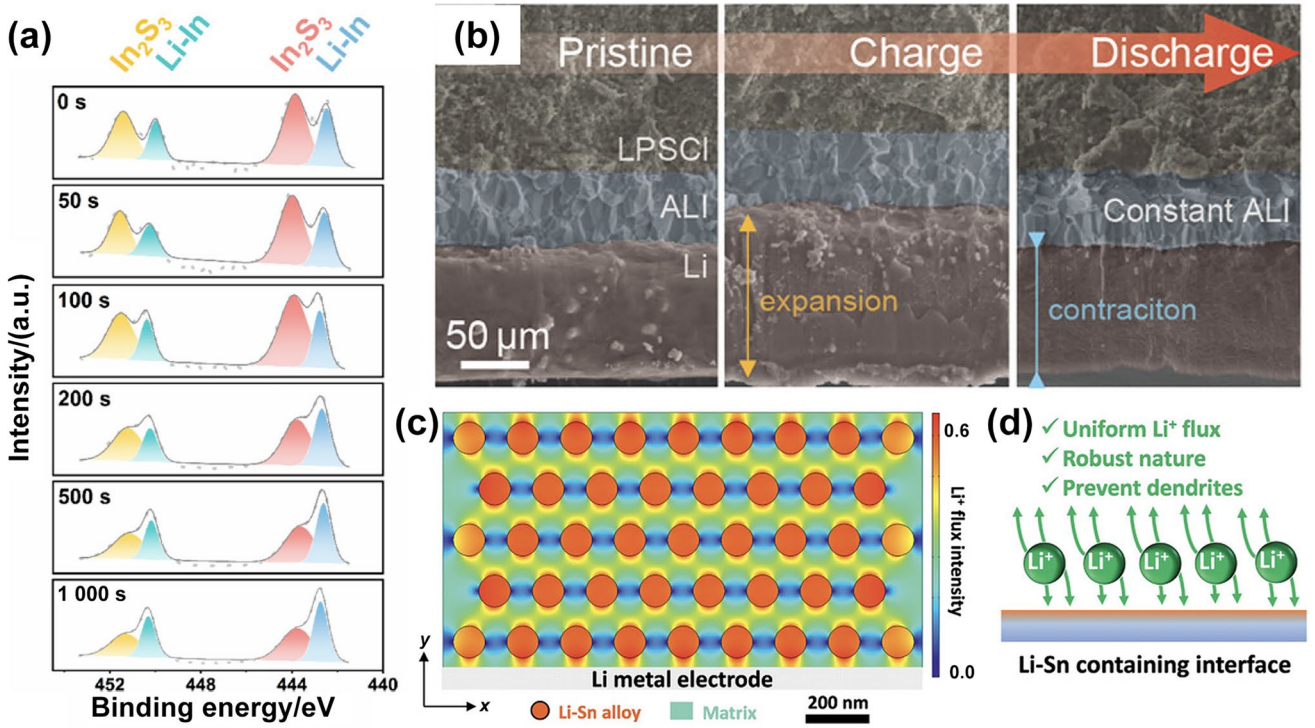

Fig. 17 Li-alloy interlayers for improving the interfacial stability. **a** In-depth XPS profile of the SEI on the indium anode. Reprinted with permission from Ref. [117]. Copyright © 2021, American Chemical Society. **b** Cross-sectional SEM images of the LPSCl/Ag-Li interfaces in the full cell after the first cycle. Reprinted with permission from Ref. [56]. Copyright © 2021, Wiley-VCH. **c** Distribution of the Li^+ flux simulated by the finite element method. **d** Schematic diagram of the working mechanism of the Li-Sn interface derived from in situ reactions between Li and the gc-$Li_{3.2}P_{0.8}Sn_{0.2}S_4$ electrolyte. Reprinted with permission from Ref. [225]. Copyright © 2021, Wiley-VCH

Li plating/stripping was established. Based on their findings, only excess alloy components could lead to severe side reactions at the interface. The corresponding positive effect of Li alloys in stabilizing the interface was also confirmed by theoretical studies. As shown in Fig. 17c, d, simulations based on the finite element method indicated that Li-Sn alloys in the interface layer accelerated the diffusion of Li^+ through the interface and improved the uniformity of the Li^+ flux, contributing to stable cycling of the cell. Based on these findings, later studies revealed that CuCl- or CuBr-doped argyrodite-type sulfide electrolytes and Bi,O-co-doped Li_3PS_4 electrolytes also exhibited outstanding stability toward Li metal anodes [226–230].

3.3 Li-Alloy in the Anode

3.3.1 Mechanical Constraints

Li-containing alloys are characterized by robust mechanical strength and proficient electron and Li^+ conductivity attributes and have high potential as the structural matrices in composite Li anodes. The alloying process is facilitated by melting a surplus of Li and other alloy constituents at elevated temperatures. Upon subsequent cooling, the composite anode adopts a form, in which the unalloyed Li metal is confined within the construct of the alloy phase-based skeleton [231, 232]. Continuous mechanical rolling at room temperature can also accelerate the alloying process [233]. Since Li-containing alloys consistently exhibit higher potentials than pristine Li, the cycling process is governed primarily by the deposition/dissolution of Li metal, which is expertly regulated via cutoff voltage manipulation. Consequently, the alloy components persist as a stable framework, which does not participate in the alloying/dealloying contributions to the capacity evolution.

Initial investigations revealed a three-dimensional (3D) skeleton structure manifested by fibrous Li_7B_6 encapsulating free Li metal within the Li-B anode framework [159, 160, 234]. Furthermore, Wu et al. examined the impact of Mg doping on Li-LiB alloy anodes and reported an increase in the affinity between Li and the LiB skeleton consequent to Mg incorporation. The preparation process of this anode is shown in Fig. 18a. After Li stripping, the residual Li-deficient component (Li-Mg alloy) within the Mg-doped Li-LiB anode was found to facilitate robust interconnections among the LiB fibers, thus fortifying the structural integrity

[235]. However, the direct contact between the Li metal in the composite anode and SSEs, particularly the sulfide electrolytes, created a delay, accentuating the potential for an additional interlayer between the Mg-doped Li-LiB anode and the sulfide electrolyte [236].

The performance of the Li-Mg alloy-composed skeleton was also verified. Yang et al. engineered an Li-Mg anode incorporating 25% (by weight) Mg for employment in LLZTO-based ASSLBs [112]. SEM imaging revealed a scaffold structure of Li-deficient Li-Mg alloys characterized by nanoscale pores following dealloying; this was subsequently amenable to Li infiltration during the deposition process, culminating in the reformulation of Li-rich Li-Mg alloys. This dynamic process is visually shown in Fig. 18b. Evidently, this design conferred structural stability to the anode, preventing any erosion of the contact between the anode and garnet electrolyte. However, despite the enhancement in kinetics conferred by Mg addition (Fig. 18c), room temperature operability remains confined by its chemical diffusion coefficient, necessitating elevated temperature or increased external pressure, as indicated by the simulation results depicted in Fig. 18d [55].

In parallel, the incorporated Cu mesh, Ni mesh, or Ni particles can serve as alternative anode skeletons within the composite Li anode, although these entities serve predominantly as electronic conductors rather than ionic conductors [237–239]. The robust skeletal architecture with intrapore conduits effectively mitigates the volume fluctuations of the anode during cycling. Nevertheless, the high densities of Cu and Ni produce an increased mass fraction of inactive constituents within the battery assembly, potentially impeding the increase of cell-level specific capacity.

3.3.2 Promotion of Li Diffusion and Li Deposition

In addition to their foundational role as structural scaffolds, Li alloys can fulfill an additional noteworthy function as proficient functional constituents within the anode, attributed to their inherent lithiophilicity and elevated Li^+ diffusion coefficients [240–243]. The prevailing application of these materials encompasses their ability to effectively modulate the surface tension of Li metal through alloying, thereby enhancing the wettability of the anode toward SSEs, with a particular emphasis on oxide- and sulfide-based electrolytes [244–246]. A compelling instance is manifested through the utilization of molten Li-Sn composite alloys, wherein substrates are progressively wetted with increasing Sn mass ratios, culminating in complete wetting achieved

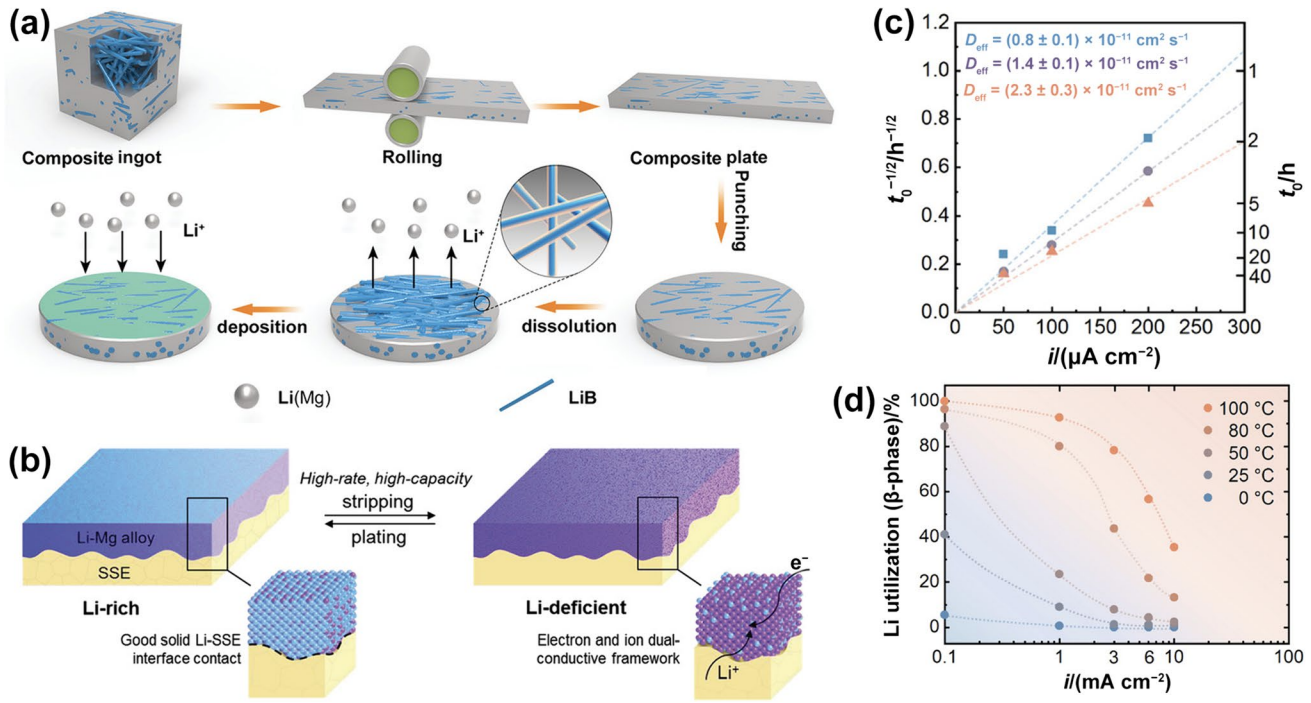

Fig. 18 Li-alloy skeletons in the anode. **a** Fabrication process and electrochemical behavior of the Mg-doped Li-LiB anode. Reprinted with permission from Ref. [235]. Copyright © 2020, Wiley-VCH. **b** Li stripping/plating behavior in the cell with the garnet-type SSE and the Li-Mg alloy anode. Reprinted with permission from Ref. [112]. Copyright © 2018, Wiley-VCH. **c** Effective Li diffusion coefficient of Li and Li-Mg alloys. The orange, gray and blue lines correspond to Li, $Li_{0.95}Mg_{0.5}$ and $Li_{0.9}Mg_{0.1}$, respectively. **d** Simulated Li utilization of the $Li_{0.9}Mg_{0.1}$ electrode as a function of current density at different temperatures. Reprinted with permission from Ref. [55]. Copyright © 2019, Wiley-VCH

at Sn contents exceeding 50%, as illustrated in Fig. 19a. This, in turn, creates a marked enhancement in interfacial contact, as corroborated by the discernibly low interfacial resistance (merely 7 Ω cm^{-2}) demonstrated by the symmetric Li-Sn|garnet|Li-Sn cell configuration. In stark contrast, the counterpart employing a pristine Li anode exhibits notably compromised interfacial contact, as evidenced by a substantially elevated interfacial resistance measuring approximately 1 000 Ω cm^{-2} [247].

Moreover, the incorporation of alloying elements within the anode matrix can exert a regulatory influence on the deposition of lithium. Theoretical computations reveal the evident proclivity of lithium atoms for mutual aggregation, thereby prompting an inclination toward undue expansion along specific orientations and provoking the formation of lithium dendrites. This tendency of lithium atoms to coalesce has been characterized succinctly in terms of cohesive energy; its manifestation has been illuminated through thorough first-principle calculations, yielding a computed cohesive energy (E_{coh}) of − 1.61 eV between lithium atoms [248, 249]. Notably, instances arise where the adsorption energy of lithium atoms onto the substrate decreases below the stipulated threshold of cohesive energy, thereby amplifying the propensity for lithium atom aggregation. Conversely, scenarios characterized by the substrate's adsorption energy surpassing the magnitude of the cohesive energy culminate in the uniform deposition of lithium atoms upon the substrate.

In light of these considerations, a notable contribution comes from the work of Li et al., who introduced an innovative $Li_{22}Sn_5$-enhanced composite Li anode supplemented with an LiC_6 scaffold, denoted as LiSnC; this electrode was specifically tailored for use in sulfide-based ASSLBs (Fig. 19b) [250]. A comparative analysis of the surface morphology of the LiSnC electrode (Fig. 19c) and the unmodified bare Li electrode (Fig. 19d) after lithium stripping showed compelling results. The adsorption energy of Li on $Li_{22}Sn_5$ significantly exceeded E_{coh}, preventing the deposited Li from aggregating into dendrites. Furthermore, the interconnected $Li_{22}Sn_5$ network played a pivotal role in replenishing the consumed lithium from the anode's bulk to the interface in a timely manner, thereby preventing the deterioration

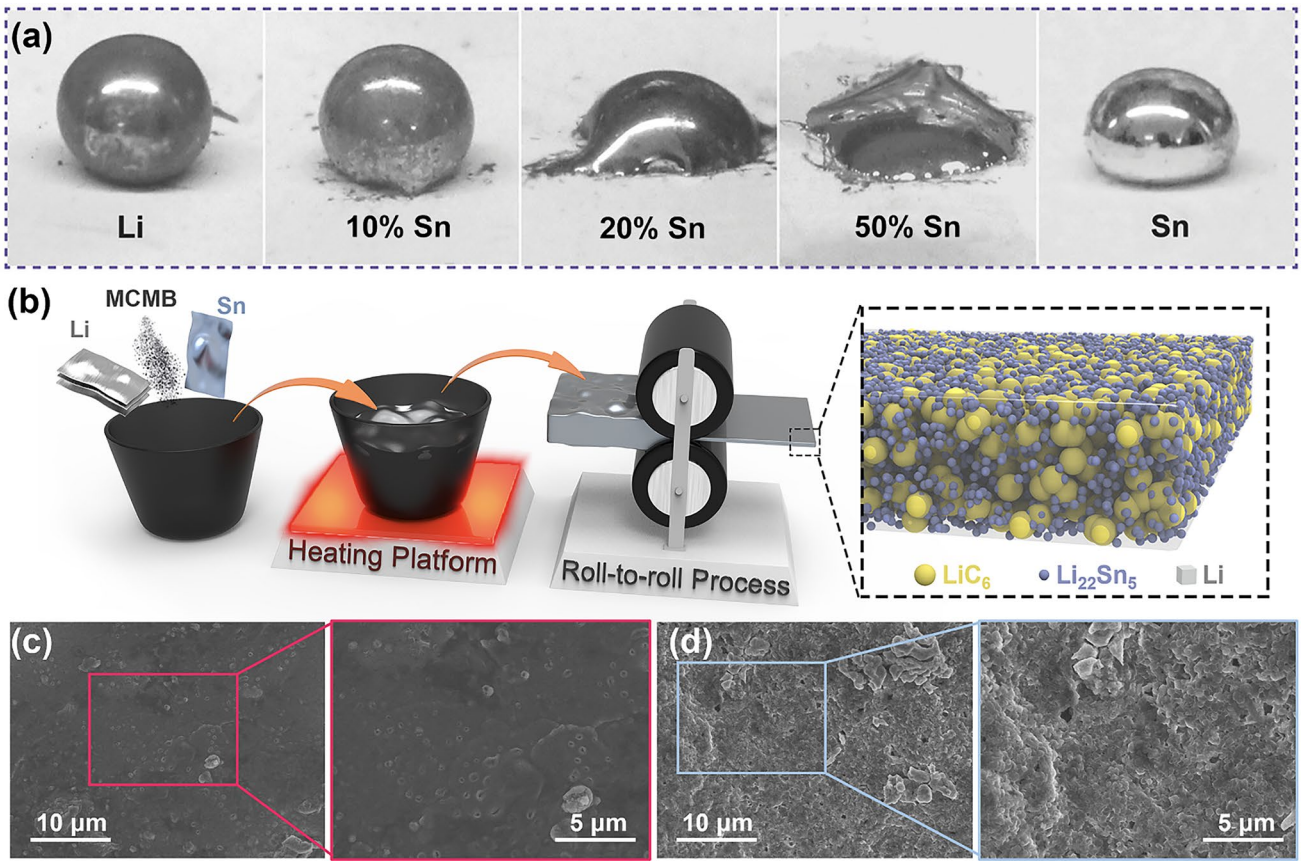

Fig. 19 Li alloys in the anode to promote Li deposition and diffusion. **a** Wetting ability of several molten Li-Sn alloys on Al_2O_3 substrates (the Sn contents of 10%, 20% and 50% are referred to weight percentages). Reprinted with permission from Ref. [247]. Copyright © 2017, Wiley-VCH. **b** Preparation process of the LiSnC electrode. Comparison of the surface morphology of the **c** LiSnC electrode and **d** bare Li electrode after Li stripping. Reprinted with permission from Ref. [250]. Copyright © 2023, Elsevier

of interfacial contacts between the anode and the sulfide electrolyte due to lithium depletion-induced porosity. This synergistic interplay exploits on the advantages of the three-dimensional design inherent to the composite anode due to the cooperative dynamics facilitated by $Li_{22}Sn_5$ and LiC_6 constituents.

The latest improvements in the performance of ASSLBs with Li alloys mentioned above are further summarized in Table 2. Generally, when both the cathode and the SSE are fixed, ASSLBs employing alloy anodes often demonstrate higher capacity retention and stabler CEs over the long term, at the expense of cell-level energy density. Additionally, cells with non-prelithiated alloy anodes may exhibit a lower initial CE due to the trapped lithium within the alloy and interface passivation. Nevertheless, the performance of alloy anodes is still widely acknowledged, as evidenced by the frequent use of Li-In alloys as reference electrodes. In addition, numerous studies focusing on electrolyte or cathode modifications still prefer Li-In alloys as anodes to ensure the stability of the anode/electrolyte interface.

Whether the alloy functions as the interface layer or the functional component within the anode, it essentially remains an Li metal anode, involving only the stripping/plating of metallic lithium during charging/discharging. Longstanding as the "holy grail" among anode materials, metallic lithium always enables the highest energy density of full cells. Introducing Li alloys into the surface or bulk of an Li-metal anode can improve the cycling stability by regulating the electrochemical behavior of Li. However, the effects of these modifications are still limited, as ASSLBs with alloy-modified anodes or alloy interlayers still exhibit a tendency for earlier failure during prolonged electrochemical cycling than those with pure alloy anodes. Additionally, the general applicability of these strategies across various electrolyte systems needs further discussion.

4 Conclusions and Perspectives

The practical attainment of ASSLBs faces a formidable challenge pertaining to the inherently unstable interface between the anode and SSE. This interface instability causes the following concerns: pronounced side reactions stemming from significant Fermi level disparities between the anode and SSE materials, compromising anode material utilization and overall battery performance; the intrusion of Li metal into the electrolyte due to electrolyte mechanical failures or concurrent Li^+ and electron flows; and contact loss issues during Li stripping. Among the various strategies for enhancing interface performance, the adoption of Li-alloy materials has garnered substantial attention, and these materials have exhibited efficacy in diverse contexts. In detail, there are three major Li-alloy material applications in ASSLBs: (1) as anodes, suppressing side reactions and Li metal intrusions; (2) as interlayers, ensuring contact and mitigating interphase overpotentials; and (3) within lithium-dominant anodes, lowering the nucleation potential and regulating Li^+ plating. This review provides Li-alloy thermodynamics, kinetics, and mechanics, substantiating property-application correlations while delving into the working principles and the applicability of Li alloys.

4.1 Thermodynamics

Three types of phase diagrams for Li-alloy systems are systematically discussed in terms of solubility. On the basis of the phase diagram, the redox potential and the specific capacity of Li alloy materials are correlated with their electrochemical performance when applied as anodes, and the detailed theoretical derivation process is shown. The Li-Mg alloy with the lowest average potential and Li-Si with the highest specific capacity may be promising candidates for use in alloy anodes. Moreover, the evolution of the phase structure accompanied by the crystal structure evolution of Li alloys during the lithiation/delithiation process is provided. In addition, this review proposes that more attention should be focused on the crystal structure evolution of Li alloys to consider their electrochemical performance.

4.2 Kinetics

Li-ion diffusion within alloys plays a vital role in shaping the electrochemical performance of ASSLBs. Two discernible modes of lithium diffusion, i.e., the interstitial and vacancy diffusion, are described, with direct hopping and coordination mechanisms delineating each mode. In addition, the diffusion coefficient serves as a critical metric in the context of alloy anodes undergoing phase transitions during electrochemical cycling. Moreover, the phenomenon in which lithium dendrites form in alloy anodes when deposition rates exceed diffusion rates should be considered in future studies.

4.3 Mechanics

In ASSLBs, the fracture and pulverization of alloy particles during cycling, coupled with void formation due to delithiation, elevate the charge carrier transport pathway tortuosity, increasing the battery resistance. Volume variations influence the battery pressure, impacting the electrochemical performance. The alloy's particle size and its partial molar volume of Li contribute to the pressure evolution. Mechanical properties also affect battery failure mechanisms, including contact loss and electrolyte fracture. Establishing the

Table 2 Summary of the performance of ASSLBs with Li alloys in recent reports

Anode	Cathode (areal loading)	Electrolyte	Test conditions	Capacity retention	References
Ag-C composite (mass ratio of Ag:C = 1:3)	$LiNi_{0.90}Co_{0.05}Mn_{0.05}O_2$ (6.8 mAh cm^{-2})	Li_6PS_5Cl	0.5 C 60 °C	89%, 1 000th	[57]
In-Li (mass ratio of In:Li = 98:2)	$LiNbO_3$-coated $LiNi_{0.6}Co_{0.2}Mn_{0.2}O_2$ (4 mAh cm^{-2})	Li_6PS_5Cl	3.8 mA cm^{-2} 25 °C	100%, 800th	[78]
$Li_{0.8}Al$	S (1 mg cm^{-2})	$Li_{10}GeP_2S_{12}$	0.2 C 25 °C	93.29%, 200th	[59]
$Al_{94.5}In_{5.5}$	$LiNi_{0.6}Mn_{0.2}Co_{0.2}O_2$ (2.1 mAh cm^{-2})	Li_6PS_5Cl	2 mA cm^{-2} 25 °C	100%, 500th	[151]
Composite anode with nano-Si (mass ratio of Si:SE:carbon black is 6:3:1)	Li_2SiO_x-coated $LiNi_{0.8}Mn_{0.1}Co_{0.1}O_2$ (20 mg cm^{-2})	Li_6PS_5Cl	C/3 RT	71.5%, 650th	[84]
Lithiated Si-hard carbon hybrid anode (mass ratio of Li:Si:HC = 23:29:44)	$LiNi_{0.8}Mn_{0.1}Co_{0.1}O_2$ (18.66 mg cm^{-2})	Li_6PS_5Cl	5.86 mA cm^{-2} 55 °C	80%, 1 033th; 61.5%, 5 000th	[116]
99.9% (by weight) micro-Si	$LiNi_{0.8}Mn_{0.1}Co_{0.1}O_2$ (25 mg cm^{-2})	Li_6PS_5Cl	5 mA cm^{-2} RT	80%, 500th	[114]
Li metal with the Li_ySn-Li_3N interlayer	$LiNi_{0.5}Co_{0.2}Mn_{0.3}O_2$ (1 mg cm^{-2})	$Li_{6.4}La_3Zr_{1.4}Ta_{0.6}O_{12}$	0.25 C 25 °C	92.6%, 200th	[207]
Li metal with the Li_xIn_y-Li_3N layer	$LiFePO_4$ (2 mg cm^{-2})	$Li_{6.4}La_3Zr_{1.4}Ta_{0.6}O_{12}$	0.2 C RT	92.4%, 110th	[209]
Li metal	$LiNi_{0.8}Mn_{0.1}Co_{0.1}O_2$ (3–4 mg cm^{-2})	$Li_{6.5}La_3Zr_{1.5}Ta_{0.5}O_{12}$ pellet with an LiF-LaF_3 interlayer	0.5 C RT	89%, 200th	[205]
Li metal anode with the composition gradient of Li-LiAl-LiF	$LiNi_{0.5}Co_{0.2}Mn_{0.3}O_2$ (4 mg cm^{-2})	$Li_{6.5}La_3Zr_{1.5}Ta_{0.5}O_{12}$	1.3 mA cm^{-2} RT	80%, 200th	[213]
Li anode with the Ag-Li layer	$LiNi_{0.6}Co_{0.2}Mn_{0.2}O_2$ (13 mg cm^{-2})	Li_6PS_5Cl	0.2 C 55 °C	93%, 140th	[56]
Li anode with an $Mg_{16}Bi_{84}$ interlayer	Cl-doped $LiNi_{0.8}Mn_{0.1}Co_{0.1}O_2$ (25.5 mg cm^{-2})	Li_6PS_5Cl	15.3 mA cm^{-2} 80 °C	64.3%, 300th	[115]
Li metal	$LiCoO_2$ (8.9 mg cm^{-2})	Glass-ceramic $Li_{3.2}P_{0.8}Sn_{0.2}S_4$	0.1 C RT	77%, 60th	[225]
Li metal	$LiCoO_2$ (2 mg cm^{-2})	Li_6PS_5Cl with Mg and F incorporation	0.2 C RT	93.3%, 100th	[251]
Li metal	$LiNi_{0.6}Mn_{0.2}Co_{0.2}O_2$ (1.34 mAh cm^{-2})	Li_6PS_5Cl-CEL (mass ratio of Li_6PS_5Cl: $Li_{10}GeP_2S_{12}$ = 9:1)	0.1 C RT	93.7%, 100th	[223]
Li metal with Cu_2O-GO coated Cu skeleton	$LiCoO_2$ (2.75 mg cm^{-2})	$Li_{10}GeP_2S_{12}$	0.1 C RT	92.9%, 120th	[237]
Mg doped Li-LiB alloy with Ag@C layer	S (1.3 mg cm^{-2})	$Li_{9.54}Si_{1.74}P_{1.44}S_{11.7}Cl_{0.3}$	0.2 C 60 °C	82%, 60th	[236]
Li-free Ni_C_Ag anode	$LiNbO_3$-coated $LiNi_{0.8}Co_{0.1}Mn_{0.1}O_2$ (17 mg cm^{-2})	$Li_6PS_5Cl_{0.5}Br_{0.5}$	0.5 mA cm^{-2} 30 °C	58.83%, 100th	[238]
Composite Li anode with LiC_6 skeleton and $Li_{22}Sn_5$	Li_2ZrF_6-coated $LiNi_{0.9}Co_{0.05}Mn_{0.05}O_2$ (6.24 mg cm^{-2})	Li_6PS_5Cl	0.2 C RT	73%, 80th	[250]

connection between alloy mechanical properties and battery failure mechanisms is crucial for advancing ASSLBs through advanced characterization techniques and theoretical analysis.

4.4 Application

Li alloys exhibit an advantageous capacity to mitigate side reactions and suppress dendrite growth when employed as

anode materials because of their elevated electrode potential relative to lithium and distinctive alloying electrode reactions. However, the practical feasibility of employing alloy-based anodes within ASSLBs warrants careful consideration. This is particularly pertinent when the alloy reaction is confined to the two-phase region. Consequently, the effective specific capacity of the alloy may markedly deviate from the requisites of high-energy-density battery applications. Moreover, even Si, heralded as a premier Li metalloid, encounters challenges in achieving high CEs within ASSLBs. In response, two strategies have emerged to address this predicament: the formulation of composite Si anodes and the attainment of diffusion-dependent Si anodes. Furthermore, when harnessed as interface modification layers, alloys have potential for enhancing the lithium wettability to electrolytes and possibly improving the stability of the anode/electrolyte interface. Nonetheless, the extent of stability enhancement remains a subject of ongoing scholarly debate. Finally, alloys find utility as framework materials for Li metal anodes, thereby enhancing the mechanical robustness of the electrode structure and concurrently lowering the energy barrier for lithium nucleation. This multifaceted role of alloys in electrode highlights their salient potential within the realm of advanced battery technologies.

4.5 Perspectives

In prospective investigations, the development of ASSLBs with Li alloys can be promoted through advanced characterization, theoretical calculations, and innovative designs (Fig. 20). The utilization of alloy materials for optimizing the interface between the anode and electrolyte necessitates a comprehensive characterization of the intrinsic thermodynamic, kinetic, and mechanical attributes of the material employing sophisticated characterization methodologies. Advanced techniques such as X-ray tomography, neutron computed tomography (CT) and cryo-TEM can provide valuable insights into the material properties, electrochemical processes, and structural changes occurring within the ASSLBs using Li-alloy materials. These characterizations can aid in identifying challenges, guiding material design, and accelerating the development of robust ASSLBs for practical applications.

Numerous opportunities exist in the compositional design of anodes with Li alloys, and an efficient screening method is highly necessary. Fortunately, the advancement of artificial intelligence (AI) and machine learning methods can accelerate the screening process for Li alloy materials applicable in ASSLBs. Specifically, high-throughput theoretical simulations provide a feasible avenue for simulating a series of alloy properties, encompassing potential, capacity, diffusion kinetics, interface dynamics, and mechanical characteristics. Based on these simulations, trained AI or machine learning models are expected to conduct a comprehensive theoretical evaluation of alloys, thereby providing guidance for future experiments. Furthermore, in-depth investigations into the behavior of the Li alloy/SE interfaces can also be achieved through high-throughput computational simulations to promote the exploration of material interactions and the design of innovative battery architectures. These computational insights have potential to facilitate academia and industry in determining suitable alloy candidates.

In the context of the application of Li alloys as anodes, instances of successful integration remain relatively limited. Drawing from examples such as Samsung's silver-carbon composite materials, future advances in composite alloy anodes may converge toward enhancing intrinsically robust mechanical attributes within the anode structure. This trajectory aims to mitigate the failure of active materials arising from structural alterations during the alloying processes. However, it is imperative to underscore that certain anodes, exemplified by Li-In, may predominantly serve as transition components. The application of these electrodes as practical anode materials for high specific energy ASSLBs is rather limited. In the domain of Li alloys as interface layers, debates persist regarding the capacity of pure Li alloys as effective electronic conductors to ensure interface stability with the electrolyte. Nevertheless, incorporating alloy materials at the anode/electrolyte interface has promise for bolstering interfacial stability. Finally, envisioning Li alloys as scaffold materials for metallic Li anodes is a compelling avenue. Leveraging their inherent mechanical strength, Li alloys can serve as rigid nucleation sites, thereby effectively suppressing the growth of damaging lithium dendrites. This multifaceted role accentuates the pronounced potential inherent in the integration of Li alloys toward achieving enhanced and stable energy storage devices.

ASSLBs with Li alloys provide significant promise for future energy storage technology. Currently, ASSLBs with alloy anodes have reached a relatively high level of maturity for commercialization. Due to their enhanced safety and energy density, ASSLBs are promising alternatives to traditional lithium-ion batteries employing graphite anodes. With ongoing developments in this field, various potential applications in electric vehicles, consumer electronics, and renewable energy storage are foreseeable. The application in electric vehicles is an example. The increased energy density of ASSLBs with alloy anodes extends the cruising range on a single charge. In addition, the improved resistance of alloy anodes to dendrite formation reduces the risk of thermal runaway. Moreover, the favorable rate performance of ASSLBs with alloy anodes, as demonstrated in recent reports, facilitates the prospect of fast charging. As research progresses, the incorporation of alloys into Li metal anodes has tremendous potential for propelling commercial ASSLBs toward the ultimate goal of achieving all-solid-state Li metal batteries. At that point, the field of energy storage will experience a revolutionary transformation.

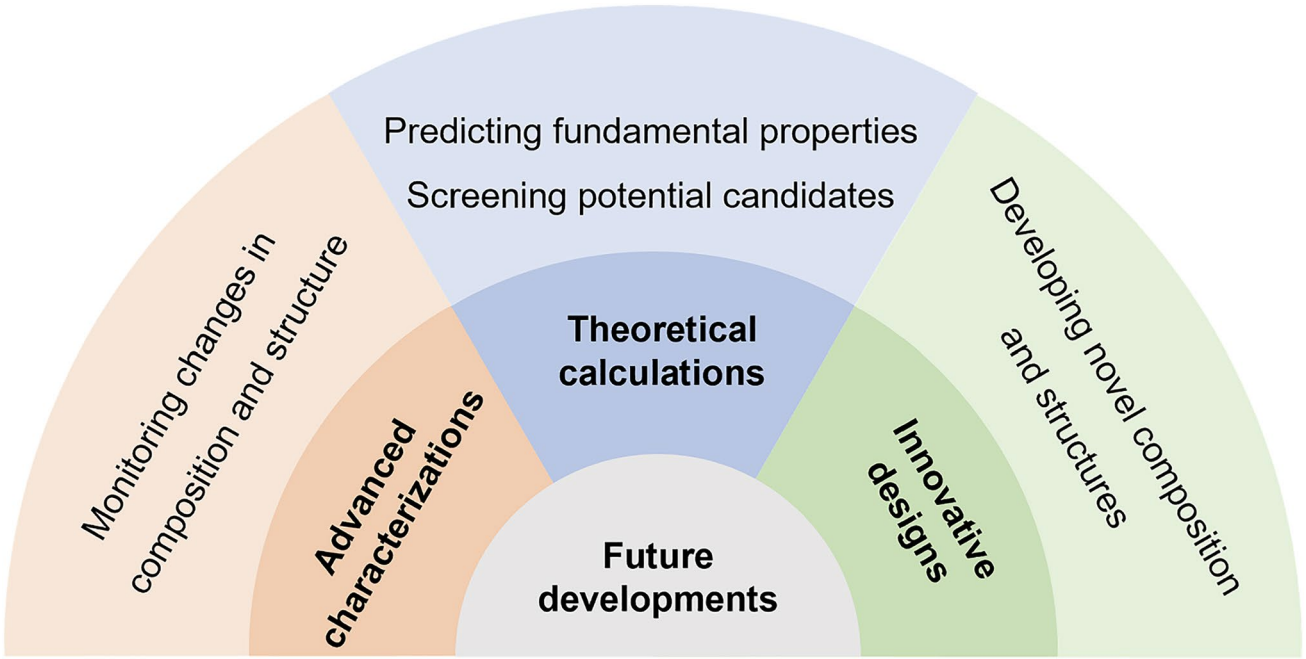

Fig. 20 Illustration of perspectives on ASSLBs with Li alloys

Acknowledgements This work was supported by National Natural Science Foundation of China (Grant Nos. 51971201, U20A20126, 52073253, and 52103350). Y. Zhong acknowledges the support by the Zhejiang Provincial Natural Science Foundation of China (No. LY23E020009). X.L. Wang acknowledges the support by Development Program of Zhejiang Province (No. 2022C01071).

Funding National Natural Science Foundation of China, 51971201, Jiangping Tu; U20A20126, Jiangping Tu; 52103350, Yu Zhong; 52073253, Xiuli Wang. Zhejiang Provincial Natural Science Foundation of China, LY23E020009, Yu Zhong. Development Program of Zhejiang Province, 2022C01071, Xiuli Wang.

Declarations

Conflict of interest The authors declare that they have no known competing financial interests or personal relationships that could have appeared to influence the work reported in this paper.

Ethical statement We hereby declare that this manuscript is the result of all authors' independent creation under the reviewer's comments. Except for the quoted contents, this manuscript does not contain any research achievements that have been published or written by other individuals or groups. We are the only authors of this manuscript. The legal responsibility of this statement should be borne by the corresponding authors.

References

1. Tarascon, J.M., Armand, M.: Issues and challenges facing rechargeable lithium batteries. Nature **414**, 359–367 (2001). https://doi.org/10.1038/35104644
2. Armand, M., Tarascon, J.M.: Building better batteries. Nature **451**, 652–657 (2008). https://doi.org/10.1038/451652a
3. Dunn, B., Kamath, H., Tarascon, J.M.: Electrical energy storage for the grid: a battery of choices. Science **334**, 928–935 (2011). https://doi.org/10.1126/science.1212741
4. Nitta, N., Wu, F.X., Lee, J.T., et al.: Li-ion battery materials: present and future. Mater. Today **18**, 252–264 (2015). https://doi.org/10.1016/j.mattod.2014.10.040
5. Zhang, J.G., Xu, W., Xiao, J., et al.: Lithium metal anodes with nonaqueous electrolytes. Chem. Rev. **120**, 13312–13348 (2020). https://doi.org/10.1021/acs.chemrev.0c00275
6. Goodenough, J.B., Park, K.S.: The Li-ion rechargeable battery: a perspective. J. Am. Chem. Soc. **135**, 1167–1176 (2013). https://doi.org/10.1021/ja3091438
7. Wang, Q., Lu, T.T., Xiao, Y.B., et al.: Leap of Li metal anodes from coin cells to pouch cells: challenges and progress. Electrochem. Energy Rev. **6**, 22 (2023). https://doi.org/10.1007/s41918-023-00185-7
8. Li, Y.L., Feng, X.N., Ren, D.S., et al.: Thermal runaway triggered by plated lithium on the anode after fast charging. ACS Appl. Mater. Interfaces **11**, 46839–46850 (2019). https://doi.org/10.1021/acsami.9b16589
9. Hou, J.X., Lu, L.G., Wang, L., et al.: Thermal runaway of Lithium-ion batteries employing $LiN(SO_2F)_2$-based concentrated electrolytes. Nat. Commun. **11**, 5100 (2020). https://doi.org/10.1038/s41467-020-18868-w
10. Jiao, S.H., Ren, X.D., Cao, R.G., et al.: Stable cycling of high-voltage lithium metal batteries in ether electrolytes. Nat. Energy **3**, 739–746 (2018). https://doi.org/10.1038/s41560-018-0199-8
11. Liu, H., Sun, X., Cheng, X.B., et al.: Working principles of lithium metal anode in pouch cells. Adv. Energy Mater. **12**, 2202518 (2022). https://doi.org/10.1002/aenm.202202518
12. Manthiram, A., Yu, X.W., Wang, S.F.: Lithium battery chemistries enabled by solid-state electrolytes. Nat. Rev. Mater. **2**, 16103 (2017). https://doi.org/10.1038/natrevmats.2016.103

13. Yang, C.P., Fu, K., Zhang, Y., et al.: Protected lithium-metal anodes in batteries: from liquid to solid. Adv. Mater. **29**, 1701169 (2017). https://doi.org/10.1002/adma.201701169
14. Yang, S.J., Hu, J.K., Jiang, F.N., et al.: Oxygen-induced thermal runaway mechanisms of Ah-level solid-state lithium metal pouch cells. ETransportation **18**, 100279 (2023). https://doi.org/10.1016/j.etran.2023.100279
15. Zhao, Q., Stalin, S., Zhao, C.Z., et al.: Designing solid-state electrolytes for safe, energy-dense batteries. Nat. Rev. Mater. **5**, 229–252 (2020). https://doi.org/10.1038/s41578-019-0165-5
16. Wu, J.H., Shen, L., Zhang, Z.H., et al.: All-solid-state lithium batteries with sulfide electrolytes and oxide cathodes. Electrochem. Energy Rev. **4**, 101–135 (2021). https://doi.org/10.1007/s41918-020-00081-4
17. Su, H., Jiang, Z., Liu, Y., et al.: Recent progress of sulfide electrolytes for all-solid-state lithium batteries. Energy Mater **2**, 205 (2022). https://doi.org/10.20517/energymater.2022.01
18. Vishnugopi, B.S., Kazyak, E., Lewis, J.A., et al.: Challenges and opportunities for fast charging of solid-state lithium metal batteries. ACS Energy Lett. **6**, 3734–3749 (2021). https://doi.org/10.1021/acsenergylett.1c01352
19. Xiao, Y.H., Wang, Y., Bo, S.H., et al.: Understanding interface stability in solid-state batteries. Nat. Rev. Mater. **5**, 105–126 (2019). https://doi.org/10.1038/s41578-019-0157-5
20. Wu, J.H., Liu, S.F., Han, F.D., et al.: Lithium/sulfide all-solid-state batteries using sulfide electrolytes. Adv. Mater. **33**, 2000751 (2021). https://doi.org/10.1002/adma.202000751
21. Su, H., Liu, Y., Zhong, Y., et al.: Stabilizing the interphase between Li and Argyrodite electrolyte through synergistic phosphating process for all-solid-state lithium batteries. Nano Energy **96**, 107104 (2022). https://doi.org/10.1016/j.nanoen.2022.107104
22. Han, F.D., Westover, A.S., Yue, J., et al.: High electronic conductivity as the origin of lithium dendrite formation within solid electrolytes. Nat. Energy **4**, 187–196 (2019). https://doi.org/10.1038/s41560-018-0312-z
23. Porz, L., Swamy, T., Sheldon, B.W., et al.: Mechanism of lithium metal penetration through inorganic solid electrolytes. Adv. Energy Mater. **7**, 1701003 (2017). https://doi.org/10.1002/aenm.201701003
24. Liu, H., Cheng, X.B., Huang, J.Q., et al.: Controlling dendrite growth in solid-state electrolytes. ACS Energy Lett. **5**, 833–843 (2020). https://doi.org/10.1021/acsenergylett.9b02660
25. Liu, X.M., Garcia-Mendez, R., Lupini, A.R., et al.: Local electronic structure variation resulting in Li 'filament' formation within solid electrolytes. Nat. Mater. **20**, 1485–1490 (2021). https://doi.org/10.1038/s41563-021-01019-x
26. Wang, C.H., Deng, T., Fan, X.L., et al.: Identifying soft breakdown in all-solid-state lithium battery. Joule **6**, 1770–1781 (2022). https://doi.org/10.1016/j.joule.2022.05.020
27. Sun, M.H., Liu, T.F., Yuan, Y.F., et al.: Visualizing lithium dendrite formation within solid-state electrolytes. ACS Energy Lett. **6**, 451–458 (2021). https://doi.org/10.1021/acsenergylett.0c02314
28. Kasemchainan, J., Zekoll, S., Spencer Jolly, D., et al.: Critical stripping current leads to dendrite formation on plating in lithium anode solid electrolyte cells. Nat. Mater. **18**, 1105–1111 (2019). https://doi.org/10.1038/s41563-019-0438-9
29. Li, J.R., Su, H., Li, M., et al.: A deformable dual-layer interphase for high-performance $Li_{10}GeP_2S_{12}$-based solid-state Li metal batteries. Chem. Eng. J. **431**, 134019 (2022). https://doi.org/10.1016/j.cej.2021.134019
30. Umeshbabu, E., Zheng, B.Z., Zhu, J.P., et al.: Stable cycling lithium-sulfur solid batteries with enhanced Li/$Li_{10}GeP_2S_{12}$ solid electrolyte interface stability. ACS Appl. Mater. Interfaces **11**, 18436–18447 (2019). https://doi.org/10.1021/acsami.9b03726
31. Xu, R., Liu, F., Ye, Y.S., et al.: A morphologically stable Li/electrolyte interface for all-solid-state batteries enabled by 3D-micropatterned garnet. Adv. Mater. **33**, 2104009 (2021). https://doi.org/10.1002/adma.202104009
32. Zhao, F.P., Sun, Q., Yu, C., et al.: Ultrastable anode interface achieved by fluorinating electrolytes for all-solid-state Li metal batteries. ACS Energy Lett. **5**, 1035–1043 (2020). https://doi.org/10.1021/acsenergylett.0c00207
33. Wang, C.H., Zhao, Y., Sun, Q., et al.: Stabilizing interface between $Li_{10}SnP_2S_{12}$ and Li metal by molecular layer deposition. Nano Energy **53**, 168–174 (2018). https://doi.org/10.1016/j.nanoen.2018.08.030
34. Wan, H.L., Liu, S.F., Deng, T., et al.: Bifunctional interphase-enabled $Li_{10}GeP_2S_{12}$ electrolytes for lithium-sulfur battery. ACS Energy Lett. **6**, 862–868 (2021). https://doi.org/10.1021/acsenergylett.0c02617
35. Ji, X., Hou, S., Wang, P.F., et al.: Solid-state electrolyte design for lithium dendrite suppression. Adv. Mater. **32**, 2002741 (2020). https://doi.org/10.1002/adma.202002741
36. Liu, Y., Su, H., Li, M., et al.: In situ formation of a Li_3N-rich interface between lithium and argyrodite solid electrolyte enabled by nitrogen doping. J. Mater. Chem. A **9**, 13531–13539 (2021). https://doi.org/10.1039/d1ta03343c
37. Bonnick, P., Muldoon, J.: The quest for the holy grail of solid-state lithium batteries. Energy Environ. Sci. **15**, 1840–1860 (2022). https://doi.org/10.1039/d2ee00842d
38. Du, M.J., Liao, K.M., Lu, Q., et al.: Recent advances in the interface engineering of solid-state Li-ion batteries with artificial buffer layers: challenges, materials, construction, and characterization. Energy Environ. Sci. **12**, 1780–1804 (2019). https://doi.org/10.1039/c9ee00515c
39. Chen, Y.M., Wang, Z.Q., Li, X.Y., et al.: Li metal deposition and stripping in a solid-state battery via Coble creep. Nature **578**, 251–255 (2020). https://doi.org/10.1038/s41586-020-1972-y
40. Rioja, R.J., Liu, J.: The evolution of Al-Li base products for aerospace and space applications. Metall. Mater. Trans. A **43**, 3325–3337 (2012). https://doi.org/10.1007/s11661-012-1155-z
41. Huang, Y.L., Shao, B.W., Han, F.D.: Li alloy anodes for high-rate and high-areal-capacity solid-state batteries. J. Mater. Chem. A **10**, 12350–12358 (2022). https://doi.org/10.1039/d2ta02339c
42. Shi, Z., Liu, M.L., Naik, D., et al.: Electrochemical properties of Li-Mg alloy electrodes for lithium batteries. J. Power Sources **92**, 70–80 (2001). https://doi.org/10.1016/s0378-7753(00)00521-8
43. Pelton, A.D.: The Cu-Li (copper-lithium) system. Bull. Alloy Phase Diagr. **7**, 142–144 (1986). https://doi.org/10.1007/BF02881552
44. Pelton, A.D.: The Ag-Li (silver-lithium) system. Bull. Alloy Phase Diagr. **7**, 223–228 (1986). https://doi.org/10.1007/BF02868993
45. Nayeb-Hashemi, A.A., Clark, J.B., Pelton, A.D.: The Li-Mg (lithium-magnesium) system. Bull. Alloy Phase Diagr. **5**, 365–374 (1984). https://doi.org/10.1007/BF02872951
46. Songster, J., Pelton, A.D.: The In-Li (indium-lithium) system. J. Phase Equilib. **12**, 37–41 (1991). https://doi.org/10.1007/BF02663671
47. Sangster, J., Bale, C.W.: The Li-Sn (lithium-tin) system. J. Phase Equilib. **19**, 70–75 (1998). https://doi.org/10.1361/105497198770342788
48. McAlister, A.J.: The Al-Li (aluminum-lithium) system. Bull. Alloy Phase Diagr. **3**, 177–183 (1982). https://doi.org/10.1007/BF02892377
49. Gąsior, W., Onderka, B., Moser, Z., et al.: Thermodynamic evaluation of Cu-Li phase diagram from EMF measurements and DTA

study. Calphad **33**, 215–220 (2009). https://doi.org/10.1016/j.calphad.2008.10.006
50. Adams, B.D., Zheng, J.M., Ren, X.D., et al.: Accurate determination of coulombic efficiency for lithium metal anodes and lithium metal batteries. Adv. Energy Mater. **8**, 1702097 (2018). https://doi.org/10.1002/aenm.201702097
51. Sun, M.H., Wei, J.K., Xu, Z., et al.: Electrochemical solid-state amorphization in the immiscible Cu-Li system. Sci. Bull. **63**, 1208–1214 (2018). https://doi.org/10.1016/j.scib.2018.06.021
52. Jin, S., Ye, Y.D., Niu, Y.J., et al.: Solid-solution-based metal alloy phase for highly reversible lithium metal anode. J. Am. Chem. Soc. **142**, 8818–8826 (2020). https://doi.org/10.1021/jacs.0c01811
53. Guo, B.C., Guo, P.Y., Zhao, G.H., et al.: A solid-solution-based Li-Mg alloy for highly stable lithium metal anodes. Sustain. Energy Fuels **6**, 4137–4145 (2022). https://doi.org/10.1039/d2se00910b
54. Braga, M.H., Dębski, A., Terlicka, S., et al.: Experimental and ab initio study of the Ag-Li system for energy storage and high-temperature solders. J. Alloys Compd. **817**, 152811 (2020). https://doi.org/10.1016/j.jallcom.2019.152811
55. Krauskopf, T., Mogwitz, B., Rosenbach, C., et al.: Diffusion limitation of lithium metal and Li-Mg alloy anodes on LLZO type solid electrolytes as a function of temperature and pressure. Adv. Energy Mater. **9**, 1902568 (2019). https://doi.org/10.1002/aenm.201902568
56. Choi, H.J., Kang, D.W., Park, J.W., et al.: In situ formed Ag-Li intermetallic layer for stable cycling of all-solid-state lithium batteries. Adv. Sci. **9**, 2103826 (2022). https://doi.org/10.1002/advs.202103826
57. Lee, Y.G., Fujiki, S., Jung, C., et al.: High-energy long-cycling all-solid-state lithium metal batteries enabled by silver-carbon composite anodes. Nat. Energy **5**, 299–308 (2020). https://doi.org/10.1038/s41560-020-0575-z
58. Prasad, N.E., Ramachandran, T.R.: Phase diagrams and phase reactions in Al-Li alloys. In: Prasad, N.E., Gokhale, A.A., Wanhill, R.J.H. (eds.) Aluminum-Lithium Alloys, pp. 61–97. Butterworth-Heinemann, Boston (2014)
59. Pan, H., Zhang, M.H., Cheng, Z., et al.: Carbon-free and binder-free Li-Al alloy anode enabling an all-solid-state Li-S battery with high energy and stability. Sci. Adv. **8**, eabn4372372 (2022). https://doi.org/10.1126/sciadv.abn4372
60. Huggins, R.A.: Lithium alloy negative electrodes. J. Power Sources **81**(82), 13–19 (1999). https://doi.org/10.1016/s0378-7753(99)00124-x
61. Boukamp, B.A., Lesh, G.C., Huggins, R.A.: All-solid lithium electrodes with mixed-conductor matrix. J. Electrochem. Soc. **128**, 725–729 (1981). https://doi.org/10.1149/1.2127495
62. Obrovac, M.N., Chevrier, V.L.: Alloy negative electrodes for Li-ion batteries. Chem. Rev. **114**, 11444–11502 (2014). https://doi.org/10.1021/cr500207g
63. Taillades, G., Sarradin, J.: Silver: high performance anode for thin film lithium ion batteries. J. Power Sources **125**, 199–205 (2004). https://doi.org/10.1016/j.jpowsour.2003.07.004
64. Beutl, A., Fürtauer, S., Flandorfer, H.: A novel apparatus for coulometric titrations in lithium containing systems. Thermochim. Acta **653**, 8–15 (2017). https://doi.org/10.1016/j.tca.2017.03.025
65. Hänsel, C., Singh, B., Kiwic, D., et al.: Favorable interfacial chemomechanics enables stable cycling of high-Li-content Li-In/Sn anodes in sulfide electrolyte-based solid-state batteries. Chem. Mater. **33**, 6029–6040 (2021). https://doi.org/10.1021/acs.chemmater.1c01431
66. Mayo, M., Morris, A.J.: Structure prediction of Li-Sn and Li-Sb intermetallics for lithium-ion batteries anodes. Chem. Mater. **29**, 5787–5795 (2017). https://doi.org/10.1021/acs.chemmater.6b04914
67. Huo, H.Y., Janek, J.: Silicon as emerging anode in solid-state batteries. ACS Energy Lett. **7**, 4005–4016 (2022). https://doi.org/10.1021/acsenergylett.2c01950
68. Pelton, A.D.: General phase diagram sections. In: Pelton, A.D. (ed.) Phase Diagrams and Thermodynamic Modeling of Solutions, pp. 103–131. Elsevier, Amsterdam (2019)
69. Li, Y.J., Li, J.P., Xiao, H., et al.: A novel 3D Li/Li_9Al_4/Li-Mg alloy anode for superior lithium metal batteries. Adv. Funct. Mater. **33**, 2213905 (2023). https://doi.org/10.1002/adfm.202213905
70. Qu, J.L., Xiao, J.W., Wang, T.S., et al.: High rate transfer mechanism of lithium ions in lithium-tin and lithium-indium alloys for lithium batteries. J. Phys. Chem. C **124**, 24644–24652 (2020). https://doi.org/10.1021/acs.jpcc.0c07880
71. Lu, Y., Zhao, C.Z., Zhang, R., et al.: The carrier transition from Li atoms to Li vacancies in solid-state lithium alloy anodes. Sci. Adv. **7**, eabi5520 (2021). https://doi.org/10.1126/sciadv.abi5520
72. Gąsior, W., Moser, Z.: Chemical diffusion coefficients in solid Al-Li alloys at low Li concentrations. Scand. J. Metall. **31**, 353–358 (2002). https://doi.org/10.1034/j.1600-0692.2002.00465.x
73. Jow, T.R., Liang, C.C.: Lithium-aluminum electrodes at ambient temperatures. J. Electrochem. Soc. **129**, 1429–1434 (1982). https://doi.org/10.1149/1.2124178
74. Korblein, A., Heitjans, P., Stockmann, H.J., et al.: Diffusion processes in solid Li-Mg and Li-Ag alloys and the spin-lattice relaxation of ^{8}Li. J. Phys. F: Met. Phys. **15**, 561–577 (1985). https://doi.org/10.1088/0305-4608/15/3/011
75. Zhang, Y., Ravi Chandran, K.S., Jagannathan, M., et al.: The nature of electrochemical delithiation of Li-Mg alloy electrodes: neutron computed tomography and analytical modeling of Li diffusion and delithiation phenomenon. J. Electrochem. Soc. **164**, A28–A38 (2016). https://doi.org/10.1149/2.0051702jes
76. Choi, Y.S., Scanlon, D.O., Lee, J.C.: Extending the performance limit of anodes: insights from diffusion kinetics of alloying anodes. Adv. Energy Mater. **11**, 2003078 (2021). https://doi.org/10.1002/aenm.202003078
77. Ye, Y.D., Xie, H.Y., Yang, Y.H., et al.: Solid-solution or intermetallic compounds: phase dependence of the Li-alloying reactions for Li-metal batteries. J. Am. Chem. Soc. **145**, 24775–24784 (2023). https://doi.org/10.1021/jacs.3c08711
78. Luo, S.T., Wang, Z.Y., Li, X.L., et al.: Growth of lithium-indium dendrites in all-solid-state lithium-based batteries with sulfide electrolytes. Nat. Commun. **12**, 6968 (2021). https://doi.org/10.1038/s41467-021-27311-7
79. Zeng, D.W., Yao, J.M., Zhang, L., et al.: Promoting favorable interfacial properties in lithium-based batteries using chlorine-rich sulfide inorganic solid-state electrolytes. Nat. Commun. **13**, 1909 (2022). https://doi.org/10.1038/s41467-022-29596-8
80. Shi, P., Cheng, X.B., Li, T., et al.: Electrochemical diagram of an ultrathin lithium metal anode in pouch cells. Adv. Mater. **31**, 1902785 (2019). https://doi.org/10.1002/adma.201902785
81. Su, Y.B., Ye, L.H., Fitzhugh, W., et al.: A more stable lithium anode by mechanical constriction for solid state batteries. Energy Environ. Sci. **13**, 908–916 (2020). https://doi.org/10.1039/c9ee04007b
82. Ye, L.H., Li, X.: A dynamic stability design strategy for lithium metal solid state batteries. Nature **593**, 218–222 (2021). https://doi.org/10.1038/s41586-021-03486-3
83. Lee, G.H., Lee, S.G., Park, S.H., et al.: Interface engineering on a Li metal anode for an electro-chemo-mechanically stable anodic interface in all-solid-state batteries. J. Mater. Chem. A **10**, 10662–10671 (2022). https://doi.org/10.1039/d1ta11066g
84. Cao, D.X., Sun, X., Li, Y.J., et al.: Long-cycling sulfide-based all-solid-state batteries enabled by electrochemo-mechanically stable electrodes. Adv. Mater. **34**, 2200401 (2022). https://doi.org/10.1002/adma.202200401

85. Wu, X.H., Billaud, J., Jerjen, I., et al.: Operando visualization of morphological dynamics in all-solid-state batteries. Adv. Energy Mater. **9**, 1901547 (2019). https://doi.org/10.1002/aenm.201901547
86. Liu, X.H., Zhong, L., Huang, S., et al.: Size-dependent fracture of silicon nanoparticles during lithiation. ACS Nano **6**, 1522–1531 (2012). https://doi.org/10.1021/nn204476h
87. Liu, H.B., Sun, Q., Zhang, H.Q., et al.: The application road of silicon-based anode in lithium-ion batteries: from liquid electrolyte to solid-state electrolyte. Energy Storage Mater. **55**, 244–263 (2023). https://doi.org/10.1016/j.ensm.2022.11.054
88. Hirai, K., Ichitsubo, T., Uda, T., et al.: Effects of volume strain due to Li-Sn compound formation on electrode potential in lithium-ion batteries. Acta Mater. **56**, 1539–1545 (2008). https://doi.org/10.1016/j.actamat.2007.12.002
89. Li, H.Y., Yamaguchi, T., Matsumoto, S., et al.: Circumventing huge volume strain in alloy anodes of lithium batteries. Nat. Commun. **11**, 1584 (2020). https://doi.org/10.1038/s41467-020-15452-0
90. Heligman, B.T., Manthiram, A.: Elemental foil anodes for lithium-ion batteries. ACS Energy Lett. **6**, 2666–2672 (2021). https://doi.org/10.1021/acsenergylett.1c01145
91. Lee, S.W., McDowell, M.T., Berla, L.A., et al.: Fracture of crystalline silicon nanopillars during electrochemical lithium insertion. Proc. Natl. Acad. Sci. U. S. A. **109**, 4080–4085 (2012). https://doi.org/10.1073/pnas.1201088109
92. Zhao, K.J., Pharr, M., Wan, Q., et al.: Concurrent reaction and plasticity during initial lithiation of crystalline silicon in lithium-ion batteries. J. Electrochem. Soc. **159**, A238–A243 (2012). https://doi.org/10.1149/2.020203jes
93. Sun, F., Dong, K., Osenberg, M., et al.: Visualizing the morphological and compositional evolution of the interface of InLi-anode|thio-LISION electrolyte in an all-solid-state Li-S cell by in operando synchrotron X-ray tomography and energy dispersive diffraction. J. Mater. Chem. A **6**, 22489–22496 (2018). https://doi.org/10.1039/c8ta08821g
94. Wu, H., Chan, G., Choi, J.W., et al.: Stable cycling of double-walled silicon nanotube battery anodes through solid-electrolyte interphase control. Nat. Nanotechnol. **7**, 310–315 (2012). https://doi.org/10.1038/nnano.2012.35
95. Liang, W.T., Yang, H., Fan, F.F., et al.: Tough germanium nanoparticles under electrochemical cycling. ACS Nano **7**, 3427–3433 (2013). https://doi.org/10.1021/nn400330h
96. Zhang, W.B., Schröder, D., Arlt, T., et al.: (Electro)chemical expansion during cycling: monitoring the pressure changes in operating solid-state lithium batteries. J. Mater. Chem. A **5**, 9929–9936 (2017). https://doi.org/10.1039/c7ta02730c
97. Hänsel, C., Kumar, P.V., Kundu, D.P.: Stack pressure effect in Li_3PS_4 and Na_3PS_4 based alkali metal solid-state cells: the dramatic implication of interlayer growth. Chem. Mater. **32**, 10501–10510 (2020). https://doi.org/10.1021/acs.chemmater.0c03444
98. Lim, H., Jun, S., Song, Y.B., et al.: Operando electrochemical pressiometry probing interfacial evolution of electrodeposited thin lithium metal anodes for all-solid-state batteries. Energy Storage Mater. **50**, 543–553 (2022). https://doi.org/10.1016/j.ensm.2022.05.050
99. Obrovac, M.N., Christensen, L., Le, D.B., et al.: Alloy design for lithium-ion battery anodes. J. Electrochem. Soc. **154**, A849 (2007). https://doi.org/10.1149/1.2752985
100. Han, S.Y., Lee, C., Lewis, J.A., et al.: Stress evolution during cycling of alloy-anode solid-state batteries. Joule **5**, 2450–2465 (2021). https://doi.org/10.1016/j.joule.2021.07.002
101. Ham, S.Y., Yang, H.D., Nunez-cuacuas, O., et al.: Assessing the critical current density of all-solid-state Li metal symmetric and full cells. Energy Storage Mater. **55**, 455–462 (2023). https://doi.org/10.1016/j.ensm.2022.12.013
102. Fan, X.L., Ji, X., Han, F.D., et al.: Fluorinated solid electrolyte interphase enables highly reversible solid-state Li metal battery. Sci. Adv. **4**, eaau9245 (2018). https://doi.org/10.1126/sciadv.aau9245
103. Lepley, N.D., Holzwarth, N.A.W., Du, Y.J.A.: Structures, Li^+ mobilities, and interfacial properties of solid electrolytes Li_3PS_4 and Li_3PO_4 from first principles. Phys. Rev. B **88**, 104103 (2013). https://doi.org/10.1103/PhysRevB.88.104103
104. Nagao, M., Hayashi, A., Tatsumisago, M., et al.: In situ SEM study of a lithium deposition and dissolution mechanism in a bulk-type solid-state cell with a Li_2S-P_2S_5 solid electrolyte. Phys. Chem. Chem. Phys. **15**, 18600 (2013). https://doi.org/10.1039/c3cp51059j
105. Yi, J.G., Zhou, D., Liang, Y.H., et al.: Enabling high-performance all-solid-state lithium batteries with high ionic conductive sulfide-based composite solid electrolyte and ex-situ artificial SEI film. J. Energy Chem. **58**, 17–24 (2021). https://doi.org/10.1016/j.jechem.2020.09.038
106. Jiang, Z., Li, Z.X., Wang, X.L., et al.: Robust Li_6PS_5I interlayer to stabilize the tailored electrolyte $Li_{9.95}SnP_2S_{11.95}F_{0.05}$/Li metal interface. ACS Appl. Mater. Interfaces **13**, 30739–30745 (2021). https://doi.org/10.1021/acsami.1c07947
107. Liu, Y., Peng, H.L., Su, H., et al.: Ultrafast synthesis of I-rich lithium argyrodite glass-ceramic electrolyte with high ionic conductivity. Adv. Mater. **34**, 2107346 (2022). https://doi.org/10.1002/adma.202107346
108. Hiratani, M.: Effect of a lithium alloy layer inserted between a lithium anode and a solid electrolyte. Solid State Ion. **28**(29/30), 1406–1410 (1988). https://doi.org/10.1016/0167-2738(88)90394-3
109. Takada, K.: Solid state lithium battery with oxysulfide glass. Solid State Ion. **86**(87/88), 877–882 (1996). https://doi.org/10.1016/0167-2738(96)00199-3
110. Notten, P., Roozeboom, F., Niessen, R., et al.: 3-D integrated all-solid-state rechargeable batteries. Adv. Mater. **19**, 4564–4567 (2007). https://doi.org/10.1002/adma.200702398
111. Han, X.G., Gong, Y.H., Fu, K., et al.: Negating interfacial impedance in garnet-based solid-state Li metal batteries. Nat. Mater. **16**, 572–579 (2017). https://doi.org/10.1038/nmat4821
112. Yang, C.P., Xie, H., Ping, W.W., et al.: An electron/ion dual-conductive alloy framework for high-rate and high-capacity solid-state lithium-metal batteries. Adv. Mater. **31**, 1804815 (2019). https://doi.org/10.1002/adma.201804815
113. Park, R.J.Y., Eschler, C.M., Fincher, C.D., et al.: Semi-solid alkali metal electrodes enabling high critical current densities in solid electrolyte batteries. Nat. Energy **6**, 314–322 (2021). https://doi.org/10.1038/s41560-021-00786-w
114. Tan, D.H.S., Chen, Y.T., Yang, H.D., et al.: Carbon-free high-loading silicon anodes enabled by sulfide solid electrolytes. Science **373**, 1494–1499 (2021). https://doi.org/10.1126/science.abg7217
115. Wan, H.L., Wang, Z.Y., Zhang, W.R., et al.: Interface design for all-solid-state lithium batteries. Nature **623**, 739–744 (2023). https://doi.org/10.1038/s41586-023-06653-w
116. Yan, W.L., Mu, Z.L., Wang, Z.X., et al.: Hard-carbon-stabilized Li-Si anodes for high-performance all-solid-state Li-ion batteries. Nat. Energy **8**, 800–813 (2023). https://doi.org/10.1038/s41560-023-01279-8
117. Wan, J., Song, Y.X., Chen, W.P., et al.: Micromechanism in all-solid-state alloy-metal batteries: regulating homogeneous lithium precipitation and flexible solid electrolyte interphase evolution. J. Am. Chem. Soc. **143**, 839–848 (2021). https://doi.org/10.1021/jacs.0c10121
118. Li, D.Q., Chu, F.L., He, Z.J., et al.: Single-material aluminum foil as anodes enabling high-performance lithium-ion batteries:

the roles of prelithiation and working mechanism. Mater. Today **58**, 80–90 (2022). https://doi.org/10.1016/j.mattod.2022.07.004
119. Kim, M.S., Deepika, N., Lee, S.H., et al.: Enabling reversible redox reactions in electrochemical cells using protected LiAl intermetallics as lithium metal anodes. Sci. Adv. **5**, eaax5587 (2019). https://doi.org/10.1126/sciadv.aax5587
120. Kamaya, N., Homma, K., Yamakawa, Y., et al.: A lithium superionic conductor. Nat. Mater. **10**, 682–686 (2011). https://doi.org/10.1038/nmat3066
121. Kato, Y., Hori, S., Saito, T., et al.: High-power all-solid-state batteries using sulfide superionic conductors. Nat. Energy **1**, 16030 (2016). https://doi.org/10.1038/nenergy.2016.30
122. Wu, Z., Li, X.H., Zheng, C., et al.: Interfaces in sulfide solid electrolyte-based all-solid-state lithium batteries: characterization, mechanism and strategy. Electrochem. Energy Rev. **6**, 10 (2023). https://doi.org/10.1007/s41918-022-00176-0
123. Nakamura, T., Amezawa, K., Kulisch, J., et al.: Guidelines for all-solid-state battery design and electrode buffer layers based on chemical potential profile calculation. ACS Appl. Mater. Interfaces **11**, 19968–19976 (2019). https://doi.org/10.1021/acsami.9b03053
124. Zhu, Y.Z., He, X.F., Mo, Y.F.: Origin of outstanding stability in the lithium solid electrolyte materials: insights from thermodynamic analyses based on first-principles calculations. ACS Appl. Mater. Interfaces **7**, 23685–23693 (2015). https://doi.org/10.1021/acsami.5b07517
125. Chen, S.J., Xie, D.J., Liu, G.Z., et al.: Sulfide solid electrolytes for all-solid-state lithium batteries: structure, conductivity, stability and application. Energy Storage Mater. **14**, 58–74 (2018). https://doi.org/10.1016/j.ensm.2018.02.020
126. Wenzel, S., Weber, D.A., Leichtweiss, T., et al.: Interphase formation and degradation of charge transfer kinetics between a lithium metal anode and highly crystalline $Li_7P_3S_{11}$ solid electrolyte. Solid State Ion. **286**, 24–33 (2016). https://doi.org/10.1016/j.ssi.2015.11.034
127. Gao, J., Zhu, J.X., Li, X.L., et al.: Rational design of mixed electronic-ionic conducting Ti-doping $Li_7La_3Zr_2O_{12}$ for lithium dendrites suppression. Adv. Funct. Mater. **31**, 2001918 (2021). https://doi.org/10.1002/adfm.202001918
128. Riegger, L.M., Schlem, R., Sann, J., et al.: Lithium-metal anode instability of the superionic halide solid electrolytes and the implications for solid-state batteries. Angew. Chem. Int. Ed. **60**, 6718–6723 (2021). https://doi.org/10.1002/anie.202015238
129. Riegger, L.M., Otto, S.K., Sadowski, M., et al.: Instability of the Li_7SiPS_8 solid electrolyte at the lithium metal anode and interphase formation. Chem. Mater. **34**, 3659–3669 (2022). https://doi.org/10.1021/acs.chemmater.1c04302
130. Il'ina, E.A., Lylin, E.D., Plekhanov, M.S.: Investigation of Li-In alloy application as anode for all-solid-state batteries. J. Phys.: Conf. Ser. **1967**, 012012 (2021). https://doi.org/10.1088/1742-6596/1967/1/012012
131. Santhosha, A.L., Medenbach, L., Buchheim, J.R., et al.: The indium-lithium electrode in solid-state lithium-ion batteries: phase formation, redox potentials, and interface stability. Batter. Supercaps **2**, 524–529 (2019). https://doi.org/10.1002/batt.201800149
132. Li, X.N., Liang, J.W., Chen, N., et al.: Water-mediated synthesis of a superionic halide solid electrolyte. Angew. Chem. Int. Ed. **58**, 16427–16432 (2019). https://doi.org/10.1002/anie.201909805
133. Park, K.H., Kaup, K., Assoud, A., et al.: High-voltage superionic halide solid electrolytes for all-solid-state Li-ion batteries. ACS Energy Lett. **5**, 533–539 (2020). https://doi.org/10.1021/acsenergylett.9b02599
134. Koç, T., Hallot, M., Quemin, E., et al.: Toward optimization of the chemical/electrochemical compatibility of halide solid electrolytes in all-solid-state batteries. ACS Energy Lett. **7**, 2979–2987 (2022). https://doi.org/10.1021/acsenergylett.2c01668
135. Liu, Y., Su, H., Zhong, Y., et al.: Revealing the impact of Cl substitution on the crystallization behavior and interfacial stability of superionic lithium argyrodites. Adv. Funct. Mater. **32**, 2207978 (2022). https://doi.org/10.1002/adfm.202207978
136. Yamada, Y., Furukawa, K., Sodeyama, K., et al.: Unusual stability of acetonitrile-based superconcentrated electrolytes for fast-charging lithium-ion batteries. J. Am. Chem. Soc. **136**, 5039–5046 (2014). https://doi.org/10.1021/ja412807w
137. Zhang, W.D., Wu, Q., Huang, J.X., et al.: Colossal granular lithium deposits enabled by the grain-coarsening effect for high-efficiency lithium metal full batteries. Adv. Mater. **32**, 2001740 (2020). https://doi.org/10.1002/adma.202001740
138. Yang, Q.F., Hu, J.L., Meng, J.W., et al.: C-F-rich oil drop as a non-expendable fluid interface modifier with low surface energy to stabilize a Li metal anode. Energy Environ. Sci. **14**, 3621–3631 (2021). https://doi.org/10.1039/d0ee03952g
139. Liu, F.F., Wang, L.F., Zhang, Z.W., et al.: A mixed lithium-ion conductive Li_2S/Li_2Se protection layer for stable lithium metal anode. Adv. Funct. Mater. **30**, 2001607 (2020). https://doi.org/10.1002/adfm.202001607
140. Chen, J., Fan, X.L., Li, Q., et al.: Electrolyte design for LiF-rich solid-electrolyte interfaces to enable high-performance microsized alloy anodes for batteries. Nat. Energy **5**, 386–397 (2020). https://doi.org/10.1038/s41560-020-0601-1
141. Ming, J., Cao, Z., Wahyudi, W., et al.: New insights on graphite anode stability in rechargeable batteries: Li ion coordination structures prevail over solid electrolyte interphases. ACS Energy Lett. **3**, 335–340 (2018). https://doi.org/10.1021/acsenergylett.7b01177
142. Gao, T., Han, Y., Fraggedakis, D., et al.: Interplay of lithium intercalation and plating on a single graphite particle. Joule **5**, 393–414 (2021). https://doi.org/10.1016/j.joule.2020.12.020
143. Lewis, J.A., Cavallaro, K.A., Liu, Y., et al.: The promise of alloy anodes for solid-state batteries. Joule **6**, 1418–1430 (2022). https://doi.org/10.1016/j.joule.2022.05.016
144. Janek, J., Zeier, W.G.: A solid future for battery development. Nat. Energy **1**, 16141 (2016). https://doi.org/10.1038/nenergy.2016.141
145. Randau, S., Weber, D.A., Kötz, O., et al.: Benchmarking the performance of all-solid-state lithium batteries. Nat. Energy **5**, 259–270 (2020). https://doi.org/10.1038/s41560-020-0565-1
146. Sun, Y.L., Suzuki, K., Hori, S., et al.: Superionic conductors: $Li_{10+\delta}[Sn_ySi_{1-y}]_{1+\delta}P_{2-\delta}S_{12}$ with a $Li_{10}GeP_2S_{12}$-type structure in the Li_3PS_4-Li_4SnS_4-Li_4SiS_4 quasi-ternary system. Chem. Mater. **29**, 5858–5864 (2017). https://doi.org/10.1021/acs.chemmater.7b00886
147. Huang, W.Z., Yoshino, K., Hori, S., et al.: Superionic lithium conductor with a cubic argyrodite-type structure in the Li-Al-Si-S system. J. Solid State Chem. **270**, 487–492 (2019). https://doi.org/10.1016/j.jssc.2018.12.015
148. Wang, C.H., Liang, J.W., Kim, J.T., et al.: Prospects of halide-based all-solid-state batteries: from material design to practical application. Sci. Adv. **8**, eadc9516 (2022). https://doi.org/10.1126/sciadv.adc9516
149. Liang, J.W., Li, X.N., Wang, S., et al.: Site-occupation-tuned superionic Li_xScCl_{3+x} halide solid electrolytes for all-solid-state batteries. J. Am. Chem. Soc. **142**, 7012–7022 (2020). https://doi.org/10.1021/jacs.0c00134
150. Kanno, R., Murayama, M., Inada, T., et al.: A self-assembled breathing interface for all-solid-state ceramic lithium batteries. Electrochem. Solid-State Lett. **7**, A455 (2004). https://doi.org/10.1149/1.1809553

151. Liu, Y., Wang, C.C., Yoon, S.G., et al.: Aluminum foil negative electrodes with multiphase microstructure for all-solid-state Li-ion batteries. Nat. Commun. **14**, 3975 (2023). https://doi.org/10.1038/s41467-023-39685-x
152. Zhong, C., Guo, C., Jin, X., et al.: Gradient electrodeposition enables high-throughput fabrication and screening of alloy anodes for high-energy lithium-ion batteries. Mater. Today Energy **18**, 100528 (2020). https://doi.org/10.1016/j.mtener.2020.100528
153. Zhou, D.B., Liu, Z.J., Lv, X.K., et al.: Electrochemical studies of LiB compound as anode material for lithium-ion battery. Electrochim. Acta **51**, 5731–5737 (2006). https://doi.org/10.1016/j.electacta.2006.03.023
154. Liu, X., Wu, X.Y., Chang, B.B., et al.: Recent progress on germanium-based anodes for lithium ion batteries: efficient lithiation strategies and mechanisms. Energy Storage Mater. **30**, 146–169 (2020). https://doi.org/10.1016/j.ensm.2020.05.010
155. He, J., Wei, Y.Q., Zhai, T.Y., et al.: Antimony-based materials as promising anodes for rechargeable lithium-ion and sodium-ion batteries. Mater. Chem. Front. **2**, 437–455 (2018). https://doi.org/10.1039/c7qm00480j
156. DeVries, L.E., Jackson, L.D., James, S.D.: Structure and anodic discharge behavior of lithium-boron alloys in the LiCl-KCl eutectic melt(II). J. Electrochem. Soc. **126**, 993–996 (1979). https://doi.org/10.1149/1.2129222
157. Sanchez, P., Belin, C., Crepy, G., et al.: Preparation and characterization of lithium-boron alloys: electrochemical studies as anodes in molten salt media, and comparison with pure lithium-involving systems. J. Mater. Sci. **27**, 240–246 (1992). https://doi.org/10.1007/BF00553862
158. Sanchez, P., Belin, C., Crepy, C., et al.: Electrochemical studies of lithium-boron alloys in non-aqueous media: comparison with pure lithium. J. Appl. Electrochem. **19**, 421–428 (1989). https://doi.org/10.1007/BF01015246
159. Netz, A., Huggins, R.A., Weppner, W.: Investigations of a number of alternative negative electrode materials for use in lithium cells. Ionics **7**, 433–439 (2001). https://doi.org/10.1007/BF02373580
160. Duan, B., Wang, W., Zhao, H., et al.: Li-B alloy as anode material for lithium/sulfur battery. ECS Electrochem. Lett. **2**, A47–A51 (2013). https://doi.org/10.1149/2.005306eel
161. Weker, J.N., Liu, N., Misra, S., et al.: In situ nanotomography and operando transmission X-ray microscopy of micron-sized Ge particles. Energy Environ. Sci. **7**, 2771–2777 (2014). https://doi.org/10.1039/c4ee01384k
162. Kennedy, T., Brandon, M., Ryan, K.M.: Advances in the application of silicon and germanium nanowires for high-performance lithium-ion batteries. Adv. Mater. **28**, 5696–5704 (2016). https://doi.org/10.1002/adma.201503978
163. Chen, G.D., Sun, J.R., Li, J.D., et al.: Revealing capacity degradation of Ge anodes in lithium-ion batteries triggered by interfacial LiH. Angew. Chem. Int. Ed. **62**, 2306141 (2023). https://doi.org/10.1002/anie.202306141
164. Weppner, W., Huggins, R.A.: Thermodynamic properties of the intermetallic systems lithium-antimony and lithium-bismuth. J. Electrochem. Soc. **125**, 7–14 (1978). https://doi.org/10.1149/1.2131401
165. Weppner, W., Huggins, R.A.: Determination of the kinetic parameters of mixed-conducting electrodes and application to the system Li_3Sb. J. Electrochem. Soc. **124**, 1569–1578 (1977). https://doi.org/10.1149/1.2133112
166. Hou, H.S., Jing, M.J., Yang, Y.C., et al.: Sb porous hollow microspheres as advanced anode materials for sodium-ion batteries. J. Mater. Chem. A **3**, 2971–2977 (2015). https://doi.org/10.1039/c4ta06476c
167. Guo, Y.G., Hu, J.S., Wan, L.J.: Nanostructured materials for electrochemical energy conversion and storage devices. Adv. Mater. **20**, 2878–2887 (2008). https://doi.org/10.1002/adma.200800627
168. Kim, H., Cho, J.: Template synthesis of hollow Sb nanoparticles as a high-performance lithium battery anode material. Chem. Mater. **20**, 1679–1681 (2008). https://doi.org/10.1021/cm703401u
169. Gong, H.X., Chen, Y.L., Chen, S.C., et al.: Fast-charging of hybrid lithium-ion/lithium-metal anodes by nanostructured hard carbon host. ACS Energy Lett. **7**, 4417–4426 (2022). https://doi.org/10.1021/acsenergylett.2c02130
170. Ko, M., Chae, S., Ma, J., et al.: Scalable synthesis of silicon-nanolayer-embedded graphite for high-energy lithium-ion batteries. Nat. Energy **1**, 16113 (2016). https://doi.org/10.1038/nenergy.2016.113
171. Son, Y., Ma, J., Kim, N., et al.: Quantification of pseudocapacitive contribution in nanocage-shaped silicon-carbon composite anode. Adv. Energy Mater. **9**, 1803480 (2019). https://doi.org/10.1002/aenm.201803480
172. Lai, Y.Z., Li, H.Y., Yang, Q., et al.: Revisit the progress of binders for a silicon-based anode from the perspective of designed binder structure and special sized silicon nanoparticles. Ind. Eng. Chem. Res. **61**, 6246–6268 (2022). https://doi.org/10.1021/acs.iecr.2c00453
173. Zhang, L., Wang, C.R., Dou, Y.H., et al.: A yolk-shell structured silicon anode with superior conductivity and high tap density for full lithium-ion batteries. Angew. Chem. Int. Ed. **58**, 8824–8828 (2019). https://doi.org/10.1002/anie.201903709
174. Yang, Z., Jiang, M.X., Cui, C., et al.: In-situ cross-linking strategy for stabilizing the LEDC of the solid-electrolyte interphase in lithium-ion batteries. Nano Energy **105**, 107993 (2023). https://doi.org/10.1016/j.nanoen.2022.107993
175. Lee, J., Jin, D., Kim, J.Y., et al.: Dry pre-lithiation for graphite-silicon diffusion-dependent electrode for all-solid-state battery. Adv. Energy Mater. **13**, 2300172 (2023). https://doi.org/10.1002/aenm.202300172
176. Zhu, B., Liu, G.L., Lv, G.X., et al.: Minimized lithium trapping by isovalent isomorphism for high initial coulombic efficiency of silicon anodes. Sci. Adv. **5**, eaax0651 (2019). https://doi.org/10.1126/sciadv.aax0651
177. Yang, Y.F., Wang, J.Y., Kim, S.C., et al.: In situ prelithiation by direct integration of lithium mesh into battery cells. Nano Lett. **23**, 5042–5047 (2023). https://doi.org/10.1021/acs.nanolett.3c00859
178. Huang, Y.L., Shao, B.W., Wang, Y., et al.: Solid-state silicon anode with extremely high initial coulombic efficiency. Energy Environ. Sci. **16**, 1569–1580 (2023). https://doi.org/10.1039/d2ee04057c
179. Zhan, X., Li, M., Li, S., et al.: Challenges and opportunities towards silicon-based all-solid-state batteries. Energy Storage Mater. **61**, 102875 (2023). https://doi.org/10.1016/j.ensm.2023.102875
180. Shoji, M., Cheng, E.J., Kimura, T., et al.: Recent progress for all solid state battery using sulfide and oxide solid electrolytes. J. Phys. D Appl. Phys. **52**, 103001 (2019). https://doi.org/10.1088/1361-6463/aaf7e2
181. Wang, Y.Y., Diao, W.Y., Fan, C.Y., et al.: Benign recycling of spent batteries towards all-solid-state lithium batteries. Chem. **25**, 8975–8981 (2019). https://doi.org/10.1002/chem.201900845
182. Cangaz, S., Hippauf, F., Reuter, F.S., et al.: Enabling high-energy solid-state batteries with stable anode interphase by the use of columnar silicon anodes. Adv. Energy Mater. **10**, 2001320 (2020). https://doi.org/10.1002/aenm.202001320
183. Han, F.D., Zhu, Y.Z., He, X.F., et al.: Electrochemical stability of $Li_{10}GeP_2S_{12}$ and $Li_7La_3Zr_2O_{12}$ solid electrolytes. Adv. Energy

Mater. **6**, 1501590 (2016). https://doi.org/10.1002/aenm.201501590
184. Schwietert, T.K., Arszelewska, V.A., Wang, C., et al.: Clarifying the relationship between redox activity and electrochemical stability in solid electrolytes. Nat. Mater. **19**, 428–435 (2020). https://doi.org/10.1038/s41563-019-0576-0
185. Wang, Y., Wu, Y.J., Wang, Z.X., et al.: Doping strategy and mechanism for oxide and sulfide solid electrolytes with high ionic conductivity. J. Mater. Chem. A **10**, 4517–4532 (2022). https://doi.org/10.1039/d1ta10966a
186. Yu, T., Ke, B.Y., Li, H.Y., et al.: Recent advances in sulfide electrolytes toward high specific energy solid-state lithium batteries. Mater. Chem. Front. **5**, 4892–4911 (2021). https://doi.org/10.1039/d1qm00474c
187. Trevey, J., Jang, J.S., Jung, Y.S., et al.: Glass-ceramic Li_2S-P_2S_5 electrolytes prepared by a single step ball billing process and their application for all-solid-state lithium-ion batteries. Electrochem. Commun. **11**, 1830–1833 (2009). https://doi.org/10.1016/j.elecom.2009.07.028
188. Dunlap, N.A., Kim, S., Jeong, J.J., et al.: Simple and inexpensive coal-tar-pitch derived Si-C anode composite for all-solid-state Li-ion batteries. Solid State Ion. **324**, 207–217 (2018). https://doi.org/10.1016/j.ssi.2018.07.013
189. Piper, D.M., Yersak, T.A., Lee, S.H.: Effect of compressive stress on electrochemical performance of silicon anodes. J. Electrochem. Soc. **160**, A77–A81 (2012). https://doi.org/10.1149/2.064301jes
190. Yamamoto, M., Terauchi, Y., Sakuda, A., et al.: Slurry mixing for fabricating silicon-composite electrodes in all-solid-state batteries with high areal capacity and cycling stability. J. Power Sources **402**, 506–512 (2018). https://doi.org/10.1016/j.jpowsour.2018.09.070
191. Cao, D.X., Sun, X., Wang, Y., et al.: Bipolar stackings high voltage and high cell level energy density sulfide based all-solid-state batteries. Energy Storage Mater. **48**, 458–465 (2022). https://doi.org/10.1016/j.ensm.2022.03.012
192. Zhang, W.B., Leichtweiß, T., Culver, S.P., et al.: The detrimental effects of carbon additives in $Li_{10}GeP_2S_{12}$-based solid-state batteries. ACS Appl. Mater. Interfaces **9**, 35888–35896 (2017). https://doi.org/10.1021/acsami.7b11530
193. Chen, C., Li, Q., Li, Y.Q., et al.: Sustainable interfaces between Si anodes and garnet electrolytes for room-temperature solid-state batteries. ACS Appl. Mater. Interfaces **10**, 2185–2190 (2018). https://doi.org/10.1021/acsami.7b16385
194. Ke, X.Y., Wang, Y., Dai, L.M., et al.: Cell failures of all-solid-state lithium metal batteries with inorganic solid electrolytes: lithium dendrites. Energy Storage Mater. **33**, 309–328 (2020). https://doi.org/10.1016/j.ensm.2020.07.024
195. Xiong, S.Z., Xu, X.Y., Jiao, X.X., et al.: Mechanical failure of solid-state electrolyte rooted in synergy of interfacial and internal defects. Adv. Energy Mater. **13**, 2203614 (2023). https://doi.org/10.1002/aenm.202203614
196. Liu, J., Yuan, H., Liu, H., et al.: Unlocking the failure mechanism of solid state lithium metal batteries. Adv. Energy Mater. **12**, 2100748 (2022). https://doi.org/10.1002/aenm.202100748
197. Kazyak, E., Garcia-Mendez, R., LePage, W.S., et al.: Li penetration in ceramic solid electrolytes: operando microscopy analysis of morphology, propagation, and reversibility. Matter **2**, 1025–1048 (2020). https://doi.org/10.1016/j.matt.2020.02.008
198. Lu, Y., Zhao, C.Z., Hu, J.K., et al.: The void formation behaviors in working solid-state Li metal batteries. Sci. Adv. **8**, eadd0510 (2022). https://doi.org/10.1126/sciadv.add0510
199. Lee, K., Kazyak, E., Wang, M.J., et al.: Analyzing void formation and rewetting of thin in situ-formed Li anodes on LLZO. Joule **6**, 2547–2565 (2022). https://doi.org/10.1016/j.joule.2022.09.009
200. Shishvan, S.S., Fleck, N.A., McMeeking, R.M., et al.: Vacancy diffusion and its consequences for void growth at the interface of a stripping metal electrode and solid electrolyte. Electrochim. Acta **467**, 143081 (2023). https://doi.org/10.1016/j.electacta.2023.143081
201. Ma, J., Zhang, S., Zheng, Y., et al.: Interelectrode talk in solid-state lithium-metal batteries. Adv. Mater. **35**, 2301892 (2023). https://doi.org/10.1002/adma.202301892
202. Kang, J., Shin, H.R., Yun, J., et al.: Chemo-mechanical failure of solid composite cathodes accelerated by high-strain anodes in all-solid-state batteries. Energy Storage Mater. **63**, 103049 (2023). https://doi.org/10.1016/j.ensm.2023.103049
203. Kato, A., Kowada, H., Deguchi, M., et al.: XPS and SEM analysis between Li/Li_3PS_4 interface with Au thin film for all-solid-state lithium batteries. Solid State Ion. **322**, 1–4 (2018). https://doi.org/10.1016/j.ssi.2018.04.011
204. Kato, A., Hayashi, A., Tatsumisago, M.: Enhancing utilization of lithium metal electrodes in all-solid-state batteries by interface modification with gold thin films. J. Power Sources **309**, 27–32 (2016). https://doi.org/10.1016/j.jpowsour.2016.01.068
205. Chen, B.T., Zhang, J.C., Zhang, T.R., et al.: Constructing a superlithiophilic 3D burr-microsphere interface on garnet for high-rate and ultra-stable solid-state Li batteries. Adv. Sci. **10**, 2207056 (2023). https://doi.org/10.1002/advs.202207056
206. Jiang, J.L., Ou, Y.H., Lu, S.Y., et al.: In-situ construction of Li-Mg/LiF conductive layer to achieve an intimate lithium-garnet interface for all-solid-state Li metal battery. Energy Storage Mater. **50**, 810–818 (2022). https://doi.org/10.1016/j.ensm.2022.06.011
207. Shi, K., Wan, Z.P., Yang, L., et al.: In situ construction of an ultra-stable conductive composite interface for high-voltage all-solid-state lithium metal batteries. Angew. Chem. Int. Ed. **59**, 11784–11788 (2020). https://doi.org/10.1002/anie.202000547
208. Zhong, Y.R., Xie, Y.J., Hwang, S., et al.: A highly efficient all-solid-state lithium/electrolyte interface induced by an energetic reaction. Angew. Chem. Int. Ed. **59**, 14003–14008 (2020). https://doi.org/10.1002/anie.202004477
209. Chen, Y., Qian, J., Hu, X., et al.: Constructing a uniform and stable mixed conductive layer to stabilize the solid-state electrolyte/Li interface by cold bonding at mild conditions. Adv. Mater. **35**, 2212096 (2023). https://doi.org/10.1002/adma.202212096
210. Lee, K., Han, S., Lee, J., et al.: Multifunctional interface for high-rate and long-durable garnet-type solid electrolyte in lithium metal batteries. ACS Energy Lett. **7**, 381–389 (2022). https://doi.org/10.1021/acsenergylett.1c02332
211. Deng, T., Ji, X., Zhao, Y., et al.: Tuning the anode-electrolyte interface chemistry for garnet-based solid-state Li metal batteries. Adv. Mater. **32**, 2000030 (2020). https://doi.org/10.1002/adma.202000030
212. He, X.Z., Ji, X., Zhang, B., et al.: Tuning interface lithiophobicity for lithium metal solid-state batteries. ACS Energy Lett. **7**, 131–139 (2022). https://doi.org/10.1021/acsenergylett.1c02122
213. Wang, T.R., Duan, J., Zhang, B., et al.: A self-regulated gradient interphase for dendrite-free solid-state Li batteries. Energy Environ. Sci. **15**, 1325–1333 (2022). https://doi.org/10.1039/d1ee03604a
214. He, G., Li, Q.W., Shen, Y.L., et al.: Flexible amalgam film enables stable lithium metal anodes with high capacities. Angew. Chem. Int. Ed. **58**, 18466–18470 (2019). https://doi.org/10.1002/anie.201911800
215. Fan, Y., Tao, T., Gao, Y.X., et al.: A self-healing amalgam interface in metal batteries. Adv. Mater. **32**, 2004798 (2020). https://doi.org/10.1002/adma.202004798
216. Zhang, Q., Wu, L., Fan, M.J., et al.: A room temperature alloying strategy to enable commercial metal foil for efficient Li/Na storage and deposition. Energy Storage Mater. **34**, 708–715 (2021). https://doi.org/10.1016/j.ensm.2020.10.028

217. Li, X.N., Liang, J.W., Li, X., et al.: High-performance all-solid-state Li-Se batteries induced by sulfide electrolytes. Energy Environ. Sci. **11**, 2828–2832 (2018). https://doi.org/10.1039/c8ee01621f
218. Fan, X.L., Yue, J., Han, F.D., et al.: High-performance all-solid-state Na-S battery enabled by casting-annealing technology. ACS Nano **12**, 3360–3368 (2018). https://doi.org/10.1021/acsnano.7b08856
219. Huo, H.Y., Chen, Y., Li, R.Y., et al.: Design of a mixed conductive garnet/Li interface for dendrite-free solid lithium metal batteries. Energy Environ. Sci. **13**, 127–134 (2020). https://doi.org/10.1039/c9ee01903k
220. Krauskopf, T., Richter, F.H., Zeier, W.G., et al.: Physicochemical concepts of the lithium metal anode in solid-state batteries. Chem. Rev. **120**, 7745–7794 (2020). https://doi.org/10.1021/acs.chemrev.0c00431
221. Pathak, R., Chen, K., Gurung, A., et al.: Fluorinated hybrid solid-electrolyte-interphase for dendrite-free lithium deposition. Nat. Commun. **11**, 93 (2020). https://doi.org/10.1038/s41467-019-13774-2
222. Li, F., Tan, Y.H., Yin, Y.C., et al.: A fluorinated alloy-type interfacial layer enabled by metal fluoride nanoparticle modification for stabilizing Li metal anodes. Chem. Sci. **10**, 9735–9739 (2019). https://doi.org/10.1039/c9sc01845j
223. Li, S., Yang, S.J., Liu, G.X., et al.: A dynamically stable mixed conducting interphase for all-solid-state lithium metal batteries. Adv. Mater. **36**, 2307768 (2024). https://doi.org/10.1002/adma.202307768
224. Liang, X., Pang, Q., Kochetkov, I.R., et al.: A facile surface chemistry route to a stabilized lithium metal anode. Nat. Energy **2**, 17119 (2017). https://doi.org/10.1038/nenergy.2017.119
225. Zhao, F.P., Alahakoon, S.H., Adair, K., et al.: An air-stable and Li-metal-compatible glass-ceramic electrolyte enabling high-performance all-solid-state Li metal batteries. Adv. Mater. **33**, 2006577 (2021). https://doi.org/10.1002/adma.202006577
226. Liu, H., Zhu, Q.S., Wang, C., et al.: High air stability and excellent Li metal compatibility of argyrodite-based electrolyte enabling superior all-solid-state Li metal batteries. Adv. Funct. Mater. **32**, 2203858 (2022). https://doi.org/10.1002/adfm.202203858
227. Ni, Y., Huang, C., Liu, H., et al.: A high air-stability and Li-metal-compatible $Li_{3+2x}XP_{1-x}Bi_xS_{4-1.5x}O_{1.5x}$ sulfide electrolyte for all-solid-state Li-metal batteries. Adv. Funct. Mater. **32**, 2205998 (2022). https://doi.org/10.1002/adfm.202205998
228. Jiang, Z., Liu, Y., Peng, H.L., et al.: Enhanced air stability and interfacial compatibility of Li-argyrodite sulfide electrolyte triggered by CuBr co-substitution for all-solid-state lithium batteries. Energy Storage Mater. **56**, 300–309 (2023). https://doi.org/10.1016/j.ensm.2023.01.018
229. Taklu, B.W., Su, W.N., Nikodimos, Y., et al.: Dual CuCl doped argyrodite superconductor to boost the interfacial compatibility and air stability for all solid-state lithium metal batteries. Nano Energy **90**, 106542 (2021). https://doi.org/10.1016/j.nanoen.2021.106542
230. Xu, B.Y., Li, X.Y., Yang, C., et al.: Interfacial chemistry enables stable cycling of all-solid-state Li metal batteries at high current densities. J. Am. Chem. Soc. **143**, 6542–6550 (2021). https://doi.org/10.1021/jacs.1c00752
231. Jia, W.S., Wang, Z.H., Li, J.Z., et al.: A dual-phase Li-Ca alloy with a patternable and lithiophilic 3D framework for improving lithium anode performance. J. Mater. Chem. A **7**, 22377–22384 (2019). https://doi.org/10.1039/c9ta08798b
232. Chen, L., Fan, X.L., Ji, X., et al.: High-energy Li metal battery with lithiated host. Joule **3**, 732–744 (2019). https://doi.org/10.1016/j.joule.2018.11.025
233. Wan, M.T., Kang, S.J., Wang, L., et al.: Mechanical rolling formation of interpenetrated lithium metal/lithium tin alloy foil for ultrahigh-rate battery anode. Nat. Commun. **11**, 829 (2020). https://doi.org/10.1038/s41467-020-14550-3
234. Ding, X.L., Lu, X., Fu, Z.W., et al.: Temperature-dependent lithium storage behavior in tetragonal boron (B_{50}) thin film anode for Li-ion batteries. Electrochim. Acta **87**, 230–235 (2013). https://doi.org/10.1016/j.electacta.2012.09.017
235. Wu, C., Huang, H.F., Lu, W.Y., et al.: Mg doped Li-LiB alloy with in situ formed lithiophilic LiB skeleton for lithium metal batteries. Adv. Sci. **7**, 1902643 (2020). https://doi.org/10.1002/advs.201902643
236. Chen, Z.R., Liang, Z.T., Zhong, H.Y., et al.: Bulk/interfacial synergetic approaches enable the stable anode for high energy density all-solid-state lithium-sulfur batteries. ACS Energy Lett. **7**, 2761–2770 (2022). https://doi.org/10.1021/acsenergylett.2c01334
237. Wang, M.Q., Peng, Z., Luo, W.W., et al.: Improving the interfacial stability between lithium and solid-state electrolyte via dipole-structured lithium layer deposited on graphene oxide. Adv. Sci. **7**, 2000237 (2020). https://doi.org/10.1002/advs.202000237
238. Park, S.H., Jun, D., Lee, G.H., et al.: Designing 3D anode based on pore-size-dependent Li deposition behavior for reversible Li-free all-solid-state batteries. Adv. Sci. **9**, 2203130 (2022). https://doi.org/10.1002/advs.202203130
239. Ye, S.F., Chen, X.J., Zhang, R., et al.: Revisiting the role of physical confinement and chemical regulation of 3D hosts for dendrite-free Li metal anode. Nano Micro Lett. **14**, 187 (2022). https://doi.org/10.1007/s40820-022-00932-3
240. Yan, K., Lu, Z.D., Lee, H.W., et al.: Selective deposition and stable encapsulation of lithium through heterogeneous seeded growth. Nat. Energy **1**, 16010 (2016). https://doi.org/10.1038/nenergy.2016.10
241. Wang, H.S., Cao, X., Gu, H.K., et al.: Improving lithium metal composite anodes with seeding and pillaring effects of silicon nanoparticles. ACS Nano **14**, 4601–4608 (2020). https://doi.org/10.1021/acsnano.0c00184
242. Zhu, J.Q., Cai, D., Li, J.R., et al.: In-situ generated Li_3N/Li-Al alloy in reduced graphene oxide framework optimizing ultra-thin lithium metal electrode for solid-state batteries. Energy Storage Mater. **49**, 546–554 (2022). https://doi.org/10.1016/j.ensm.2022.05.001
243. Wan, H.L., Wang, Z.Y., Liu, S.F., et al.: Critical interphase overpotential as a lithium dendrite-suppression criterion for all-solid-state lithium battery design. Nat. Energy **8**, 473–481 (2023). https://doi.org/10.1038/s41560-023-01231-w
244. Chen, L.H., Tong, R.A., Zhang, J.X., et al.: Reactive magnesium nitride additive: a drop-in solution for lithium/garnet wetting in all-solid-state batteries. Angew. Chem. Int. Ed. **62**, 2305099 (2023). https://doi.org/10.1002/anie.202305099
245. Qiu, H.L., Tang, T.Y., Asif, M., et al.: Stable lithium metal anode enabled by lithium metal partial alloying. Nano Energy **65**, 103989 (2019). https://doi.org/10.1016/j.nanoen.2019.103989
246. Huang, Y., Chen, B., Duan, J., et al.: Graphitic carbon nitride ($g\text{-}C_3N_4$): an interface enabler for solid-state lithium metal batteries. Angew. Chem. Int. Ed. **59**, 3699–3704 (2020). https://doi.org/10.1002/anie.201914417
247. Wang, C.W., Xie, H., Zhang, L., et al.: Universal soldering of lithium and sodium alloys on various substrates for batteries. Adv. Energy Mater. **8**, 1701963 (2018). https://doi.org/10.1002/aenm.201701963
248. Wang, T.S., Zhai, P.B., Legut, D., et al.: S-doped graphene-regional nucleation mechanism for dendrite-free lithium metal anodes. Adv. Energy Mater. **9**, 1804000 (2019). https://doi.org/10.1002/aenm.201804000
249. Xu, Y., Zheng, H.Q., Yang, H., et al.: Thermodynamic regulation of dendrite-free Li plating on Li_3Bi for stable lithium metal

batteries. Nano Lett. **21**, 8664–8670 (2021). https://doi.org/10.1021/acs.nanolett.1c02613
250. Li, J.R., Su, H., Jiang, Z., et al.: Domain-limited laminar lithium deposition behavior mediated by the design of hybrid anode for sulfide-based all-solid-state batteries. Acta Mater. **244**, 118592 (2023). https://doi.org/10.1016/j.actamat.2022.118592
251. Liu, C., Chen, B.T., Zhang, T.R., et al.: Electron redistribution enables redox-resistible Li_6PS_5Cl towards high-performance all-solid-state lithium batteries. Angew. Chem. Int. Ed. **62**, 2302655 (2023). https://doi.org/10.1002/anie.202302655

Jingru Li received her B.S. degree from Chongqing University in 2019. She is currently pursuing a Ph.D. degree under the supervision of Prof. Jiangping Tu at the School of Materials Science and Engineering, Zhejiang University. Her research mainly focuses on all-solid-state Li metal batteries.

Han Su has been a Ph.D. candidate at the School of Materials Science and Engineering at Zhejiang University since 2020. He obtained his Bachelor's degree from Chu KoChen honors college at Zhejiang University. His research mainly focuses on the lithium metal anodes and sulfide-based all-solid-state batteries.

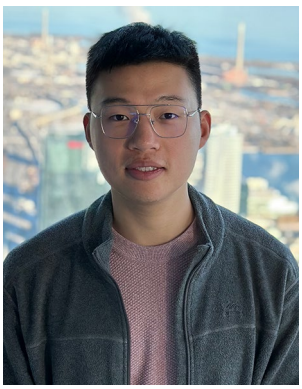

Yu Liu received his B.S. degree from Zhejiang University and has been a Ph.D. candidate at the School of Materials Science and Engineering at Zhejiang University since 2019. His research mainly focuses on sulfide electrolytes.

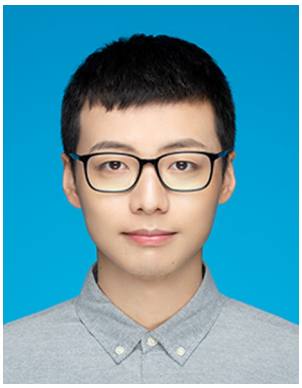

Yu Zhong is currently an assistant professor at Zhejiang University. He received his Ph.D. degree from Zhejiang University in 2019. His research mainly focuses on all-solid-state batteries.

Xiuli Wang obtained her B.S. degree (2001) and Ph.D. degree (2006) at the school of Materials Science and Engineering from Zhejiang University, respectively. After a postdoctoral fellowship in Zhejiang University, she was appointed an associated professor in 2010. During 2013–2014, she worked at Nanyang Technological University as a research fellow. Her scientific research focuses on electrochemical energy storage materials and engineering technology. She was awarded "Highly Cited Researcher" in four consecutive years (from 2015 to 2018) for her contributions in the field of engineering technology.

Jiangping Tu received his Ph.D. degree from Zhejiang University in 1994. From 1998 to 2000, he worked as a Japan Society for the Promotion of Science (JSPS) research fellow at the Department of Chemical Engineering of Hiroshima University, Japan. He has been a full professor at the school of Materials Science and Engineering at Zhejiang University since 2000. His main research interests are the fabrication and tribological properties of nanocomposites and nanocomposite coatings, novel electrochemical energy storage materials and solid electrolyte materials.